Pulmonary cell signals mediating resident memory B cell responses to influenza rechallenge.

By: Niamh Richmond

Supervisor: Prof. Tal I. Arnon
Co-supervisor: Prof. Irina Udalova

DPhil in Molecular and Cellular Medicine

University of Oxford
Keble College

Dedication

I dedicate this thesis to my loving parents and sister,

To my former mentor Prof. Zia Khan, for encouraging me in the pursuit of science,

To those who urge others to breach glass ceilings.

Acknowledgements

I want to thank everyone who contributed to my DPhil work and experience! I am truly happy to acknowledge that people have played such an important role.

First, I would like to thank Prof. Tal Arnon for providing me the opportunity to work on such an exciting area of research, for all the insight and helpful guidance throughout my studies, and for the support in writing my thesis. I want to thank my lab mates: Dr. Andrew MacLean – for the many discussions shared over science and many hours shared over mashing lungs; Dr. Gabriela Pirgova – for the many chocolate bribes sweetening incubation times; Dr. Anne Chauveau – for having answers to almost everything; Dr. Bin Xie – for having my best interests at heart and teaching me cloning; Sophia Oram – who's kindness brightens my day!

I also would like to thank my thesis committee: Prof. Irina Udalova, Dr. Emily Thornton, and Prof. Christopher Buckley, for the helpful direction and suggestions during my studies. A big thank you to Dr. Kristina Zec for taking the time to answer many microscopy questions and being so helpful, and to Dr. Benjamin Demarco for taking the interest and time to discuss the inflammasome with me. To the many senior post-docs in the institute who have helped me here and there – thank you! Collectively, those moments have had a significant impact. I also want to thank the staff of the Kennedy Institute and our animal facilities for keeping the roof standing over our heads (literally!) and being a grounding force for so many.

To my new friends here in Oxford, especially Vicky, Ali, Pedro, Mikesh, Cat, Alex, Jana, Gabrielle, and Micon; and friendships made via the student committee, especially: Fabi, Nicole, Justin, and Libby – you have all made my time here SO wonderful, and I'm truly grateful for your friendships.

To Luca, my love, beyond everything else – this path led me to you. I'm not quite sure how you've put up with me these past few years, but I'm so happy you have! Thank you for your patience, support, and belief in me.

Abstract

The capacity of the mammalian adaptive immune response to generate immunological memory has for years been exploited by systemic vaccination strategies to protect large populations from infectious diseases. Recently, evidence has emerged for the establishment of memory B cells in tissues prone to antigen exposure. These tissue-resident B cells (Brm) may be adapted toward rapid reactivation at local sites – reducing the need for systemic intervention when fighting recurring pathogens.

Here, I utilize cytometry, microscopy, and transcriptomic sequencing approaches to explore the dynamics of Brm residence in the lung and their response to secondary influenza virus infections. I propose that the induction of C-X-C motif chemokine ligands 9 and 10 (CXCL9, CXCL10) early after rechallenge are important for Brm migration and accumulation at sites of infection. Innate immune cells, including alveolar macrophages, bridge the inflammatory and adaptive immune systems in part by inducing the expression of these two chemokines.

The recruitment of Brm at sites of viral infection is associated with the rapid appearance of antibody-producing cells in the same niche. This enables the prompt delivery of antibodies in a highly localized manner at sites of viral replication. Defining the protection granted by Brm towards recurring antigens has important implications for developing immunization strategies against respiratory viruses such as influenza.

Table of Contents

Dedication.....2
Acknowledgments.....3
Abstract.....4
Table of Contents.....5
List of Figures.....7
List of Abbreviations.....8

1 Introduction ***9***

1.1 Humoral immunity – an overview **9**

1.2 B cell activation **14**

1.2.1 Stage I. Encounter with antigen: 14

1.2.2 Stage II. B-T interaction 18

1.3 Germinal center reactions **20**

1.4 Humoral memory **25**

1.4.1 Memory T cells 26

1.4.2 Long-lived plasma cells 26

1.4.3 Memory B cells 28

1.4.4 Memory B cell subsets 28

1.4.5 Memory B cell localisation 31

1.4.6 Memory B cell reactivation 34

1.5 Tissue-resident lymphocytes **37**

1.6 Resident memory B cells **39**

1.7 Pulmonary immunity **43**

1.8 Influenza virus **45**

1.8.1 An overview of infection by influenza viruses 45

1.8.2 Humoral responses to influenza virus 46

1.8.3 Potential implications of Brm on influenza vaccination strategies 48

2 Research Aims ***49***

2.1 Hypothesis **49**

2.2 Specific aims **49**

3 Materials and Methods ***50***

4 Results I: Brm residence during steady state ***61***

4.1 Introduction **61**

4.2 Visualising Brm in the lung during steady state **64**

4.3 Validating alveolar Brm cells localization inside blood-sheltered regions **68**

4.4 Exploring potential cellular partners that associate with alveolar Brm cells **71**

4.5 Investigating the role of CCR1 in Brm establishment or retention **76**

4.6 Discussion 84

5 Results II: The role of alveolar macrophages in regulating Brm cell activation 89

5.1 Introduction 89

5.2 Optimizing alveolar macrophage identification by flow cytometry 93

5.3 Alveolar macrophage depletion using clodronate liposomes causes local inflammation. 99

5.4 Alveolar macrophages orchestrate Brm cell accumulation at infected sites via activation of CXCR3 ligands early after re-infection. 103

5.5 Discussion 110

6 Results III: Identifying cellular mechanisms that act downstream of AM to induce Brm migration to infected sites. 115

6.1 Introduction 115

6.2 Innate cells, including neutrophils, monocytes, and natural killer cells, infiltrate the lung tissue with 24 hours of rechallenge. 119

6.3 Depletion of AM leads to selective loss of *Cxcl9 and Cxcl10* expression in neutrophils and reduced interferon-gamma transcription in natural killer cells. 127

6.4 Discussion 132

7 Concluding remarks and limitations of study 137

8 References 153

List of Figures

Figure 1-1 (schematic): Follicular naïve B cell routes of encounter with antigen….....17
Figure 1-2 (schematic): Naive B cells cycle through LNs via migratory cues….....20
Figure 1-3 (schematic): Bmem and PCs of differing affinities arise pre-GC and during GC reactions….....24
Figure 4-1: Pulmonary AID+ B cells and plasma cells in the BAT mouse….....67
Figure 4-2: Confocal microscopy of lungs from BAT mice 42 days post-primary infection with influenza virus. 69
Figure 4-3: Proximity of Brm to TIIAEC….....73
Figure 4-4: Proximity of Brm to alveolar macrophages….....73
Figure 4-5 (left): Normalized distances.....74
Figure 4-6: Proximity of Brm to endothelium and TIIAEC….....75
Figure 4-7: Bulk RNA sequencing of Brm reveals changes in select GPCR expression.....75
Figure 4-8: CCR1 does not affect B cell subset establishment or retention in the lung….....82
Figure 5-1 (schematic): Brm mobilize to infected sites rapidly after influenza rechallenge….....92
Figure 5-2 (above): Identification of AM and IM by flow cytometry….....96
Figure 5-3: Lung immune cell composition….....98
Figure 5-4: Lung immune cell composition after CLL treatment….....100
Figure 5-5: Lung macrophage composition in memory state LysMCre+ Clec4a2flox/DTR recipient/BAT donor chimeras after DT administration….....102
Figure 5-6: Quantitative PCR analysis of sorted AM 24 hours post-rechallenge….....104
Figure 5-7: AM bulk-sequencing sample similarity….....106
Figure 5-8: Bulk RNA-sequencing of AM at 6, 12, 18 hours post-rechallenge reveals changes in select cytokines and chemokines….....109
Figure 6-1: Lung hematopoietic scRNA sequencing experimental set-up….....120
Figure 6-2: Changes in the cellular landscape of rechallenged mice in the presence and absence of alveolar macrophages….....123
Figure 6-3: Neutrophils and NK cells are proximal to infected cells within 24 hours of rechallenge….....126
Figure 6-4: Infiltrating immune cells transcriptionally express IFNγ and CXCR3 ligands during rechallenge response in an alveolar macrophage-dependent manner….....128
Figure 6-5: Neutrophils and natural killer cells exhibit distinct transcriptional profiles during rechallenge in the absence of alveolar macrophages….....130
Figure 6-6: Neutrophils respond to interferon gamma during rechallenge….....131
Figure 6-7: Summary schematic of chemokine mediated Brm mobilization during influenza rechallenge….....131

List of Abbreviations

AfM Affinity maturation
AID Activation-induced deaminase
AM Alveolar macrophage
APRIL A proliferation-inducing ligand
BCR B cell receptor
Bmem Memory B cell
Brm Resident memory B cell
BSA Bovine serum albumin
CD Cluster of differentiation
CFP Cyan fluorescent protein
CSR Class-switch recombination
DC Dendritic cell
DMEM Dulbecco's Modified Eagle Medium
FACS Fluorescence-activated cell sorting
FBS Foetal bovine serum
FDC Follicular dendritic cell
GC Germinal center
GFP Green fluorescent protein
GPCR G-protein coupled receptor
HA Haemagglutinin
IC Immune complex
i.n. Intranasal
i.p. Intraperitoneal
i.v. Intravenous
IAV Influenza A virus
Ig Immunoglobulin
IL Interleukin
LLPC Long-lived plasma cell
LN Lymph node
MHC Major histocompatibility complex
MZ Marginal zone
NA Neuraminidase
PC Plasma cell
PD-L2 Programmed-death ligand 2
PFA Paraformaldehyde
Ptx Pertussis toxin
SCS Subcapsular sinus
SHM Somatic hypermutation
SLO Secondary lymphoid organ
SLPC Short-lived plasma cell
TCR T cell receptor
Tfh T follicular helper cell
TLR Toll-like receptor
TNF Tumour necrosis factor
Trm Resident memory T cell
VLP Virus-like particle

1 Introduction

1.1 Humoral immunity – an overview

Humoral immunity is an essential component of protection from extracellular pathogens. It encompasses the antibody-mediated neutralization of foreign antigens arising from the activation of B cells and their subsequent differentiation into antibody-producing plasma cells (PC). Antibodies can contribute to immunity by binding directly to viral and bacterial antigens, thus preventing their entry into target cells. Additionally, Fc receptors on the surface of phagocytic cells can recognize the constant region of antibodies; hence, the latter mark infected cells for phagocytosis and their ultimate destruction. Antibody coating can activate protein components of the complement system, causing pathogen opsonization by binding to complement receptors on phagocytes or inducing cell lysis directly via membrane pore formation. These alternate effector mechanisms are differentially induced depending on the isotype or class of antibody involved. The binding of antibody-antigen immune complexes (IC) to complement or Fc receptors expressed by follicular dendritic cells (FDC) in secondary lymphoid organs (SLOs) is important for FDC-mediated antigen retention and presentation during normal humoral immune responses. Bone marrow chimera experiments where radiation-resistant cells lack the expression of complement receptors CD21/35 lead to a marked decrease in the trapping of immune complexes on FDCs, demonstrate diminished IgG titers two weeks post-infection and fail to mount recall responses to subsequent infection (1, 2).

Antibodies are present throughout mammalian tissues, blood, and at mucosal surfaces. Five different isotypes of antibodies (IgD, IgM, IgG, IgA, and IgE) are structurally and functionally adapted to these different regions (3, 4). IgD and IgM are the first isotypes

expressed during B cell development. Their co-expression is commonly used to identify mature, naïve B cells (e.g., marginal zone B cells and B1 cells). The expression of IgD is lost after B cell activation; as such, its contribution to B cell function is unclear. Yet, mice deficient in IgM (IgM−/− mice) exhibit normal B cell development and maturation, with IgD replacing membrane-bound and secretory IgM, as well as the capacity to isotype-switch (5). This suggests that IgD can largely substitute for IgM and may constitute evolutionary redundancy between these two isotypes.

IgM antibodies are present prior to somatic hypermutation and thus provide immediate protection, albeit usually being of lower affinity than IgG antibodies. However, soluble IgM conforms as a 5-unit pentamer consisting of 10 antigen-binding sites, thereby compensating for affinity by exhibiting greater avidity. This structure also enables IgM to be particularly effective in activating complement, which requires the proximity of two or more antibody Fc domains. Due to the large size of IgM pentamers, this isotype is largely found in serum – yet it can transcytose across epithelium, thus prompting efficient protection at mucosal barriers as well. IgM and IgA bind to the polymeric immunoglobulin receptor (pIgR) located on the basolateral surface of epithelial cells forming mucosa. The antibody-receptor complex is then endocytosed and transported to the apical side, where pIgR is proteolytically cleaved, releasing the antibody into the mucosal secretions (6). IgA provides protection in the blood as a monomer and primarily in mucosal tissues as secretory IgA. This isotype is uniquely associated with local production by mucosal-associated lymphoid tissues (MALT), present in the gut, respiratory tract, lactating breast tissue, and other exocrine glands (salivary and tear). IgA-producing plasma cells are predominantly found in the lamina propria, where secreted IgA is further transcytosed to the lumen of the bronchi or the gut. IgA can provide immediate immunity at these barrier sites by neutralizing pathogens before

their systemic circulation. IgA is a weak activator of complement and thus less inflammatory.

IgG, in contrast, is both of high affinity, neutralizing capacity, and a strong activator of complement. It is the principal isotype in blood and extracellular fluid, protecting internal organs from systemic pathogens. There are four subclasses of IgG (IgG1, IgG2, IgG3, IgG4), with slight structural differences in their constant regions (hinges and CH2), thus conferring diverse effector functions *in vivo*. The intact antibody of human and mouse immunoglobulin (IgG) is composed of fragments: the fragment for antigen binding (Fab) and the crystallizable fragment (Fc) for binding of Fcγ receptor (FcγR). The observed functional differences in IgG subclasses are primarily due to their FcγR-binding affinities. For example, FcγRIIIa is found on the surface of natural killer cells, monocytes, macrophages, neutrophils, and T cells and is the primary receptor involved in the activation of antibody-dependent cellular cytotoxicity (ADCC). IgG3, followed closely by IgG1, displays the highest affinities for this FcγRIIIa (7), reflecting an ability to induce ADCC potently. IgG3 also has the shortest half-life of the subclasses due to interference from IgG1 for FcRn-mediated transport (8). IgG4 has a high affinity for FcγRI but weak affinities for other receptors and is a poor inducer of Fc-mediated effector functions. IgG2 has high affinity for some forms of FcγRIIA, but weak affinity for FcγRI and all other FcγRs. Thus, IgG2 and IgG4 have the least functional potency of the subclasses. Interestingly, IgG4 antibodies are often formed following repeated or long-term exposure to antigens in a non-infectious setting and may become the dominant subclass in response to allergens along with IgE (9).

The fifth and final antibody subclass, IgE, is present at very low levels throughout circulation but is tightly bound to mast cell surfaces through the high-affinity IgE receptor, FcεRI (10). Antigen-binding to IgE triggers mast cells to release powerful chemical

mediators, such as histidine, that induce type I hypersensitivity (allergic) reactions.

The observed alternation of antibody isotype is due to class-switch recombination (CSR). Every mature B cell begins by expressing IgM as its B-cell receptor (BCR); therefore, the first antibody produced during an immune response is IgM. Later, however, the same assembled variable (V) region contributing to the antigen-binding site of the antibody may be expressed in IgA, IgG, or IgE format. This change is known as isotype switching and occurs after a naive B cell has become activated in response to mitogenic signals delivered by pathogens (antigen stimulation) and external signals, including cytokines released by T cells. The structural variation of different isotypes is generated by linking different heavy-chain constant regions (C_H) to the same V region. The heavy chain confers functionally distinct properties of each isotype, and the C_H regions are encoded separately in genes located downstream of the V genes at the heavy-chain locus. CSR occurs through a nonhomologous DNA recombination mechanism guided by stretches of repetitive DNA known as switch regions, containing ~150 repeats of the sequence [(GAGCT)n (GGGGGT)], where n is between 3-7 (11). The double-stranded DNA is nicked and broken at two selected S-regions by the activity of a series of enzymes, including activation-induced cytidine deaminase (AID), uracil DNA glycosylase, and apyrimidinic/apurinic (AP)-endonuclease. The pre-existing sequence between these regions is subsequently excised from the chromosome, allowing nonhomologous end joining of the newly exposed C_H sequence to the same V region.

CSR allows fine-tuning of antibody responses due to the diverse functional characteristics of isotypes in terms of their ability to bind Fc receptors on the surface of phagocytic cells, their activation of the complement system, and their ability to be transported across compartments of the body to reach alternate tissues. In contrast, the specificity of an antibody, determined by the V region, which can change through the course

of an immune response through somatic hypermutation (SHM) and affinity maturation (AfM). A mammalian organism's BCR repertoire diversity is mainly obtained by somatic gene rearrangements (called VDJ recombination) during B cell development, where one variable (V), one diversity (D), and one joining (J) gene segment combine in a stochastic fashion. However, increasing affinity towards an antigen is achieved during humoral immune responses by the accumulation of point mutations within the V region. Only a small fraction of the altered antigen receptors generated by SHM will have increased affinity for the antigen. Those that do are preferentially stimulated by the antigen to survive and proliferate, whereas most other B cells die by apoptosis. Repeated cycles of somatic hypermutation followed by antigen-driven proliferation of selected clones of memory B cells causes antibodies of increasingly higher affinity to become abundant during an immune response, providing progressively better protection against the pathogen.

The germinal center (described in detail in section **1.3**) is an established site of SH and AfM, B cell selection and clonal expansion. Importantly, B cells that mature in germinal centers can emerge as isotype-switched plasmablasts and memory B cells in response to disease. Aside from immediate antibody production, a vital component of the humoral immune system is the establishment of immunological memory. This phenomenon is a hallmark of adaptive immunity. It enables more efficient immune responses to pathogens encountered previously, both in terms of the rapidity of the response and the efficacy. The maintenance of humoral memory is primarily mediated by two cell types: long-lived plasma cells (LLPCs) and memory B cells (Bmem). What triggers a naïve B cell to differentiate into an antibody-producing PC or a memory B cell are important areas of ongoing research. Yet, critical components of this fate decision frequently occur during germinal center reactions. In the following sections, I discuss how naïve B cells become activated and the role of the

germinal center in driving affinity maturation and differentiation into memory compartments.

1.2 B cell activation

The differentiation of naïve B cells into either PC or Bmem in response to antigen encounters is crucial for adaptive immune responses. B cell activation is triggered after the recognition of a foreign antigen through the B cell receptor (BCR), distributed on the surface of naïve B cells. Successful B cell activation is associated with the formation of signaling BCR microclusters (12), which further depends on cytoskeletal ezrin- and actin-defined networks to modulate BCR diffusion (13). This can occur in response to soluble antigen, or antigen present on the surface of antigen-presenting cells (APCs), including dendritic cells (DCs), follicular dendritic cells (FDCs), or macrophages. To maximize the likelihood of encountering cognate antigen, naïve B cells have evolved to shuttle between and localize within secondary lymphoid organs (SLOs, lymph nodes and spleen) – tissues that are explicitly organized to catalyze encounters with antigen.

1.2.1 Stage I. Encounter with antigen:

The location at which B cells first encounter antigen depends on the route of infection (for example, mucosal, intravenous, or intradermal). Naïve B cells circulate through the secondary lymphoid organs, including the spleen and peripheral LNs to increase the likelihood of antigen encounter. Small antigens (<70kDa) may circulate directly into lymph node follicles via conduits extending from a network of lymphatic vessels called the subcapsular sinus (SCS) (14). These follicular conduits co-stain with antibodies to ER-TR7, gp38, and fibronectin, indicating they are collagenous fibers in extracellular matrix, likely deriving from fibroblast reticular cells. Other studies suggest small antigens can potentially

diffuse across small pores within the SCS, wherein they come into direct contact with follicular B cells (15). Irrespective of how they arrive, small antigens can directly stimulate follicular B cells in proximity to the SCS.

Larger antigens (>70kDa), in contrast, are captured by CD11b+CD169+MHCII+ macrophages lining the SCS and medulla of lymph nodes and subsequently presented to follicular B cells (16). Depleting these macrophages with clodronate liposomes (CLL) results in higher antigen presence in blood and lymph, indicative of their filtration capacity in capturing antigen. After injection of fluorescently tagged vesicular stomatitis virus (VSV) and adenovirus, virions are readily detectable at B cell–macrophage interfaces for at least four hours, suggesting that SCS macrophages facilitate the shuttling of viral particles across the SCS floor for presentation to B cells (16). Further studies visualized fluorescence-tagged immune complexes (IC) during live two-photon microscopy to reveal that within 2 hours following subcutaneous injection, IC accumulated on the surface of peripheral lymph node SCS macrophages, followed by 40% of follicular B cells labeled with IC by 8 hours post-injection (17). Non-cognate B cells capture antigens from SCS macrophages and deliver them to follicular dendritic cells (FDC) in a complement-dependent manner, as CR2-/- B cells (complement receptor-deficient) are unable to capture IC (17). The inability of CR2-/- B cells to capture IC resulted in impaired transport of IC into the follicle from the subcapsular space and substantial delay in FDC deposition at 8 hours post-injection. Antigen-specific B cells (e.g., phycoerythrin) capture PE immune complexes from SCS macrophage processes via their BCR and further relocate to the T/B border zone within 24 hours, consistent with crosslinking of the BCR by cognate antigen (17). Similar studies in parallel utilizing protein-coated beads show that by 24 hours after antigen injection, most follicular B cells have encountered antigen and polarize toward the B cell-T cell boundary area (18). Cognate B

cells also acquire opsonized antigen from follicular dendritic cells (FDC), as observed during two-photon live-imaging studies within primary follicles (19). In time-course experiments, cognate B cells that newly entered a draining LN could be observed capturing FDC-displayed antigen nine days after the initial immunization and continued to lead to B cell activation, as assessed by CD83 and CD86 induction. Thus, FDCs provide a mechanism to increase the chance of antigen encounters even by rare antigen-specific B cells (19).

Follicular B cells in the spleen also migrate over FDCs, where they capture opsonized antigens (20). In the absence of immunization or BCR activity, marginal zone B cells (generally located between the white and red pulp) constitutively shuttle between the marginal zone and splenic follicles. This trafficking is regulated by a balance between the attraction of B cells towards the follicles via the chemokine receptor CXCR5 and sphingosine-1-phosphate receptor 1 (S1PR1), which opposes CXCR5-mediated signals and promotes migration toward the marginal zone compartment (20). After immunization, naïve, marginal zone (MZ) B cells capture C3-coated antigens within the marginal zone sinus and transport them into the follicles where they are transferred to FDCs, thus comprising a significant means of antigen transport and exposure in the spleen. Despite the efficient manner by which MZ B cells carry opsonized antigens into the follicles, preventing MZ B cell migration or reducing their ability to capture ICs does not impair the development of germinal center B cells (21). Thus, alternative routes are likely to deliver antigen into the splenic follicle.

Antigens can also be captured in the periphery by tissue-resident DCs, which may subsequently home to SLOs and deliver them to naïve follicular B cells (22). Lymphoid-homing DCs also present processed antigen in the context of MHC class II to T follicular helper (Tfh) cells in the T-cell zones of the secondary lymphoid organs, leading both to Tfh

migration towards the T-B border, further increasing T cell help for B cell activation, as well as the clonal activation of antigen-specific T cells.

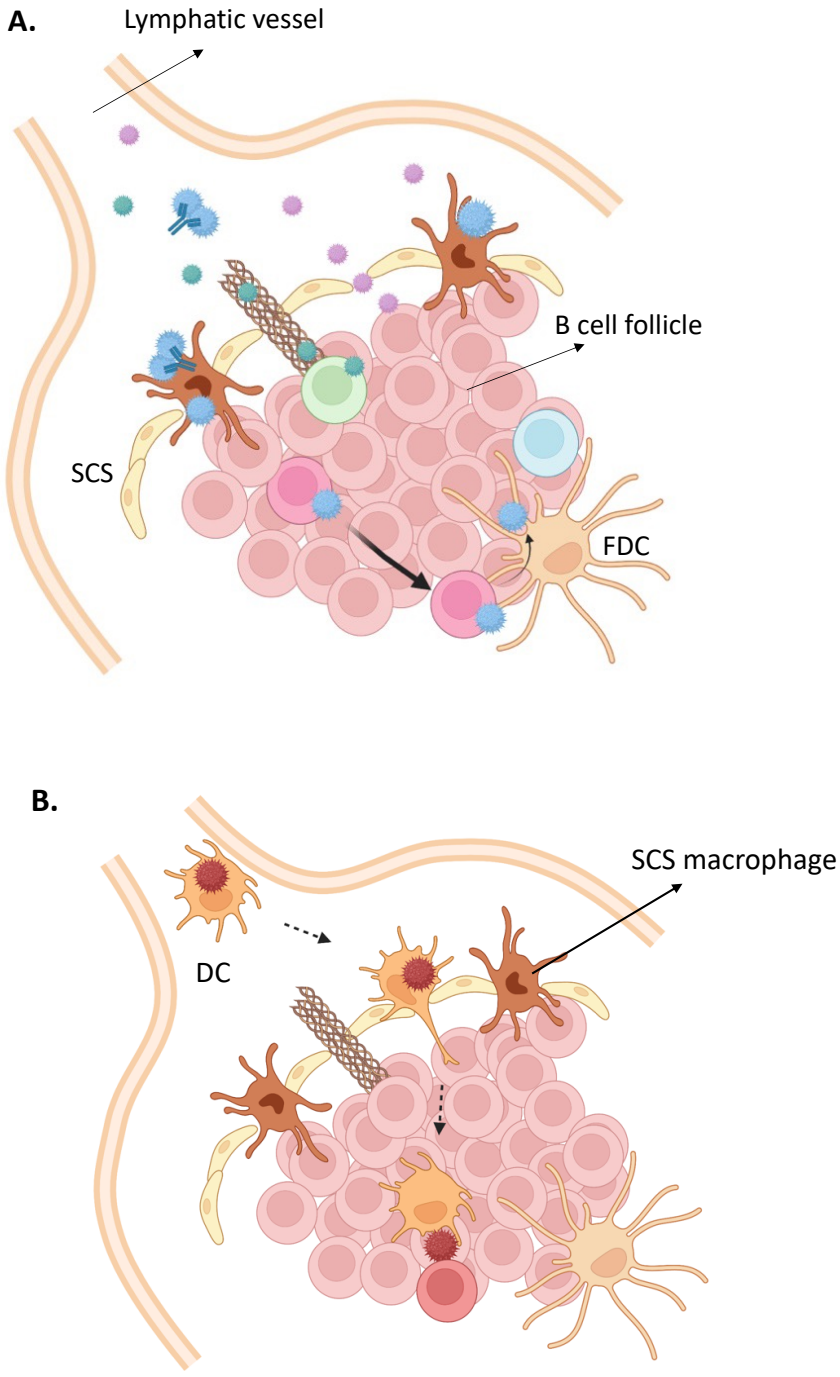


Figure 1-1 (schematic): Follicular naïve B cell routes of encounter with antigen.
A) Small antigens access the follicle via gaps in the SCS lining (purple antigen) or via conduits (green antigen and brown collagen fibers) and is then encountered by cognate B cells. Larger particulate and/or opsonized antigens (blue antigens) are captured and displayed by SCS macrophages and then presented directly by cognate B cells or is transported by noncognate B cells to FDCs for later

encounter with cognate B cells. B) Antigen (red) is carried within DCs into the follicle where it is presented on their cell surface and encountered by cognate B cells. Image created with Biorender.com.

1.2.2 Stage II. B-T interaction

As a result of prolonged contact with FDC or SCS macrophages, antigen-specific B cells having acquired cognate antigen migrate in a CCR7-dependent manner to B-T boundaries within the cortex of SLOs, where they may present antigen to CD4+ helper T cells and receive CD4+ T cell help, amplifying their activation. This positioning can last for days, increasing the kinetic of T and B cell interactions. While T cell-independent antigens can activate B cells via cross-linking of the BCR to polysaccharides or TLRs, T cell-dependent antibody responses require activated CD4+ T cells specific for peptides from the same pathogen (although they need not recognize the same epitope). Antigen-presenting dendritic cells are common activators of CD4+ T cells. If an activated helper T cell recognizes the appropriate peptide-MHC class II complex on the B cell surface, this triggers helper T cells to synthesize cell-bound and secreted effector molecules that synergize in activating the B cell. Thus, it is of crucial importance that B and T cells co-localize in the same anatomical region to ensure humoral responses to T-dependent antigens. Shortly after BCR stimulation, antigen-specific B cells increase their expression of CCR7 by ~threefold (23) and distribute along the B-T border. Their positioning is a result of a balance between chemoattraction to CCL21 (a ligand for CCR7) expressed by fibroblastic reticular cells (FRC) within the T zone and CXCL13-expressing follicular stroma (the ligand for CXCR5). Furthermore, at this stage, antigen-specific B cells down-regulate S1PR1 while up-regulating S1PR2, thus promoting their retention in lymphoid organs (24) and enhancing their ability to localize to the center of the follicle, where germinal centers eventually form (25).

A particularly important T cell effector molecule for the proliferation of antigen-specific B cells is a membrane-bound member of the tumor necrosis factor (TNF) called CD40 ligand (CD40L). The binding of CD40L to CD40 in the surface of the B cell drives the latter into the cell cycle and is essential for B cell responses to T-dependent antigens. CD40L-deficient mice fail to mount Ig responses to T-dependent antigens, such as TNP, in isotypes other than IgM, whereas wildtype animals additionally produced IgG, IgA, and IgE antigen-specific antibodies (26). Furthermore, the addition of CD40L *in vitro* stimulates B cell MCHII and CD23 expression and triggers their proliferation (in combination with IL-4) as measured by tritiated thymidine uptake (27).

Analysis of immunized HKI65 mice, having BCRs that specifically bind the hapten arsonate, thus facilitating their histological detection, demonstrate that following activation, pre-GC B cells proliferate within the periphery of splenic follicles before central GC formation (28). Several studies further established later that these pre-GC activated B cells subsequently move to the inter- and outer follicular regions in an EBI2-dependent manner preceding germinal center reactions. EBI2-deficient B cells fail to distribute along the B-T border and instead accumulate in the center of B cell follicles, colocalizing with FDC, in both spleen and lymph nodes (29). Critically, plasmablast (PB) frequencies of EBI2-deficient B cells are 10-20% that of wildtype B cells yet normally contribute to germinal center B cells. Overexpression of EBI2 induced exaggerated plasmablast responses and smaller germinal centers (29). Thus, EBI2 expression in responding B cells is required for the efficient generation of T cell-dependent extrafollicular plasmablasts and the associated early antibody response.

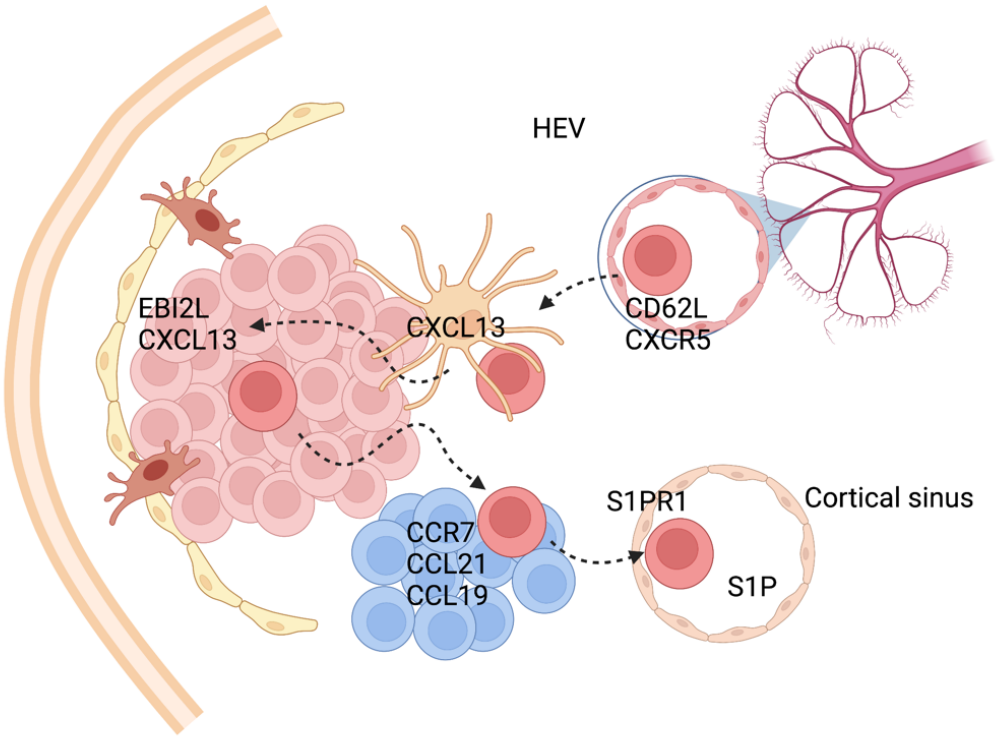


Figure 1-2 (schematic): Naive B cells cycle through LNs via migratory cues.
B cells enter LNs from an HEV using CD62L to initiate rolling, followed by chemokine-mediated inside out activation of integrins (LFA-1 and VLA-4) which facilitate firm adhesion and eventually transmigration into the LN. Upon entry, the cells migrate to the follicle (pink cells) in a CXCR5-CXCL13–dependent manner. When activated, they are attracted to the outer follicle due to both CXCL13 and EBI2 ligand (EBI2L). B cells then cell travel through the T cell zone (blue cells) using CCR7 to respond to CCL21/19 before exiting via a cortical sinus in a sphingosine 1-phosphate receptor type 1 (S1P1)-dependent manner (23). Image created with Biorender.com.

1.3 Germinal center reactions

High-affinity antibodies are required for protection against a wide variety of pathogens – a variety that is astounding in the face of a limited genome. Part of how the immune system copes with this diversity of antigens is by V(D)J recombination and clonal selection theory, which explains how a staggering number of unique immunoglobulins are generated during B cell development before antigen encounter. However, cognate diversification alone does not account for the progressive increase in antibody affinity after antigen exposure, often by orders of magnitude. This post-exposure process is termed

affinity maturation and frequently occurs during germinal center (GC) reactions.

Within 4-5 days after immunization, while some activated B cells differentiate into plasmablasts and migrate to extrafollicular sites, others differentiate into GC B cells and migrate back from the B-T border to the FDC-rich follicle center. Both affinity maturation and clonal expansion of activated B cells occur in GCs, within the B cell follicles of SLOs. As the GC reaction progresses, a T zone-proximal "dark zone" develops where high-affinity GC B cell clones undergo bursts of proliferation and somatic mutation. Additionally, a T zone-distal "light zone" develops containing GC B cells, antigen-bearing FDC, and T follicular helper cells (Tfh) that support GC B cell selection and differentiation events. These cells provide several survival signals to GC B cells, including CD40L, PD-1, BAFF, IL-4, and IL-21, which compete with Fas-FasL interactions (reviewed in (30)). The organization of GCs into dark and light zones is facilitated by opposing gradients of CXCL12 and CXCL13, where GC B-cell positioning in the dark zone depends on the high expression of the CXCL12 receptor, CXCR4 (31). As B cells in the dark zone give rise to a population of cells expressing closely related antibodies that differ in their ability to bind antigen, they subsequently migrate to the light zone, where they test their unique receptors on FDC-bound antigen to potentially receive help from cognate Tfh cells. This ensures the positive selection of cells expressing higher-affinity antibodies. The segregation of these two zones requires that GC B cells migrate dynamically between them, a behavior known as cyclic reentry (32).

While several transcription factors and epigenetic regulators are necessary for maintaining the GC phenotype, BCL6 is a primary transcriptional regulator sufficient to determine the GC B cell program (33). BCL6 targets and represses the cell-cycle regulator *Myc*, as well as the *Prdm1*, the gene encoding B lymphocyte-induced maturation protein-1 (Blimp-1), raising the threshold for GC B cell positive selection and PC differentiation,

respectively (34, 35). BCL6 also suppresses the expression of the antiapoptotic gene *Bcl2*, prompting a high rate of apoptosis among GC B cells that aren't rescued by antigen, underlying affinity-based selection (36). Crucially, BCL6 also helps B cells undergoing SHM and CSR to tolerate the physiological DNA breaks that occur by repressing the activity of DNA damage sensors such as p53 (37).

Where Bcl6 is critical for establishing GC B cell phenotype, the mutator enzyme AID is essential for SHM and affinity maturation. AID deaminates cytidine to uracil directly on DNA, creating U:G mismatches that, upon repair, lead to point mutations in variable regions of immunoglobulin genes. Mismatch repair with error-prone DNA polymerases such as *Polh* can result in further mutations other than the AID-dependent C/G-to-T/A transition scattered around the AID target (38). Overall, AID-dependent mutations arise at a rate of 1 per 1,000 bp per cell generation (approximately one million times the baseline rate of mutation of the genome) (38). These mutations generate the sequence diversity upon which affinity-based selection will ensue.

During GC reactions, B cells are not only selected for their high affinity but are also sorted into different fates. B cells exiting GCs are either plasmablasts (PBs) (which can then become terminally differentiated PCs) or Bmem. The mechanisms regulating PB and Bmem fates are not yet fully understood and are areas of current investigation. In addition to positive selection, Tfh cell help is thought to play a prominent role in driving cells toward the PB fate. *In vivo*, delivery of T cell antigen to B cells via the cell-surface lectin DEC-205 triggers the expansion of the DEC-205+ PB population and greatly increases serum antibody levels (39), demonstrating that Tfh cell help has at least the potential to trigger PB differentiation from GC B cells. Other work supports a role for BCR signaling as a driver of PB export from the GC. For example, elegant experiments have separated CSR from SHM by utilizing

Aicda$^{cre/-}$ *Igh*$^{96K/+}$ *R26*$^{LSL-YFP}$ mice (with genetically targeted Ig heavy chain (*Igh*) alleles carrying *loxP* sites upstream of the μ and γ1 constant regions (*Igh*^{96K})), wherein Cre expression upon BCR activation forces B cells to switch toward IgG1 in the absence of AID (40). After immunization, 79% of antigen-specific PCs (in bone marrow) were class-switched in these animals, revealing IgG1-mediated positive selection independent of SHM (40). The finding that IgG1 BCRs become enriched among bone marrow PCs but not in the GC or Bmem compartments strongly suggests that BCR signaling affects PB differentiation.

Less is known about the selection of GC B cells into the Bmem compartment. Recent studies have identified Bmem precursors (pre-Bmem) within the LZ of GCs, which have transcriptional features overlapping with terminally differentiated Bmem, and display functional features suggestive of memory – such as the ability to survive longer and respond more rapidly and robustly to stimulation *in vitro* (41, 42). Bmem differentiation has been shown to require cessation of proliferation, downregulation of Bcl6, and upregulation of antiapoptotic factors such as Bcl2 (43, 44). Thus, the Bmem fate choice differs from DZ reentry and PB differentiation pathways as it involves the long-term survival of B cells that are not positively selected to proliferate. In fact, strong Tfh cell help appears to inhibit Bmem differentiation, partly by inducing downregulation of the transcription factor Bach2 and upregulation of mTORC1, both of which counter the Bmem fate choice (45, 46). The signals triggering pre-Bmem to survive but not to proliferate are currently unknown. A conceptual framework supported by recent data has been proposed in which affinity is the primary determinant of GC B cell fate decisions (47, 48). B cells with no or low affinity for antigen die by neglect. Of those that do not die, B cells with the lowest affinity exit the GC as Bmem; those with intermediate affinity reenter the DZ for further proliferation; and those with the highest affinity are exported to the PB and PC compartments.

It is important to note that recent and emerging data describe SHM and affinity maturation to also occur outside of the GC during extrafollicular responses (EF), with EF responses tending to give rise to early, lower-affinity antibody responses (reviewed in (49)). The type of infection or immunopathological state can skew the GC or EF responses to one or another, with the molecular mechanisms governing this switch currently being investigated. Antibody affinity is also reported to influence separate waves of Bmem development: prior to and during GC reactions. The former is composed primarily of immunoglobulin M (IgM)-expressing B cells that have undergone a small number of divisions, and the latter Bmem emerge after B cells acquire affinity-enhancing somatic mutations and undergo class switch recombination (48, 50).

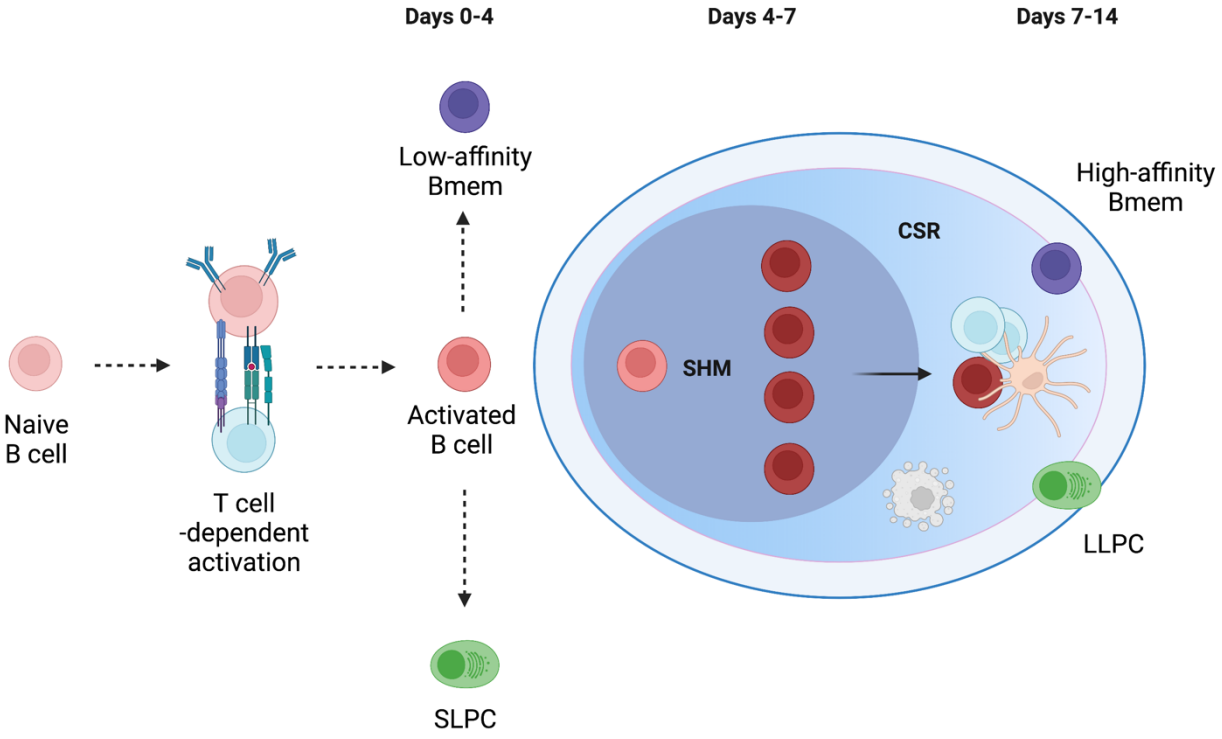


Figure 1-3 (schematic): Bmem and PCs of differing affinities arise pre-GC and during GC reactions. Upon BCR recognition of cognate antigen, naïve B cells become activated (illustrated in a T-dependent manner involving MHC II synapse and CD40L co-stimulation). Activated B cells move to the border of the B cell follicle and T cell zones by modifying the expression of chemokine receptors,

and form cognate pairs through physical interactions. These interactions can induce B cell class-switch recombination to change their initial IgD and IgM isotypes to IgG, IgA or IgE. This drives the early differentiation of low-affinity plasmablasts, and pre-germinal center B cells that re-enter the B cell follicle with T follicular helper cells to seed a new germinal center (GC). Within the GC, T follicular helper cells induce somatic hypermutation in germinal center B cells and direct them to differentiate into high-affinity PCs and Bmem. Image created with Biorender.com.

1.4 Humoral memory

One of the earliest written reports of immunological memory is from 430 BC, described in Thucydides' account of the plague that struck Athens during the Peloponnesian war. He writes "...it was with those who had recovered from the disease that the sick and the dying found most compassion. These knew what it was from experience and had now no fear for themselves; for the same man was never attacked twice—never at least fatally. And such persons not only received the congratulations of others, but themselves also, in the elation of the moment, half entertained the vain hope that they were for the future safe from any disease whatsoever" (51). While wishing for the extent of cross-protective immunity to encompass all diseases whatsoever has indeed proven to be in vain, Thucydides acknowledges two fundamental properties of mammalian immunity – memory and specificity. In other words, the capacity for the adaptive immune system to establish anamnestic responses to recurring antigens.

Immunological memory is granted by the development of three main cell subsets during primary reactions: memory T cells, memory B cells, and long-lived plasma cells. Compared with their naïve counterparts, memory lymphocytes have less stringent requirements for subsequent activation via antigenic and costimulatory receptors, increased proliferative potential, and a more rapid effector response. In addition, memory cells can

traffic through both SLOs and peripheral tissues, giving them access to peripheral tissues or SLOs poorly accessed by naïve or effector lymphocytes, respectively.

1.4.1 Memory T cells

This chapter aims to introduce important aspects of humoral memory; however, it is important to note the role memory T cells undoubtedly have in granting resistance to recurring pathogens. CD4+ memory T cells can provide important cues to reactivate Bmem; vaccination with T cell epitopes (or vectors encoding such epitopes) designed to elicit cytotoxic CD8+ memory T cells can protect mice, humans, and non-human primates from viral infections via B cell-independent mechanisms (52, 53). Furthermore, the presence of memory T cells in peripheral tissue correlates with protective immunity. For example, influenza- and MCMV-induced memory CD8+ T cells provide protection from local, heterotypic challenges (vaccinia virus, coronaviruses, influenza viruses) in an antigen-dependent fashion (53-55).

1.4.2 Long-lived plasma cells

Long-lived plasma cells (LLPCs) grant immunological memory by constitutively secreting antibodies to previously encountered pathogens for years after their initial formation (56, 57). Indeed, the half-life of some antibodies against measles and mumps isolated from human serum is estimated at 200+ years (56)! Granted that Bmem frequencies are poor predictors of antibody titers, it was presumed that LLPCs, later discovered in the bone marrow, must exist to replenish the antibody pool (58). Differentiated PCs are generated early in the humoral response from recently activated B cells or emerge a few days later from GCs. During proliferation and until the completion of differentiation, these cells are termed plasmablasts. PCs generated independently of the GC

are located outside the B cell follicle in secondary lymphoid organs, thus called extrafollicular PCs. These PCs display shorter life spans than their GC-derived counterparts, often persisting for only a few days before undergoing apoptosis (59). Hence, they are commonly referred to as short-lived PCs (SLPCs). Notably, some PCs that form in a T cell–independent manner from differentiated B1 B cells are long-lived (60). IRF4 and BLIMP1 are two transcription factors required for the differentiation and maturation of PCs. The latter is also being important for establishing the metabolic program required for LLPCs to produce and secrete antibodies (61-63). PCs that emerge from GC reactions tend to leave secondary lymphoid organs and subsequently establish residency within the bone marrow (64). This homing process is mediated by the chemotactic receptors S1PR1 and CXCR4, and the transcription factor KLF2, which promotes the expression of the integrins required for retention in the bone marrow (65). After treatment with FTY720, an inhibitor of S1PR1, or genetic ablation of S1PR1, plasma cells develop normally in SLOs but fail to egress into the blood or home to the bone marrow (65). Similarly, CXCR4-deficient plasma cells fail to accumulate in the bone marrow, which is rich in the ligand CXCL12 (66). The survival of bone marrow–resident PCs relies on the cytokines APRIL and IL-6, secreted by several cell types within the bone marrow (67), and prosurvival signals from stromal cells. Recently, three subsets of LLPCs have been identified in the human intestinal tract, two of which carbon dated to median age of 11 and 22 years (57), strongly suggesting that the gut also serves as a niche for the survival and maintenance of these cells. More research is needed to identify the factors which may support their longevity in the intestine.

1.4.3 Memory B cells

Memory B cells do not constitutively secrete antibodies. Instead, they differentiate rapidly into antibody-secreting cells (ASC) or seed novel germinal centers to generate further antigen-specific diversification during secondary humoral immune responses. These subsets can be established in response to differing immunizations and are detectable by changes in cell surface phenotype. Memory B cells can also be found in several diverse microanatomical niches, which may influence their immediate response upon rechallenge.

1.4.4 Memory B cell subsets

In mice, in response to immunization with influenza virus, malaria, and hapten-carrier with alum antigen, five different subsets of memory B cells can be found according to the expression of CD80, PD-L2, and CD73 (68, 69). 12-20 weeks after intraperitoneal immunization with NP-CGG in alum, these markers are expressed bimodally among Bmem, with distinct positive and negative populations: triple negative (PD-L2−/CD80−/CD73−), triple positive (PD-L2+/CD80+/CD73+), CD73 single positive (PD-L2−/CD80−/CD73+), CD80/PD-L2 positive CD73 negative (PD-L2+/CD80+/CD73−), and PD-L2 positive CD80 negative (69). CD80 and PD-L2 belong to the B7 family of immune regulatory ligands and bind to the CD28 family of receptors on lymphocytes, providing costimulatory or coinhibitory signals. CD73 has enzymatic activity and converts ADP/ATP to adenosine, catalyzing a shift from a pro-inflammatory ATP-driven state to an anti-inflammatory environment induced by adenosine. Interestingly, upon transfer into recipient mice having irrelevant BCR specificity (AM14-KI × Vκ8R-KI BALB/c mice) and immunization with NP-OVA in alum one day later, double positive (PD-L2+/CD80+) NP-specific Bmem generated 5- and 13-fold more NP+ IgG1+ AFCs than did single positive B cells or double negative Bmem, demonstrating a propensity for the double positive Bmem to differentiate more rapidly into

APC (70). This configuration is irrespective of isotype switch during the primary response, as it holds for both IgG1+/PD-L2+/CD80+ Bmem (which give rise to IgG1+ ASC) and IgM+/PD-L2+/CD80+ Bmem (which give rise to both IgM+ and IgG1+ ASC). Importantly, all three subsets generate more IgM+ ASC than naïve B cells (70). However, double positive IgG+ Bmem are unable to establish germinal centers by 10.5 days after immunization. In contrast, double negative (PD-L2−/CD80−) Bmem generate few APC when challenged with antigen but establish an equivalent number of germinal centers compared to naïve B cells. Thus, these two markers alone are enough to denote a predisposition for Bmem to differentiate into APC or re-enter GCs upon re-activation.

Intriguingly, the presence of memory T cells in addition to Bmem during the secondary immunization greatly augments Bmem subset responses but is not essential (70). The functional significance of CD73 expression within Bmem subsets is not yet fully understood but is associated with greater somatic hypermutation, a higher affinity for antigen, and a robust ability for APC differentiation upon re-infection (71). The segregation of function into different MBC subsets is proposed to ensure self-renewal while enabling robust responses to external signals. This suggests that secondary responses have evolved to be particularly suited for pathogens that mutate, as the double negative subset contains Bmem that can respond to such adaptations, even if the antibody secreted from the progeny of double positive Bmem has little cross-reactivity with a novel pathogen.

In humans, CD27 is a widely used marker to distinguish many Bmem from precursor naïve and GCBC populations (72). CD27 is a member of the TNF-receptor superfamily and binds to CD70, playing a key role in both T cell differentiation and B cell activation. The phenotyping of CD70+ B mem cells identifies many peripheral blood and tonsillar human Bmem with somatically mutated V(D)J genes and demarcates Bmem deriving from germinal

center reactions, where it is progressively upregulated as the germinal center matures (72, 73). However, CD27- Bmem can be both germinal center-derived and from germinal center-independent pathways (73). CD27- Bmem can be further subdivided based on Fc receptor-like 4 (FCRL4) expression, which can enhance Toll-like receptor signaling and dampen BCR activity (74). FCRL4+/CD27− Bmem are a specialized population rarely found in healthy individuals but are upregulated in patients with malaria, HIV, and rheumatoid arthritis (75-77). In health, they are scarcely found in peripheral blood, bone marrow, or spleen but more commonly in the mesenteric lymph nodes, tonsils, and intestinal lymphoid tissues (78). The extracellular domain of FCRL4 functions as a low-affinity receptor for IgA, in line with their association with mucosal tissue (79).

In both mice and humans, another subset of Bmem defined by the expression of the transcription factor T-bet (Tbet+ Bmem) have been found (80). Tbet+ Bmem are commonly referred to as “age-associated B cells” due to their prevalence in the context of murine aging. They are also associated with autoimmune conditions, including rheumatoid arthritis, systemic lupus erythematosus, and Crohn’s disease (81). Moreover, they develop naturally after some viral infections, including influenza. Key studies have recently shown both Tbet+ and Tbet- subsets to develop during GC reactions after influenza infections, which are stable and endure indefinitely with minimal interconversion (82). In both humans and mice, Tbet-high Bmem are restricted to the spleen, bone marrow, and peripheral blood compartments, whereas Tbet-low Bmem recirculate through the lymphatics and are additionally found in mesenteric lymph nodes and tonsils. Chyme samples obtained from patients undergoing thoracic duct surgery reveal Tbet-high cells to be virtually absent in this major lymphatic vessel, in contrast to other Bmem subsets (82). Functionally, Tbet expression is required for the development of influenza hemagglutinin (HA) stalk-specific IgG2c antibodies and for

durable neutralizing titers to influenza, as conditional depletion of the Tbet gene in B cells causes significant loss of IgG2c antibody titers that are not compensated for by other IgG isotypes (82).

1.4.5 Memory B cell localization

Memory B cells are primarily found in the spleen, recirculating through peripheral blood, bone marrow, and secondary lymphoid organs, and in peripheral mucosal tissues. In humans, the adult spleen has been found to host approximately 9 billion CD27+ Bmem; the tonsil ~1 billion; the bone marrow and peripheral blood following closely behind at $6.6x10^8$and $9.2x10^7$, respectively (83). Despite being the greatest reservoirs of Bmem, the spleen and tonsils appear dispensable for adequate humoral responses to secondary challenges, as evidenced via immunization after their surgical removal (splenectomy and tonsillectomy) (83, 84). It follows that Bmem are also found in large numbers in peripheral tissues, including the lung, gut, and gingiva. In the absence of secondary lymphoid organs (splenectomized Lta−/− mice, irradiated and reconstituted with normal bone marrow), neutralizing antibody-specific antibodies are still produced and detected 120 days after primary infection (84). Upon homotypic rechallenge of influenza virus, these SLO-deficient mice do not lose weight and have negligible viral titers, suggestive of a robust humoral memory response. While the ratio of IgM:IgG antibody in chimeric mice is higher than in wildtype controls, recipients still exhibit considerable isotype-switching in the absence of SLOs. Further investigation revealed that inducible bronchus-associated lymphoid tissue (iBALT) was robustly formed in the bronchi and lung tissue of the mice after influenza challenge and were maintained long-term – likely contributing to the amnestic response observed, being the only source of lymphoid tissue present (84). This demonstrates that

memory cells in peripheral tissues can respond to and clear a rechallenge infection locally without first expanding in SLOs.

A central finding was separately made by the observation that in response to a peripheral mucosal infection (influenza virus administered intranasally), Bmem circulate and disperse widely to SLOs (85). Frequency differences between SLOs suggest an influence of local tissue factors on trafficking. IgG Bmem are detected earlier and establish higher frequencies in Peyer's patches (PPs) compared with the inguinal lymph nodes, even though immune responses to influenza do not occur in either site (85). Bmem numbers increase and stabilize at tissue-specific frequencies without contraction of the Bmem pool during the period of analysis. Within the lung, a rapid influx of IgG and IgA Bmem established relatively high frequencies that were maintained long-term (85).

Splenic Bmem are naturally detected both in the marginal zone (MZ) and the follicles (86). In mice, these Bmem are known to express CCR6 and are dependent on CCR6/CCL20 signaling, most likely deriving from CCL20-expressing CD4+T cells, for their positioning (87). In CCR6-deficient mice, there is a 6-fold increase in the follicular localization of Bmem compared to wildtype animals. In humans, the relationship between CD27+ B cells in MZs and follicles and antigenically naïve MZ B cells is unclear. In fact, the mechanisms that retain Bmem in a particular niche are not entirely clear in both species. Overall, Bmem express CXCR5 (88), a primary receptor for follicular localization; hence it is reasonable that Bmem circulate in SLO follicles. As naïve B cells and Bmem traffic through many of the same lymphatic tissues, it is likely they may rely on similar cues to enter alternate sites, with subtle differences driving Bmem biases. For example, Bmem expressing high levels of integrin α4β7 may be attracted by the high endothelial venules of PP and mucosal lymphoid tissues, which express higher levels of the ligand (89, 90). Classical B cell entry into lymphoid

organs has been extensively studied in lymph nodes, wherein they enter from circulation by crossing high endothelial venules (HEVs) in a CD62L-dependent matter (reviewed in (91)). CD62L recognizes a family of mucin-like glycoproteins, which are heavily sulphated, fucosylated, and sialylated when on HEV endothelial cells. The interaction of CD62L with its ligand on HEVs mediated tethering and rolling into the lymph node through a multistep adhesion and migration cascade. In mice, the HEV endothelium abundantly expresses CCL21 in homeostatic conditions, attracting CCR7+ B cells (and T cells). Stromal cells produce CXCL13 and CXCL12, which can be transcytosed to the surface of HEV, further attracting CXCR5+ and CXCR4+ lymphocytes. The integrin LFA1 mediates B cell adhesion and arrest on HEVs ((91).

Differential distribution of Bmem in tissue-specific SLOs, blood, and lymph, may also reflect differences in the rate of egress of lymphocytes from each tissue. Bmem migration along an increasing sphingosine-1-phosphate (S1P) concentration gradient between the lymphoid tissue interior and adjacent blood or lymph underlies lymphocyte egress (25, 92). Local overproduction of S1P in lymphoid tissues due to local inflammation leads to disruption of the S1P concentration gradient or down-regulation of cell receptors for S1P (25, 92). This results in a transient block in lymphocyte egress from lymphoid tissues. Thus, high Bmem frequencies in constitutively active lymphoid tissues may be a consequence of both preferential entry and delayed egress. Further research of the locations of Bmem and how they are maintained is needed, especially considering newly uncovered heterogeneity.

The maintenance of Bmem in individual niches has not yet been fully characterized, but recent studies, in contrast to previously reported literature, point towards a critical requirement for BCR and BAFFR signals (93). Depleting the BCR after Bmem establishment resulted in the significant loss of Bmem numbers; interrupting CD79A signaling (a

transmembrane protein associated with the BCR critical for signaling from the receptor) affected Bmem maintenance. Furthermore, genetic depletion of BAFFR or antibody blockade treatment with anti-BAFF resulted in the loss of splenic, blood-circulating, and lung-resident Bmem (93). Two additional BCR-related proteins are known to be essential for Bmem persistence: Syk tyrosine kinase (SYK) and phospholipase Cγ2 (PLCγ2), an enzyme that is phosphorylated and activated by SYK (94, 95). Thus, BCR activity is robustly required for Bmem durability. Interestingly, the antigen specificity of the Bmem BCR is not important for their maintenance, excluding any requisite for residual antigen (96). Utilizing a very elegant "BCR switch" Cre recombinase genetic reporter model, Maruyama et al. show that Bmem developed against the NP antigen (NP-specific BCRs) and converted to alternate PE-specific BCRs 8 weeks later during the memory phase, display the same longevity and capacity to respond as control NP-BCRs (96). These experiments demonstrate that the humoral immune response can generate true memory cells independently of persisting immunizing antigens. As Bmem are long-lived cells, with many having a half-life longer than the animal's life span (97), identifying factors that impart their survival could be very important for immunization strategies.

1.4.6 Memory B cell reactivation

Reactivation of Bmem requires BCR stimulation and can occur both T-dependently and T-independently. Interestingly, optimal reactivation appears to be impacted by Bmem localization in SLOs, however, inhabiting this niche is not strictly required. To assess Bmem reactivation, many investigators use adoptive transfer of Bmem from immunized wildtypes animals into immunocompromised recipients (incapable of mounting a significant primary B cell response), which are then challenged to assess Bmem contribution to humoral

immunity in the memory context. For example, RAG1−/− mice, deficient in T and B cells, have been used as a host for the adoptive transfer of memory B cells from mice previously immunized with human cytomegalovirus (HCMV). Upon challenge with HCMV-DBs, noninfectious enveloped particles consisting of viral tegument proteins contained in a complete viral envelope, HCMV-specific IgG was detectable in sera, compared to undetectable levels in RAG1−/− mice transferred with naïve B cells (98). Similarly, antibody-based depletion of CD4+ T cells in wildtype recipients had no effect on the ability of transferred Bmem to respond to rechallenge. In contrast, immunization of recipient RAG-1−/− mice after transfer with wildtype Bmem with the soluble, monomeric antigen gB did not produce significant antibody titers (98). Thus, Bmem reactivation can occur without T-cell help, depending on the structure of the antigen.

In follow-up studies, Weisel et al. observe diminished antibody titers in TNF/LTα−/− mice (lacking most lymphoid structures other than spleen) reconstituted with wildtype bone marrow from immunized animals and further rechallenged with virus-like particles (VLPs) (99). Serum antibody levels after rechallenge were further drastically diminished by 10^3-fold after splenectomy (99), suggesting that Bmem homing to SLOs is important for their reactivation. Further evidence for a specific niche being a requirement for Bmem reactivation is granted simply by the observation that antigen challenge provided at the same time or shortly afterward (2 hours) does not elicit an antibody response from Bmem. Only after 24 hours, and optimally between 48 hours and seven days after transfer, can Bmem reactivate functionally, suggesting they must home to reactivate (98, 99). More robust, functional evidence in support is the observation that antibody blockade of CXCL13, the ligand for B cell and Bmem receptor CXCR5, impaired Bmem-derived antibody titers from developing in a dose-dependent manner. CXCL13, a B lymphocyte chemoattractant

chemokine produced by stromal cells within the follicles of peripheral lymphoid organs, directs CXCR5-expressing B cells into these areas. As CXCL13 is expressed in RAG1−/− mice, adoptive transfer of B cells from VLP-immune wildtype mice normally show homing to follicle-like structures in the white pulp of RAG1−/− spleens (99). After treating the recipient with blocking anti-CXCL13 Abs, transferred B cells failed to organize in follicular clusters and appeared as a ring of cells around the white pulp areas. Furthermore, in anti-CXCL13–treated recipients, antigen-mediated reactivation of adoptively transferred MBCs resulted in significantly decreased virus-specific serum IgG titers 4, 8, and 11 days later and significantly smaller extrafollicular clusters of IgG+ plasmablasts (99).

Regarding T-dependent reactivation, the microanatomical localization of Bmem subsets close to Tfh cells in SLOs has been of significant interest. Intravital microscopy and sequencing analysis reveal that in lymph nodes, Bmem cluster in subcapsular proliferative foci (SPF) where they interact with Tfh cells, as evidenced by frequent, short-lived contacts between these two cell types (100). Subsequent rechallenge immunization induced proliferation and differentiation into PCs within three days, in this same subcapsular region (100). In parallel, some Brm cells were also seen to enter the GC, suggesting two distinct sites of activation may exist. Similarly, memory Tfh are found both within the B cell follicles of draining lymph nodes and outside the follicle in the spleen (101). To address the functional outcome of memory Tfh/memory B-cell interaction *in vivo* after rechallenge, local or circulating Bmem were induced by NP-KLH (NP hapten conjugated keyhole limpet hemocyanin) administration via intraperitoneal (i.p.) or subcutaneous injection. Thirty days after immunization, local (dLN) or circulating (splenic) memory Tfh cells were transferred into the previously immunized recipient. Following an NP-OVA i.p. injection, the NP-specific B-cell response was monitored five days after. Notably, local memory Tfh cells induce higher

production of class-switched and high-affinity Ig by memory B cells, while circulating memory Tfh cells induce more secondary GC (101).

1.5 Tissue-resident lymphocytes

Much of the adaptive immune response has been studied in the context of blood and lymphoid organs; however, many leukocyte lineages have the capacity for residence in peripheral tissues, including memory B cells, memory T cells, innate lymphoid cells (ILCs), macrophages, natural killer (NK) cells, and plasma cells. Indeed, for many leukocyte subsets, residence is more the "norm" than a lifestyle of recirculation. These resident populations have critical roles in immune surveillance, protective immunity, and organ homeostasis.

Most understanding about memory resident lymphocytes comes from extensive T cell analyses. Elegant studies wherein dorsal root ganglia latently infected with herpes simplex virus (HSV), thus containing HSV-specific, GFP-tagged, CD8+ memory T cells, were transplanted into recipient mice with congenitally marked HSV-specific CD8+ memory T cells. This enabled the authors to assess the recruitment capacity of circulating memory T cells versus resident memory T cells within the graft to a novel infection (102). After rechallenging the recipient mice, almost all antigen-specific T cells responding to this virus challenge originated from newly recruited T cells from the circulation, even though the ganglia contained roughly equal numbers of both resident (primary transplant donor) and recruited (primary transplant recipient) T cell populations (102). This strongly supports the concept that that subsets of memory T cells fail to recirculate.

Moreover, it has been established that local memory T cells can provide greater protection upon subsequent infection compared to distal sites. In support of this, B cell-deficient μMT mice infected and boosted with HSV in the ipsilateral flank, show 100-fold

better control of infection than those immunized in the contralateral flank (102). Subsequent studies have demonstrated resident memory T cells (Trm) to reside in the skin, wherein a localized vaccinia virus (VACV) skin infection generates long-lived non-recirculating CD8+ skin Trm cells (103). These skin Trm cells are potent effector cells and are superior to circulating central memory T cells at providing rapid long-term protection against cutaneous re-infection (103). These findings have motivated researchers to establish tissue-resident T cells as part of immunization strategies, to best protect against local antigens. As such, a "prime and pull" vaccination strategy was developed, wherein conventional parenteral vaccination elicits systemic T-cell responses (prime), followed by the recruitment of activated T cells using a topical chemokine application to the restrictive genital tract (pull) (104), thereby allowing recruited T cells to establish a long-term niche and mediate protective immunity. As T cells upregulate CXCR3 upon activation, the authors used CXCL9 and CXCL10 (the ligands for CXCR3) to attract the activated T cells by chemotaxis. The two chemokines were applied topically to the vaginal cavity of subcutaneously immunized mice, which successfully recruited CXCR3+ effector T cells to the vagina (104). Crucially, mice infected intravaginally with a lethal dose of HSV 4 weeks after the prime and pull protocol lose significantly less weight, exhibit very few clinical symptoms, and have a 100% survival rate compared to the 36% survival rate of the prime-only cohort (104). This work validates immunization efforts to establish resident memory lymphocyte populations.

The mechanisms by which memory T cells become Trm, and subsequently their complete phenotypic identification, remains somewhat unresolved. Often, Trm are distinguished by the upregulation of CD69 (105) in correlation with stimulation via the TCR. Yet, the persistence of antigen is dispensable for the establishment and maintenance of

Trm; hence the factors promoting their residency remain ill-defined. Nevertheless, the transcriptional downregulation of S1PR1 is required for the establishment of CD8+Trm cells in the skin after topical administration of 2,4-dinitro-1-fluorobenzene (DNFB) (106). These Trm are characterized by low KLF2 expression, a transcription factor that promotes expression of the recirculation molecules CD62L and S1PR1 (106). Consequently, the latter's repression may induce retention of Trm within the tissue. At the same time, CD69 represses S1PR1 surface expression, suggesting that inhibition of the S1P chemotactic cues may be essential for tissue-resident lymphocytes to resist egress. For some Trm, the expression of integrin αEβ7 (CD103) or its ligand, E-cadherin, contributes to their maintenance (107). However, not all Trm express CD103, suggesting that such interactions do not constitute a universal mechanism for retaining Trm cells (107). Thus, further work is needed to define molecular factors that regulate Trm residency.

1.6 Resident memory B cells

The discovery and study of resident memory B cells (Brm) has lagged behind that of resident memory T cells, possibly due to the preconception that long-lived antibodies circulate systemically throughout the body, thus negating an obvious need for local production by Bmem upon reactivation (108). However, clear evidence has emerged of their existence, which raises important questions about their protective functions at barrier sites and potentially major implications for immunization strategies delivered at local, antigen-exposed sites.

Like Trm, Brm share many of the same phenotypic markers of residence, including upregulated CD69 and downregulated CD62L expression. As previously discussed, this suppresses lymphocyte egress from tissue into the blood by antagonizing S1PR1 signaling

and reduces their ability to traverse HEVs, respectively. Brm in the lung also upregulate CXCR3 expression, a chemokine receptor that responds to the interferon-inducible chemokines, CXCL9, 10, and 11 (reviewed in (109)). Onodera et al. first identified a population of CD69+/CXCR3+ Bmem cells in the lung after influenza infection persisting 80+ days after primary infection (110). The authors also observed rapid proliferation of lung Bmem by 2-3 days after rechallenge infection, with the subsequent appearance of IgA- and IgG-expressing PCs by day 4. Adoptive transfer of either the lung HA-specific Bmem population or splenic HA-specific Bmem (along with CD4+ T cells from the same donors) into recipient *scid* mice, strongly demonstrates a greater protective capacity of the lung-Bmem population – with significantly reduced viral titers and greater antibody concentrations in BALF upon rechallenge compared to splenic counterparts (110). Interestingly, this only occurs with the pretreatment of recipient mice with CpG oligonucleotides to induce iBALT in the lung tissue prior to adoptive transfer. These findings suggest there is a lung-homing population of Bmem that confers greater protection than systemic counterparts, which also exhibits phenotypic hallmarks of tissue residence.

Follow-up studies revealed that lung Bmem are protected from intravascular CD38 antibody staining, suggesting they localize in the tissue and not from capillaries exposed to circulation (111). Lung Bmem populations generated after primary influenza infection also exhibit greater cross-protective immunity than splenic Bmem counterparts, as revealed by similar adoptive transfer experiments into recipient *scid* mice wherein rechallenge was performed with homotypic or heterotypic influenza strains. Lung Bmem produce higher numbers of plasma cells than splenic Bmem after boosting with drifted, heterotypic influenza virus (111). Upon depletion of GC reactions two weeks after primary infection (utilizing a *Bcl6* inducible knockout mouse), cross-reactive lung Bmem are significantly

reduced. In contrast, strain-specific lung Bmem remain intact, thus suggesting the origin of cross-protective lung Bmem is from ongoing GC reactions (111). Of note, the development of cross-reactive Bmem at day 30 post primary infection is associated with the persistence of the influenza virus antigen in the lung at this timepoint, compared to its absence in splenic tissue.

A landmark study establishing the identification of lung Bmem as *bone fide* Brm utilized parabiosis experiments to definitively test their recirculation capacity (112). After primary infection with influenza virus, antigen-specific Bmem from CD45.1 mice surgically paired to uninfected CD45.2 mice do not migrate to the naïve lung (whereas naïve B cells equilibrate to equal frequencies in the spleens and LN of both animals). Furthermore, regardless of whether the surgically paired partner is treated with LPS to induce inflammation or previously infected with the same influenza virus, Brm do not migrate to the paired animals' lung tissue – demonstrating that antigen-specific memory cells in the lung are maintained as tissue-resident cells. This phenomenon was only striking for lung Bmem, as splenic Bmem and mLN Bmem populations were found in the organs of their paired partners (although not at equal frequencies). Finally, concurrent infection of surgically paired mice with two different strains of influenza reveals that Brm develop in response to local infection, requiring local antigen (112). Using anti-CD40L blockade to collapse germinal centers has also revealed that Brm depend on early T-dependent reactions to be established, but not for their maintenance (suggesting they are GC-derived) (112). Importantly, the presence of Brm in the lung confers protection against recurring antigens, as animals with influenza-specific Brm in the lung generate secondary PC responses more rapidly than mice with memory B cells at systemic sites (induced by intraperitoneal priming). By four days after the rechallenge, intranasally primed mice have

hundreds of thousands of influenza-specific PCs in their lungs, whereas within IP-primed mice, PCs are virtually absent. Importantly, the accelerated secondary response in the lungs occurs despite treatment with FTY720, the S1PR1 agonist, validating that the response is generated *in situ* from precursors already in the lung (112).

Throughout the conduction of experiments encompassed in this thesis, several additional reports of Brm in both mice and humans have been reported (113, 114). A recent study recovered multiple tissues (spleen, intestine, bone marrow, blood, tonsils, and lymph nodes) from the same human cadaveric donors to reveal substantial heterogeneity within B cell subsets amongst donors (114). Antibody screening and sequencing analysis reveal a gut-resident memory phenotype in humans (including CD69+) (114). Barker et al. also report that human lungs bear class-switched B cells with a resident memory phenotype (CD69+) (113) and murine Brm develop after pneumococcal infection. In mice, two further studies published in the last year report binary subsets of Brm in lungs after influenza or Sars-CoV-2 infection, distinguishable by CXCR3 and CCR6 expression and harboring different antigen specificities (115, 116). Granted their relevance to the context of our experiments, the details of these recent findings will be considered in more depth in the discussion sections of the following chapters.

While there is an invigorating interest in discovering more about Brm biology, very little is known about their function contributions to health and disease. Tissue-resident memory B cells are likely poised at mucosal barriers to make antibodies promptly after a secondary encounter with antigen. This capacity will likely accelerate pathogen clearance directly, by neutralizing activity or complement activation, or indirectly, through the FcR-dependent functions of phagocytic or cytolytic cell types. At the same time, excessive Brm

activity may be detrimental upon encounter with allergens or autoantigens by over-production of inflammatory cues and may exacerbate disease.

1.7 Pulmonary immunity

The lungs are an exceptionally important organ for protection from the external environment and the foundation for gas exchange. Managing immune responses across this delicate tissue is essential for host survival, to prevent lung damage while protecting against inhaled pathogens.

Large particles are often trapped in the nasopharynx and cleared by coughing and sneezing. Further down the respiratory tract, smaller particles are captured on a mucociliary surface and moved back to the upper airways via ciliary action. Several antimicrobial compounds exist within this mucous layer, including surfactant proteins, lipopolysaccharide binding protein (LPB), and complement components. At the terminal branches, the alveoli contain a small number of immune cells, almost entirely comprised of alveolar macrophages (AM). AM phagocytose and kill microbes, and secrete an excess of antimicrobials, including lysozyme, antimicrobial peptides, and proteases. AM are furthermore important for recruiting additional immune cells into the lung parenchyma and airspaces upon infection via secreting several cytokines and chemokines. During resting states, within the interstitial spaces of the lung, T cells and DCs exist between alveolar epithelial cells. Utilizing two-photon intravital microscopy, DCs can be seen extending their dendrites into airway lumens and directly uptake antigens present in the airspace (117). Immunohistochemistry has also revealed the presence of CD103+/CD3+/CD8+ T cells located intra-epithelially above the basement membrane of the small airways, where they bind epithelial cadherin (E-cadherin), expressed by the alveolar epithelial cells (118). Neutrophils and mast cells are found in low

frequencies, with most innate cells infiltrating only upon inflammation. The resident population of immune cells in the lungs allows for immunosurveillance and rapid responses to antigens. Notably, the architectural cells of the lung, including the epithelium, endothelium, and stroma, can also respond directly to pathogens and initiate inflammatory cascades linking the innate and adaptive immune responses.

Concerning adaptive immune responses, the lungs are aptly supplied with draining lymph nodes (mediastinal and hilar lymph nodes) located beside and external to the branching airways. Yet, within the tissue of the lung, tertiary lymphoid structures form in response to inflammation – the iBALT – which enable local, mucosal adaptive responses independent of systemic responses. A variety of B cell subsets are found within iBALT, including naïve B cells, memory B cells, and GC B cells. T cells and dendritic cells typically surround the B cell follicle of the iBALT. Two types of B cell follicles have been described in iBALT in response to different pathogens: a classic follicle containing follicular dendritic cells (FDCs) and CXCL12+ follicular stromal cells and a non-classical B cell follicle that lacks FDCs and instead uses podoplanin (PDPN)+ CXCL12+ fibroblast-like stromal cells to maintain the B cell area (119). The latter grants B cell recruitment and follicle formation via attracting CXCR4-expressing B cells even in the absence of CXCL13+ FDC recruitment of CXCR5+ B cells (119). Lymphatic endothelial cells (LECs) appear in the lungs within seven days after *M. pulmonis* infection surrounding iBALT and secrete CCL21, likely supporting T cell recruitment and survival (120). Pulmonary infections are often associated with the formation of iBALT, which supports the proliferation of B and T cells. Granted the observations that effective humoral responses to some respiratory viruses can occur in the absence of SLOs (84), it follows that iBALT may facilitate primary immune responses and support the generation of memory lymphocytes. Indeed, following influenza infection, antigen-specific CD8+ T cells,

germinal center B cells (Fas+/GL7+), and influenza nucleoprotein (NP) antigen NP-IgM and IgG antibodies are nonetheless present in the lungs and BALF of splenectomized, lymphotoxin knockout mice (LTKO-S) lacking secondary lymphoid organs (121). It follows that confocal microscopy confirms the presence of iBALT structures in the lungs of LTKO mice within 10 days of infection (121). Follow-up studies demonstrated that memory CD8+T cells developed in the absence of SLOs following influenza infection (84), yet the formation of Bmem in these tertiary lymphoid structures is currently understudied and has not yet been shown.

1.8 Influenza virus

1.8.1 An overview of infection by influenza viruses

It is not a coincidence that many studies investigating adaptive immune responses utilize influenza viruses as an immunogen. Influenza viruses are among the most common causes of human respiratory infections (122), causing high morbidity and mortality particularly for the elderly, infants, and individuals with chronic diseases. Approximately 200,000 hospitalizations and 36,000 deaths in the United States are due to influenza viruses in a typical endemic season (123). Pandemic influenza viruses occasionally, emerge causing excessive mortality (124). Typically, influenza A virus (IAV) is the cause of pandemic flu, whereas influenza B and C viruses frequently cause endemics.

Influenza viruses (of the family Orthomyxoviridae) are enveloped negative-strand RNA viruses covered with protrusions of three proteins: hemagglutinin (HA), neuraminidase (NA), and matrix 2 (M2). The HA molecule binds receptors on specific host cells, initiating infection. Antibodies against the HA protein prevent receptor binding and are effective at preventing re-infection with the same strain. Influenza viruses accumulate point mutations

during replication because their RNA polymerase complex has no proofreading activity (122). Their genes have high mutation rates, which may produce selective advantages for viral strains by allowing them to evade preexisting immunity. Influenza viruses can evade previously acquired immunity via antigenic drift (in which mutations limit or prevent antibody binding) or antigenic shift (in which the virus acquires HA of a new subtype by reassortment between two influenza A viruses) (122). Influenza viruses infect both the upper and lower respiratory tracts, as the epithelial cells of the bronchi, bronchioles, and alveoli are all equivalent targets of influenza virus (with some strains also directly infecting alveolar macrophages). Three characteristic alveolar changes are seen in early influenza pathogenesis in humans: capillary thrombosis, necrosis of the alveolar wall, and development of hyaline membranes.

The first influenza A virus was isolated from pigs in 1930 (125), followed by the isolation of the first human influenza A viruses in 1933 (126), which were found to be capable of infecting ferrets (the only species among "many other species"), thus identifying them as an excellent laboratory model for human influenza. In a series of pioneering papers, Shope reported on the histopathologic changes in the respiratory tract of pigs, ferrets, and mice, describing changes compatible with those in human influenza virus infection (127, 128). Importantly, mice are susceptible to infection with human and swine influenza viruses (129) but cannot transmit the infection to other mice (89), and human cases demonstrate additional pathologies such as the formation of hyaline membranes.

1.8.2 Humoral responses to influenza virus

Antibodies alone can prevent influenza infection (reviewed in (130)). Importantly, recall response in exposed or vaccinated adults is characterized by activation of preexisting

Bmem (131), precursing an influenza-specific plasmablast response. Previous exposures to certain influenza strains shape subsequent responses, suggesting that they are drawn from Bmem against cross-reactive strains (131). Within the context of influenza infection, antibody responses are largely characterized against the surface glycoproteins HA, NA, and M1/2 (132). In both humans and mice, after primary infection with either seasonal or pandemic strains of flu, neutralizing IgM, IgG, and IgA influenza-specific antibodies are reported to develop (85, 133-136). A recent clinical trial of 47 human volunteers shows IgA influenza-specific antibodies in nasal lavage and serum to correlate inversely with viral shedding (137). Interestingly, the conversion of an anti-HA stalk antibody from an IgG1 backbone to IgA1 or IgA2m2, significantly increased hemagglutinin inhibition activity of this antibody (138), suggesting IgA anti-HA stalk antibodies may have greater receptor binding site (RBS)-blocking efficiency than IgG anti-HA stalk antibodies. Yet, murine IgA knock-out models exhibit similar morbidity and mortality rates as wildtype mice, suggesting that at least in this species, IgA is not essential for protection against influenza (139). In contrast, the depletion of IgG in bronchoalveolar lavage fluid (BAL) results in far greater lethality upon influenza challenge, highlighting an important role of IgG in protection against this virus (133). In this study, authors filtered out immunoglobulin in BAL isolated from previously infected animals via absorption against a Protein-G Sepharose column before transferring control, IgG- or IgM-depleted BAL into naïve recipients and subsequently challenging with a heterotypic influenza virus. This permitted the authors to assess the contribution of specific isotypes in protection against subsequent infections.

1.8.3 Potential implications of Brm on influenza vaccination strategies

Current strategies against influenza diseases include infection prevention through vaccination, or administration of antiviral drugs (140). Clinical studies have shown the influenza vaccine to be 70% – 90% effective in preventing influenza A illness in healthy young adults, with moderately lower efficacy in the elderly (140). Alas, seasonal influenza vaccines must be reformulated each year to account for antigenic drift since the majority of generated antibodies are strain-specific. Since Brm offer protection at local exposure sites and exhibit greater cross-reactivity to heterotypic strains than recirculating splenic or lymph node Bmem, it would be strategic to consider the nature of the lung Bmem compartment during vaccine design. In summary, based on murine studies, influenza infection in the lung generates local humoral responses that may be of higher or different protective quality than those elicited by vaccines administered intramuscularly.

2 Research Aims

2.1 Hypothesis

The establishment of resident memory B cells in the lung after primary challenge with influenza suggests they are poised at sites of original antigen exposure as an adaptation toward rapid reactivation upon rechallenge. I hypothesize that chemotactic cues within the lung tissue mediate the retention of Brm during the resting state and direct their migration during recall. Furthermore, I hypothesize that Brm uniquely express several chemotactic receptors to facilitate their sensitivity in responding to pulmonary stress signals.

2.2 Specific aims

The research aims I will address in this thesis are:

1. To characterize the Brm niche during resting state and identify unique G-protein coupled receptors that may be required for their establishment or retention in the lung.

2. To assess whether alveolar macrophages are important upstream mediators of Brm reactivation upon rechallenge infection with influenza.

3. To comprehensively describe the secondary immune response during recall which potentially affects Brm migration – and identify the chemotactic cues responsible for such activity.

3 Materials and Methods

Animals

Male and female mice at 8-12 weeks of age were used in this project. All mice were housed in the Biological Services Unit at the Kennedy Institute of Rheumatology, University of Oxford. All procedures carried out on animals are approved by the Home Office under the United Kingdom Animals (Scientific Procedures) Act 1986. Project licenses P1F0EF2FE and PP2527171.

Original mouse strains:

Mouse: Rosa26-tdTomato: B6.Cg-Gt(ROSA)26Sortm9(CAG-tdTomato)Hze/J	Jackson Laboratory	Cat# 007909; RRID:IMSR_JAX:007909
Mouse: BLIMP1-mVenus: Prdm1-mVenus	Provided by M. Saitou (141)	Riken accession CDB0460T
Mouse: AID-cre: B6.129P2-Aicdatm1(cre)Mnz/J	Jackson Laboratory	Cat# 007770; RRID:IMSR_JAX:007770

Influenza infection

For infection with the X31 recombinant strain of influenza (142), mice weighing ≥20g were anaesthetized and intranasally administered 2x10^4 PFU of X31 in sterile PBS (Sigma-Aldrich). Mouse weight and behavior were monitored every day for seven days following infection. For rechallenge experiments, high-dose challenge was performed using 1x10^6 PFU of X31 influenza or 1x10^6 PFU of CFP-S-flu strains (clone E10). The X31 strain was donated by Oliver Bannard and propagated in-house. The CFP-S-flu is a single-cycle fluorescent reporter strain of influenza A virus prepared as previously published (143, 144). Briefly, plasmids encoding eCFP were cloned into the pPoll vector. 293T cells were transfected with Lipofectamine 2000 (Invitrogen), in the presence of expression plasmid pCDNA3.1, which contained expression of full-length HA. This permits viral coating of HA and secretion from the

293T. The resulting viral particles were used as seed to infect a stable H3-expressing MDCK-SIAT1 cell line, thus generating viral particles which carry the genes for all IAV proteins except HA, and in its place eCFP, but that are coated with H3 HA to allow sialic acid-binding and single cycle infection. Stocks of this CFP-S-Flu were produced by infecting HA-expressing SIAT1 cells in DMEM (0.1%BSA, 1%P/S) and two hours later adding 1µg/ml TPCK-treated trypsin (Sigma T-1426). The virus supernatant was collected after 48h of incubation at 37°C. The production of CFP-S-flu was performed by A. MacLean with guidance from A. Townsend.

Bone marrow chimeras

Mice were lethally irradiated (11Gy) in two dosages, separated by 4 hours. Long bones of the lower limbs of donor mice were collected into DMEM collection medium (10% FBS, 1% penicillin/streptomycin, 1% HEPES). Bones were cleaned and bone marrow removed by dissecting the ends of the femur or tibia and flushing clean sterile DMEM through the bones. Cells were resuspended at ~1x10^7 cells/ml and each recipient mouse received i.v. ~2.5x10^6 total cells.

For **chest-shielded chimeras**, mice were anesthetized prior to irradiation with 100 mg/kg ketamine and 25mg/Kg Xylazine i.p. Lead blocks (3cm x 3cm x 0.5 cm) were secured to the chests of the animals covering the region from the neck to the abdomen with surgical tape, within rodent pie cages. Limbs of the animals were positioned in an outstretched manner using traction cords.

Clodronate liposome (CLL) treatment

Mice were anaesthetized, and 40µl of clodronate liposomes (Liposoma BV, Cat# CP-010-010) was administered intranasally, twice on d-6 and twice on d-3 (CLL was substituted for PBS in control animals).

In vivo (IV) labelling

Mice were intravenously administered 2.5µg of fluorescently conjugated anti-CD45 in 200 µl PBS. After four minutes, the animals were euthanized, and their lungs perfused with 10mL cold PBS through the right ventricle of the heart. The lungs were then immediately harvested and the heart, esophagus, thymus, mediastinal lymph nodes, and trachea removed.

Flow cytometry and cell sorting

Lungs were removed and individual lobes were collected into RPMI. Lungs were digested in 1mg/ml collagenase D (Roche, Cat# 11088858001) and 10µg/ml DNAse I (Merck, cat# DN25) in RPMI (with 25mM HEPES) for 30 minutes at 37°C. Following digestion, the lung tissue was homogenized through a 100µm filter. Cell suspensions were incubated with Fc block (anti-mouse CD16/32, Biolgend, cat #101320) in FACS buffer (2% FBS, 0.1% sodium azide, 1mM EDTA in sterile PBS) for 15min, and were then stained in FACS buffer using predetermined optimal antibody concentrations for 30min. Cell suspensions were washed, labelled with secondary labelling agents for 20min and resuspended in FACS buffer for data acquisition on Fortessa X20 or LSRII analyzers (BD Biosciences). For cell sorting, samples were prepared as above and sorted on a FACSAria III (BD Biosciences). For bulk RNA sequencing of alveolar macrophages, approximately 10,000 cells were sorted directly into 350µl lysis buffer (RNeasy Micro Kit, Buffer RLT), immediately snap-frozen on dry ice and stored at -80°C.

Immunofluorescence staining and confocal microscopy

Mice were euthanized with a single dose of i.p. pentobarbitone; upon confirmation of death, the lungs were perfused intracardiacally with periodate-lysine-paraformaldehyde (PLP) buffer. The trachea was then exposed, and 0.7-1ml of 1% low-melt agarose was

injected intratracheally into the lungs before solidifying by washing with cold sterile PBS (and using suture material to tie off the trachea). Individual lung lobes were dissected and fixed in 10mL PLP buffer for 24h shaking at 4°C. After washing, the lungs were incubated in 10mL of 30% sucrose at 4°C for 24h for cryoprotection. Individual lobes were then immersed in OCT and frozen in a methanol-dry-ice bath. 20-25µm tissue sections were taken on a cryostat at -23°C (Lecia Biosystems). Sections were blocked with mouse/rat serum and FC block in staining solution (5% normal mouse/rat serum, 0.3% Triton-X100 (Sigma), 0.2% FBS, 0.1% sodium azide) for 30min. Primary stains were carried out at predetermined optimal concentrations for 3h in staining solution. Secondary antibodies were applied for 2h and slides were washed in PBS and mounted using Fluoromount-G (Cambridge Bioscience Ltd.). Confocal microscopy was performed on an upright ZEISS LSM880 or an inverted ZEISS LSM980. Please see **Appendix 1, Table 1** for the list of antibodies used.

Image analysis

Image files obtained from confocal microscopes were analyzed using Imaris software (versions 9.3-9.8). For calculation of the distances between cells, the Imaris Spots or Surfaces function was used to mark cells of equivalent mean fluorescent intensity (MFI) within a specified channel, and manually inspected. This information, together with image metadata, then supplied an Excel file with distance statistics for each individually measured cell-pair. The raw data from these files was used as input to Prism (Version 9) for graphical representation.

Flow cytometry analysis

Flow cytometric data was analyzed on FlowJo v10 (BD Biosciences). The raw data from these files was used as input to Prism (Version 9) for graphical representation.

Cell culture

293T and gp-293 cells were grown in DMEM with 4mM L-glutamine, 25mM glucose, 1mM sodium pyruvate (Life Technologies) and added 1%Penicillin-Streptomycin, 1% HEPES and 10% FBS. Cultures were split at 85-95% confluence, typically every 2-3d. Cells were maintained in a sterile, humidified environment of 5% carbon dioxide, 95% oxygen at 37ºC. Culture flasks and plastics were obtained from Sarstedt Ltd.

Generation of CCL3/5-IgFc fusion proteins and CCR5 overexpression cell lines

cDNA encoding CCL3 and CCL5 was generated by high-fidelity RT-PCR from splenocytes isolated from immunized mice, with primer-based addition of restriction enzyme cut sites. The sequence was then inserted into the CS-1Fc mut pIRESpuro vector (donated by Prof. Oferm Mandelboim, The Hebrew University of Jerusalem), containing the Fc domain sequence of IgG. A His tag was added to the 3' end of the Fc sequence, for purification purposes. This entire cassette (target gene through to His tag) was then cloned into the pQCXIX vector (Clontech, 631515), containing an IRES-eGFP cassette. Amplification was carried out in competent DH5α cells (Invitrogen). Retroviral particles containing CCL3IgFc-pQCXIX were packaged according to Clontech guidelines in GP-293 cells by co-transfection with the pVSVg vector (Clontech; PT3343-5), and 293T cells were then transduced by spinfection. GFP+ cells were then sorted by FACS to establish a stably expressing cell line, 293-CCL3IgFc+His.

cDNA encoding CCR1 and CCR5 was generated by high-fidelity RT-PCR from splenocytes isolated from immunized mice, with primer-based addition of restriction enzyme cut sites, and subsequently cloned into the MSCV-IRES-GFP plasmid (Addgene, 20672). Amplification was carried out in competent DH5α cells (Invitrogen). PLAT-E cells were transfected with the

retroviral vector using lipofectamine (Thermo Fisher), and WeHi cells were then transduced by spinfection. GFP+ cells were then sorted by FACS to establish a stably expressing cell line, WeHi-CCR5-O/E.

CCL3-IgFc protein purification

Briefly, supernatant from 293-CCL3IgFc+His cultures was filtered and diluted 1:1 in binding buffer (PBS, 0.05% sodium azide, pH8), incubated with Ni-NTA agarose beads (Qiagen) and applied to an equilibrated centrifuge column (Pierce). After the application of wash buffers containing increasing concentrations of imidazole (10mM, 20mM in PBS pH8), elution buffer (250mM imidazole, PBS) was added and eluant were collected in 0.5ml fractions. Protein concentrations were measured via OD values and target fractions were pooled and concentrated utilizing VivaSpin500 columns (Sartorious).

Ponceau staining

To detect and assess protein size (of IgFc fusion proteins), SDS-PAGE was performed (with BioRad TGX gels) in denatured conditions (samples mixed with Laemmli buffer and 20mM DDT, heated to 100 deg C) utilizing the Turbo-Blot transfer apparatus and system. Membranes were submerged in Ponceau S solution to stain, then rinsed and imaged for protein detection (Precision Plus Protein™ Dual Color Standards, Bio-Rad, 1610394, was used as a ladder).

RNA sequencing analysis

Single cell RNA-seq

B6 mice were infected with X31 influenza and were allowed to reach a memory phase (day 42 post primary infection). The mice were divided into 3 groups (n=3). One group was assessed without rechallenge. The second group was pre-treated with PBS liposomes intranasally on days 6 and 3 before being rechallenged with X31 influenza. The third group was pre-treated as above with CLL liposomes followed by rechallenge with X31 influenza. One day after rechallenging, the mice were *in vivo* labelled with CD45 for 4min prior to tissue collection. Lungs were processed, stained, and sorted as described above. Briefly, the lung tissue was digested in 1mg/ml Collagenase D and 10ug/ml DNase1 in RPMI for 45min. After digestion, cells were Fc-blocked stained and sorted. 60,000 cells (per sample) were sorted directly into FBS, then stained with TotalSeq hashing antibodies, pooled and stained with CITESeq antibodies for 30min further processing. The cells were stained with DNA-barcoded TotalSeq C Abs (Biolegend) according to the manufacturer's instructions. TotalSeq antibody-oligonucleotide conjugates contain a capture sequence complementary to the Template Switch Oligo (TSO) on the Single Cell 5' Gel Bead oligos. The following TotalSeq C antibody-oligonucleotide conjugates were used:

TotalSeq-C0301 anti-mouse Hashtag 1, Clone M1/42; 30-F11 Biolegend Cat# 155861; RRID:AB_2800693
TotalSeq-C0302 anti-mouse Hashtag 2, Clone M1/42; 30-F11 Biolegend Cat# 155863; RRID:AB_2800694
TotalSeq-C0303 anti-mouse Hashtag 3, Clone M1/42; 30-F11 Biolegend Cat# 155865; RRID:AB_2800695

Three sample pools were generated, each containing 3 individual samples – with single replicates of each condition pooled separately. For example, "sample_pool_1" comprises of

three samples (resting_1, rechallenged_1, CLL_1) labelled with hashtags and multiplexed together through a single capture channel. Thus, each of the three sample pools represent one experimental replicate with one technical replicate for each condition.

The sample hash tag oligo identifiers and sequences and details of the multiplexed samples were provided by the sequencing facility (file: "sample.metadata.tsv"), in which:

hto_id	library_id	sample_id	condition	replicate	sex	sequence
C0301_TotalSeqC	pool_1	resting_1	resting	1	female	ACCCACCAGTAAGAC
C0301_TotalSeqC	pool_3	resting_3	resting	3	male	ACCCACCAGTAAGAC
C0301_TotalSeqC	pool_2	rechallenged	rechallenged	2	female	ACCCACCAGTAAGAC
C0302_TotalSeqC	pool_1	rechallenged	rechallenged	1	female	GGTCGAGAGCATTCA
C0302_TotalSeqC	pool_2	resting_2	resting	2	female	GGTCGAGAGCATTCA
C0302_TotalSeqC	pool_3	rechallenged	rechallenged	3	male	GGTCGAGAGCATTCA
C0303_TotalSeqC	pool_2	CLL_2	CLL	2	female	CTTGCCGCATGTCAT
C0303_TotalSeqC	pool_1	CLL_1	CLL	1	female	CTTGCCGCATGTCAT
C0303_TotalSeqC	pool_3	CLL_3	CLL	3	male	CTTGCCGCATGTCAT

(Note, only thee TotalSeqC antibody-oligonucleotide conjugates were needed as three separate pools were generated – within each pool, three distinct TotalSeqC sequences could distinguish each of the three original samples).

Approximately 20,000 cells per sample pool were loaded onto the 10X Genomics Chromium Controller (Chip K); all sample pools were loaded onto the same 10x chip. Library preparation was performed by Moustafa Attar at the Wellcome Trust Center, Oxford University. Gene expression, feature barcoding and BCR sequencing libraries were prepared using the 10x Genomics Single Cell 5' Reagent Kits v2 (Dual Index) following manufacturer user guide (CG000330 Rev B). The final libraries were diluted to ~10nM for storage. The 10nM library was denatured and further diluted prior to loading on the NovaSeq6000 sequencing platform (Illumina, v1.5 chemistry, 28bp/98bp paired end for gene expression and feature barcoding, 150bp paired end for BCR libraries).

Initial processing of reads was performed by Lada Koneva and Stephen Sansom, at the genomic center at the Kennedy Institute. Sequence reads were mapped using CellRanger multi (version 6.0.0) with the 10x mouse reference transcriptome (version 2020-A). Cells were demultiplexed using GMM-Demux (version 0.2.1.3). The reads matrix was then provided to me to perform the analysis. Only cells with >200 genes and <10% mitochondrial reads were included. The analysis was performed using Suerat. Highly variable genes (HVG) were identified within each sample separately (n_top_genes=2000, flavour="Seurat_v3", using counts) and then combined, retaining only the subset that was discovered in at least 2 samples (n=2906 genes). Conserved cluster markers were identified as those that were commonly identified for the clusters in each of the three conditions (Seurat FindMarkers, Wilcoxon test, BH adjusted $p < 0.05$). For composition and within-cluster differential expression analysis the dendritic cell (DC) clusters were merged into a single DC cluster. Cluster differential expression analysis between the cells of the "rechallenged" and "CLL-treated rechallenged" conditions was performed using the Seurat FindMarkers function (Wilcoxon test, BH adjusted $p < 0.05$). Geneset scores were computed using the AUCell algorithm and were visualized without thresholding.
Dataset deposited: Gene Expression Omnibus (GSE194058).

Bulk RNA-seq (Brm)

Reads were provided by Dr. Andrew MacLean (sequencing was performed using an Illumina NextSeq 500 System). Downstream processing and analysis was performed using Partek Flow software. QC analysis was performed with the fastQC package. Reads were then aligned using STAR against the mouse genome assembly (GRCm38 (mm10) UCSC transcripts). The read counts were used for the identification of global differential gene

expression between specified populations using the edgeR package. Genes were considered differentially expressed between populations if they had an adjusted p-value (FDR) of less than 0.05. Inter- and intragroup variability was assessed by principal component (PC) analysis applied to filtered and variance stabilized transformed (VST) count data generated using the DESeq2 package, and by Spearman's correlation (r_s) values between samples calculated from TMM-normalized and filtered count data (gene counts were filtered for features detected at least 50x across all samples). Dataset deposited: Gene Expression Omnibus (GSE183135).

Bulk RNA-seq (alveolar macrophages)

B6 mice were infected with X31 influenza and were allowed to reach a memory phase (day 42 post primary infection). The mice were divided into 4 groups of three (n=3). One group was assessed without rechallenge (resting state), the other three groups were collected at 6 hours, 12 hours, and 18 hours after rechallenge. Downstream processing and analysis were performed using Partek Flow software. QC analysis was performed with the fastQC package. Reads were then aligned using STAR against the mouse genome assembly (GRCm38 (mm10) UCSC transcripts). The read counts were used for the identification of global differential gene expression between specified populations using the edgeR package. Genes were considered differentially expressed between populations if they had an adjusted p-value (FDR) of less than 0.05. DEG analysis was performed via DESeq2 on median ratio (MR)-normalized and filtered counts (gene counts were filtered for features detected at least 25x across all samples). Pathway analysis was performed utilizing ReactomeGSA.

Quantitative PCR (qPCR)

Quantitative PCR was performed on lung alveolar macrophages (i.v. $CD45^-$ $F4/80^+$ $CD11c^+$ $SiglecF^+$), monocytes (i.v. $CD45^-$ $F4/80^-$ $CD11c^-$, $Ly6g^-$ $Ly6c^+$) and neutrophils (i.v. $CD45^-$ $F4/80^-$ $CD11c^-$ $Ly6g^+$ $Ly6c^-$) and dendritic cells (i.v. $CD45^-$ $F4/80^-Ly6G^-$ $MHCII^{hi}$ $CD11c^+$). A minimum of 10,000 cells from each population were sorted directly into lysis buffer with 2-ME (Qiagen RNeasy Plus Micro Kit). Reverse transcription was performed with High-Capacity cDNA Reverse Transcription Kit (Applied Biosystems, 4368814). Quantitative PCR was performed using the following TaqMan assays:

GAPDH (Mm99999915), *Cxcl9* (Mm00434946), *Cxcl10* (Mm00445235), *Ccl3* (Mm00441259), *Ccl5* (Mm01302427) and *Ccl4* (Mm00443111).

Data acquisition was performed on an Applied Biosystems Viia 7 Real-Time PCR System.

All gene expression were normalized to an internal housekeeping gene (GAPDH) mRNA and calculated as $2^{-(\mathrm{CThk}-\mathrm{CTgene})*10{,}000}$.

Statistical tests and analyses

Where normal distribution could be determined (using Shapiro-Wilk test for normality), comparisons between two groups were made using unpaired Student's t-tests. Paired Student's t-tests were used when measuring the difference between two variables in the same subject (**Figure 4-2B and C**). In other (non-parametric) cases, statistical comparisons between two variables were performed using Mann-Whitney U tests. For multiple comparisons of normally distributed datasets with one independent variable, one-way ANOVA was used (**Figure 6-4B**) followed by Tukey post-hoc test. Graphpad Prism 8 (GraphPad software Inc.) was used to perform statistical analysis and for graphical representation of data. P values were calculated and represented as follows: $^*(p < 0.5)$; $^{**}(p < 0.01)$; $^{***}(p < 0.001)$.

4 Results I: Brm residence during steady state

4.1 Introduction

B cells rely on niche-specific cues to direct their differentiation, migration, and effector functions from their development through to their activation. The bone marrow (BM) serves as a complex microenvironment within which B cell development and PC retention occur (reviewed in (145)). In the BM niche, the CXCL12-CXCR4 axis is essential for the attraction or retention of B cell precursors and plasma cells (PCs). Deficiency of CXCR4 results in a severe reduction of both pro-B and pre-B cells in fetal liver and bone marrow from as early as embryonic stage E18.5 (146). PCs exhibit niche-specific sensitivity to CXCR12 signaling as, in the absence of CXCR4, they fail to accumulate normally in the bone marrow and are found elevated in the blood (147). It is suggested that CXCL12-high reticular cells, lining BM sinuses away from the surface of the bone, associate with pre-pro-B-cells in support of their differentiation towards pro-B cells. Furthermore, mature PCs home to CXCL12-high reticular cells in the BM. Stromal IL-17-expressing cells present in the BM, distinct from CXCL12-high reticular cells, are also important for supporting the development of pro-B cells by mediating the expression of MCL1 and thus their survival (148). CXCL12 is also found highly expressed in the splenic red pulp and lymph node medullary cords, additional sites of PC localization (147), and is required for normal PC positions in the spleen. Thus, the CXCR4/CXCL12 receptor-ligand pair regulates B cell development, BM lodgment and localization of PCs in spleen and lymph nodes (149). Positioning of germinal center (GC) B cells also depends on the CXCL12-CXCR4 axis, as CXCR4-deficient cells are excluded from the dark zone in the context of a wild-type GC (150, 151). CXCL13, in contrast, is found highly expressed in the light zone of GCs and is important for the

positioning of this zone at the pole of the GC distal to the T zone (31). CXCL13-deficient mice demonstrated atypical light zone formation in the center of the GC or near the T zone (150).

Outside of the BM, in secondary and tertiary lymphoid organs, follicular dendritic cells (FDCs) maintain primary follicle identity and germinal center clustering – thus promoting long-term antigen display (152). FDCs are stromal cells with the striking capacity to capture, retain and present antigens. In the absence of FDCs, B cell areas overlap with T zone stromal cells and are infiltrated by T cells and DCs, suggesting that FDCs play an important role in maintaining the structure and integrity of the B cell follicle (152). FDCs are also thought to contribute B cell trophic factors, such as IL-6, BAFF, sonic hedgehog, and hepatocyte growth factor (reviewed in (153)); however, many of these studies are limited to *in vitro* assays and have yet to be robustly demonstrated *in vivo*. What remains undisputed is that engagement of BCRs with FDC-retained antigen is critical for GC development, B cell survival, Ig class-switching, and memory B cell development (153).

Memory B cells tend to be stationed strategically at sites where they are likely to re-encounter antigen. The splenic marginal zone and the subcapsular sinus of lymph nodes are two well-known reservoirs of memory B cells. They are also found in the blood, the bone marrow, tonsillar mucosal epithelium, and, recently, as tissue-resident cells in the lung following infection. Within lymph nodes, memory B cells are located in close association with CD169+ macrophages – specialized cells capable of capturing and presenting antigen to B cells (100). They share this niche with follicular memory T cells, innate lymphocytes, and NKT cells, which are well-adapted to provide co-stimulatory signals, such as CD40L, to advance the secondary antibody response (100). In the mouse spleen, memory B cells are found in both the marginal zone and the follicle (86), the distribution of which appears to change over time after immunization and is possibly dependent on the immunogen. IgG+

memory B cells have been reported proximal to GCs in the spleen, adjacent to CD4+ T cells, in contrast to localization of IgM+ memory cells in the follicle (154). The reactivation of the IgG+ subset can be abolished after CD4+ depletion, indicating their dependence on cognate interactions with helper T cells. Interestingly, IgG+ memory B cells isolated from peripheral blood are found to migrate towards CXCL13 *in vitro* (they are not sensitive to CXCL12), suggesting they may eventually circulate to follicles of secondary lymphoid organs, including the spleen (155).

Unlike at any other site, tissue-resident memory B cells (Brm) are uniquely positioned within non-lymphoid tissue that lacks the typical structural elements supporting B cell migration, survival, and activation in secondary and tertiary lymphoid organs. Allie et al. demonstrate that Brm establishment requires local antigen (156), but it is not yet known what maintains their survival and retention in the tissue. Furthermore, we report the sparse distribution of alveolar Brm amongst the lung parenchyma, outside of iBALT clusters (157) and not necessarily in contact with other B cells. This is in stark contrast to memory B cell localization in the follicles of secondary and tertiary lymphoid organs. Thus, I hypothesized that Brm must have unique mechanisms to maintain residency, which likely involve niche-specific neighboring cells and chemokine receptor-ligand pair signaling in the lung.

In this chapter, I aim to characterize the cellular environment within which Brm reside during steady-state conditions, to probe for potential cellular cues that may contribute to their retention in the lung tissue.

Objectives:

1) Characterize the alveolar Brm niche during steady state to identify neighbouring cells.
2) Determine whether chemokine receptor CCR1 is necessary for Brm retention in the lung.

4.2 Visualizing Brm in the lung during steady-state

Our lab previously established the BAT reporter mouse model (Blimp1^{mVenus} AID$^{Cre/+}$ Rosa26^{tdTomato}) to track lung Brm cells *in situ*. In this model, *Aicda*(AID)$^{Cre/+}$ Rosa26^{tdTomato} reporter mice, in which B cells are irreversibly labeled after activation by expression of the fluorescent protein tdTomato, are crossed to a *Prdm1*^{mVenus} (Blimp1^{mVenus}) strain, where mVenus expression under the *Prdm1* regulator elements permits detection of PCs (157). This allows us to distinguish between 'red' memory B cells (expressing tdTomato) and 'yellow' PCs (expressing both tdTomato and mVenus).

In previous work from the lab, we used 2-photon microscopy to characterize the location and behavior of Brm and PCs in live and static lung sections. This analysis showed that during the memory phase, aggregates of tdTomato^{+} Venus^{neg} GL7^{+} cells are found adjacent to and within iBALT-like structures, likely representing ongoing GC reactions. PCs (tdTomato^{+} Venus^{+}) are chiefly found confined to large clusters at branching points of large airways or contained within the outer perimeter of iBALT-like structures. In contrast, and of interest, many tdTomato^{+} Venus^{neg} GL7^{neg} cells did not aggregate but were instead distributed sparsely throughout the lung parenchyma in close contact with alveoli. Different from the observed high motility of tdTomato^{+} B cells within iBALT, these parenchymal Brm cells exhibited limited migratory capacity and were often seen to perform restricted surveillance behavior, locally probing alveolar walls (157). Flow cytometry analysis revealed that lung tdTomato^{+} Venus^{neg} GL7^{neg} cells closely resemble the non-recirculating resident memory B cell subset previously described (156), including upregulation of CD69, CXCR3, PDL2, and CD80, as well as downregulation the migratory receptor CD62L. Thus, Brm are enriched in the parenchymal tdTomato^{+} observed by 2-photon microscopy.

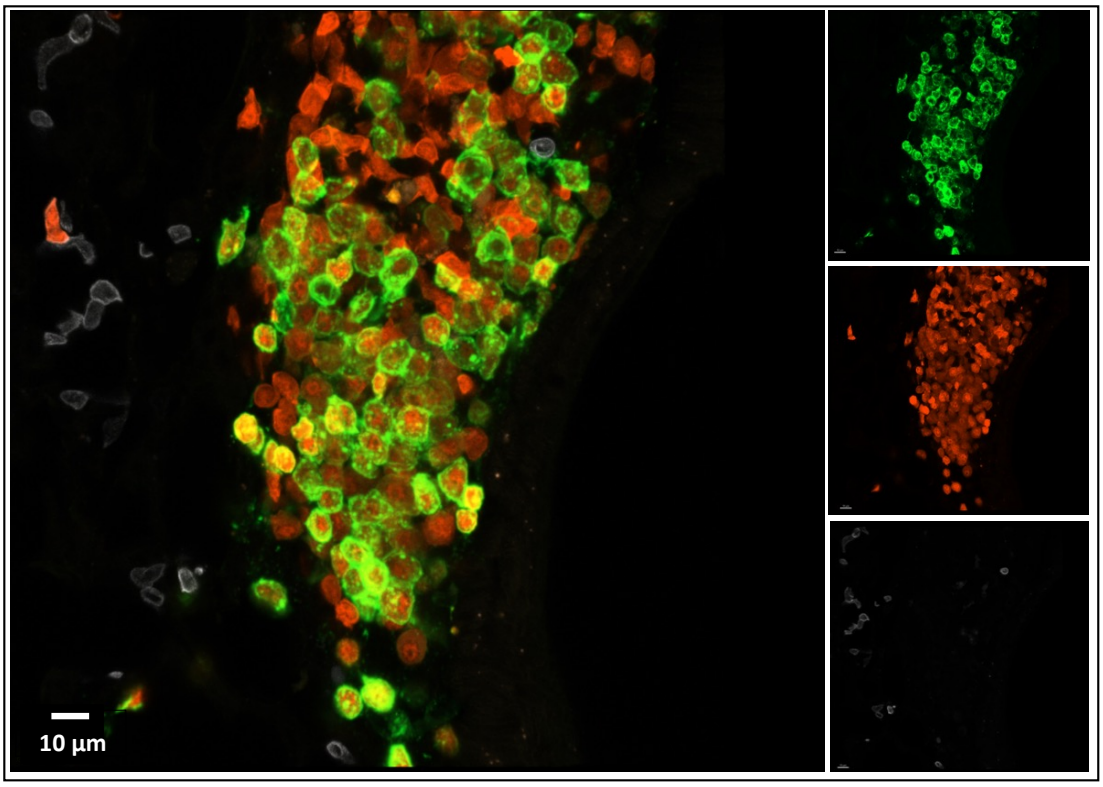
While 2-photon analysis provides excellent coverage of large areas because it penetrates deeply into tissues, it lacks the resolution needed to dissect more specific details about the cellular architecture of the lung. Therefore, to investigate the Brm niche, I used confocal microscopy to begin exploring the identity of cells neighboring Brm, including key structural and cellular components, to gain insight into possible mechanisms that regulate the unusual distribution of Brm cells in the lung. I hypothesized that granted the localization of Brm distributed around alveolar walls they are likely in close proximity to type I and type II epithelial cells, as well as the endothelial cell capillary network of the lung. To address this, I optimized immunofluorescent staining of target cells and examined lung sections from memory-stage BAT mice.

To establish Brm, I infected BAT mice with the X31 influenza strain >40 days prior to lung collection. The X31 influenza strain was generated ~50 years ago by simultaneous inoculation of chick embryos with a low-yielding, heat-inactivated H3N2 Hong Kong virus (A/Aichi/2/68 strain; referred to as A2) and the high-yielding, infective H1N1 A/Puerto Rico/8/34 strain (PR8; referred to as AO) (142). The subsequent selection was made "based on suppression of the parental or recombinant virus of AO serotype with specific antiserum and limiting diluting passage to permit the emergence of Hong Kong-like virus of good growth potential." This generated a high-yielding recombinant, X-31, with identical surface glycoprotein genes of the A/Aichi/2/68 strain and the internal protein genes of PR8. The virulence of X31 in mice is intermediate between wildtype human H3N2 isolates and PR8 in that a dose of approximately 10^6 plaque-forming units (PFU) of X31 during primary challenge is required to induce mortality in mice (158, 159). The X31 and PR8 virus strains have since been used together, in alteration, to perform heterotypic challenges and

evaluate cross-protective immunity, as the surface proteins from each are of distinct subtypes (112, 144).

Consistent with previous 2-photon observations from the lab, by confocal microscopy, I observed iBALT-like structures with tdTomato+ Venus+ plasma cells in dense clusters associated with airway branch points (**Fig. 4-1A**) and tdTomato^{+} Venus^{neg} cells distributed across the interstitium between the walls of pulmonary alveoli (**Fig. 4-1B**)

A.



B.

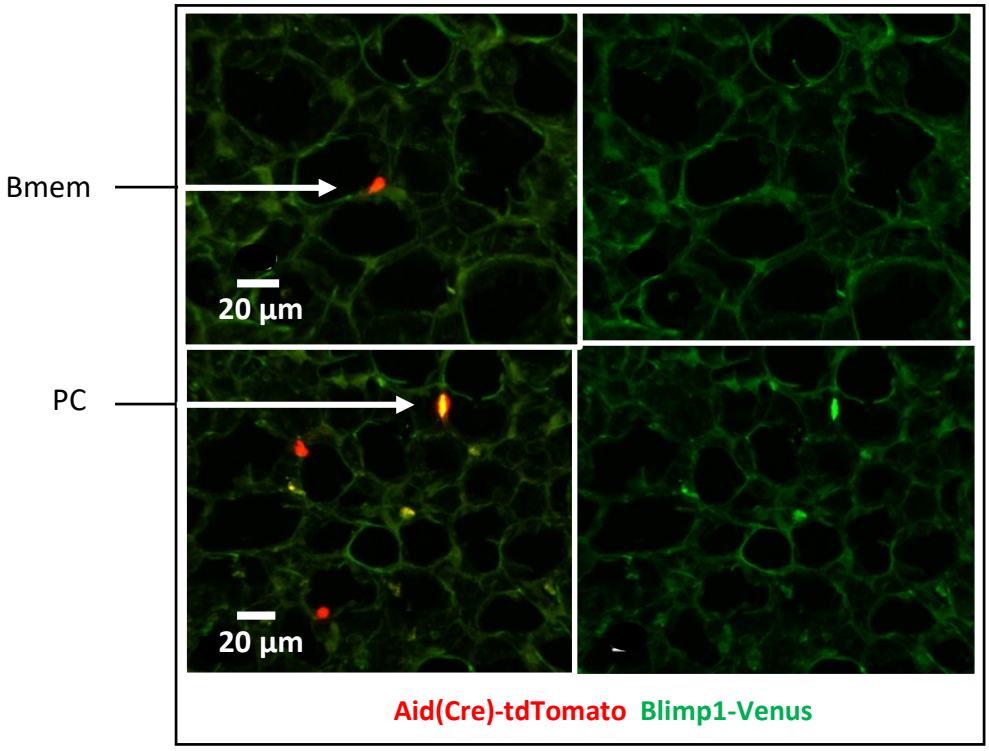


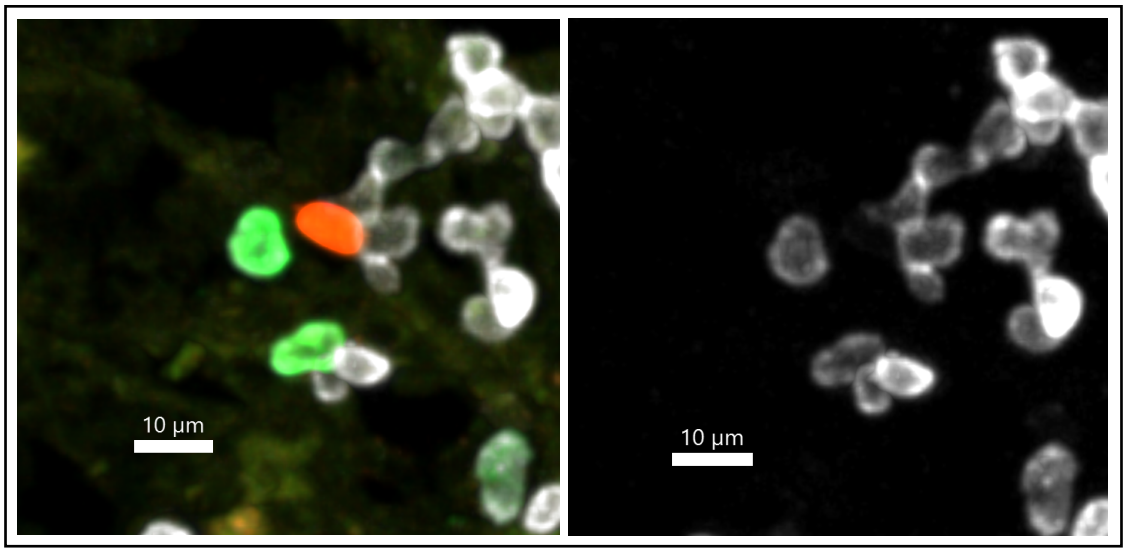
Figure 4-1: Pulmonary AID+ B cells and plasma cells in the BAT mouse.
Confocal microscopy of BAT lung d42 post influenza X31 infection [25 µM thick sections].
A) Representative image of an iBALT-like structure adjacent to an airway.
B) Representative image of AID+ Bmem and rare AID+ Blimp+ plasma cell around alveoli (autofluorescence in Venus channel amplified to visualize surrounding structure).

I investigated the fraction of tdTomato^{+} Venus^{neg} cells dispersed across the alveoli and withing the lung parenchyma rather than those associated with iBALT-like structures. Isotype-switched B cells are well-characterized in iBALT, whereas nothing is known about Brm positioning in the alveoli. Thus, we were most curious to understand the function and relevance of these previously unreported cells, which we term “alveolar Brm cells” in the context of recall influenza infections.

4.3 Validating alveolar Brm cells localization inside blood-sheltered regions

Studies from our lab demonstrate that the tdTomato^{+} Venus^{neg} cells observed via imaging persist in lung tissue after treatment with FTY720. This compound is an S1PR1 inhibitor that sequesters lymphocytes in secondary lymphoid organs and thymus, thereby preventing activated and memory B cells from circulating and entering peripheral tissues (160-162). This suggests that tdTomato^{+} Venus^{neg} cells imaged in histology sections primarily encompass those of local tissue residence, as opposed to circulating cells. However, it is still possible that while most of these cells are tissue-resident, a proportion of the imaged tdTomato^{+} Venus^{neg} cells may be a recirculating subset of previously activated B cells. To further validate whether imaged cells are exposed to circulation and more directly compare them to our flow cytometry subsets, I included the use of an intravenous anti-CD45 antibody administered 4 minutes before euthanasia to label cells exposed to blood (163) prior to collection (**Fig. 4-2A**). I then quantified the number of labeled versus unlabeled tdTomato+ cells (**Fig. 4-2B, left**) per tile. I compared these numbers to those obtained by flow cytometry (**Fig. 4-2B, right**). A representative image of a histology section obtained during image acquisition for analysis is included in **Figure 4-2C**.

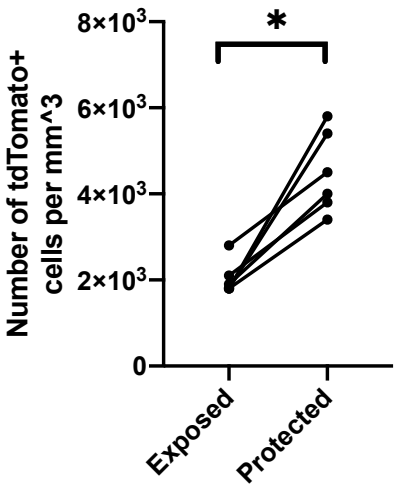
A.



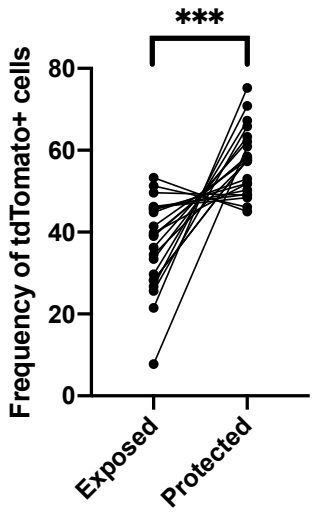
Aid(Cre)-tdTomato Blimp1-Venus In-vivo CD45-APC

B.

tdTomato+ cells exposed to blood via microscopy



Proportion of all tdTomato+ cells exposed to blood by flow cytometry



C.

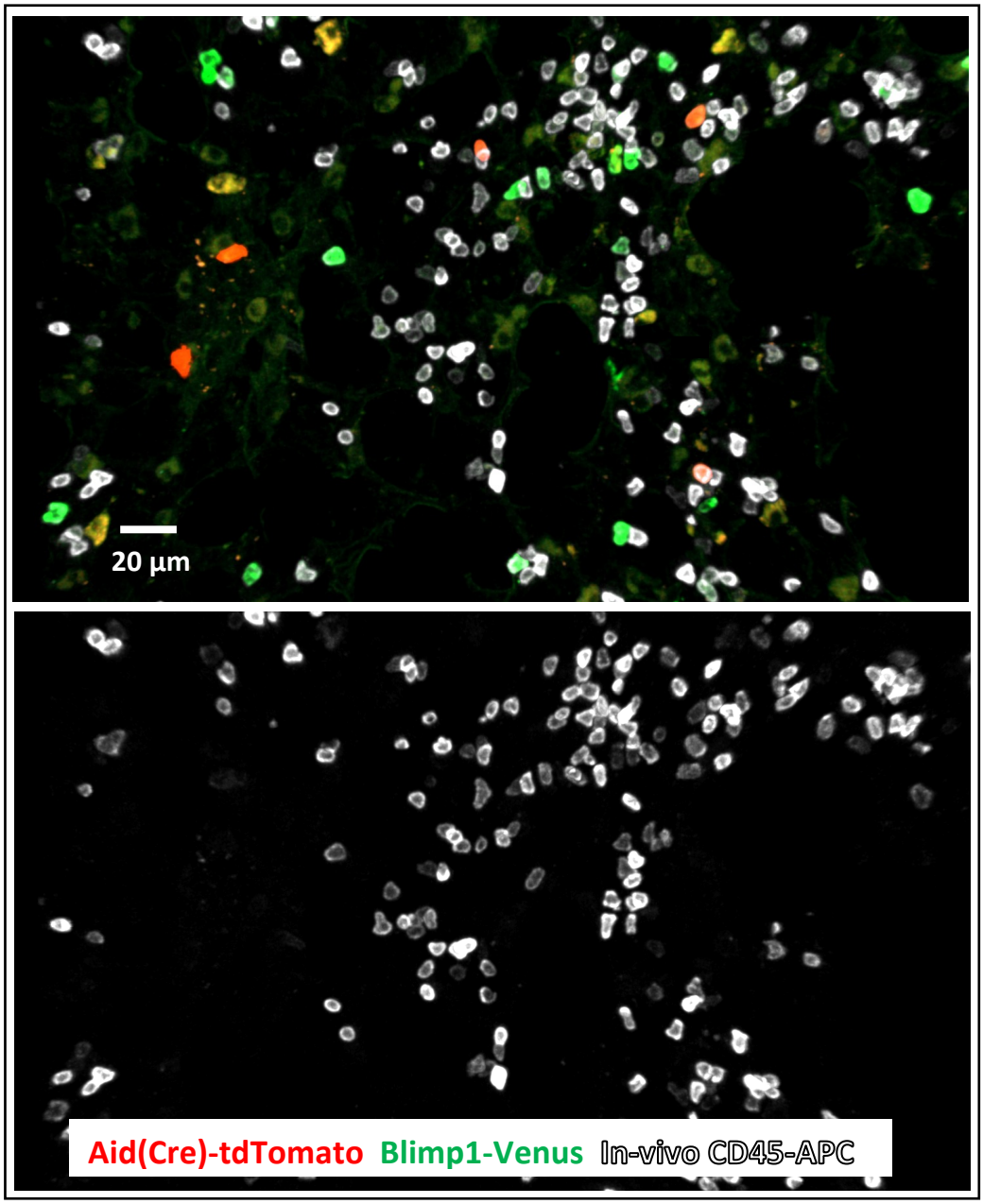


Figure 4-2: Confocal microscopy of lungs from BAT mice 42 days post-primary infection with influenza virus.

A) Close-up of Brm (tdTom+) proximal to cells exposed to circulation [scale bar represents 10 µM].
B) (Left) Summary of quantification using Imaris software to classify cells and standardise mean fluorescence intensity of labelled objects. Each pair represents the projected cubic millimetre quantification from original 500 x 500 x 20 µM tiles [N=3, n=2]. Paired t-test (passed Shapiro-Wilk test for normality), * = $p<0.05$.
C) (Right) Summary of quantification from flow cytometry analysis gated on live singlets, tdTomato$^+$ cells that are CD45 IV-label negative (protected) or positive (exposed) [N=3, n=5]. Paired t-test (passed Shapiro-Wilk test for normality), * = $p<0.05$.
D) Representative image of a tile used to quantify tdTomato+ cells in histology sections [25 µM thick].

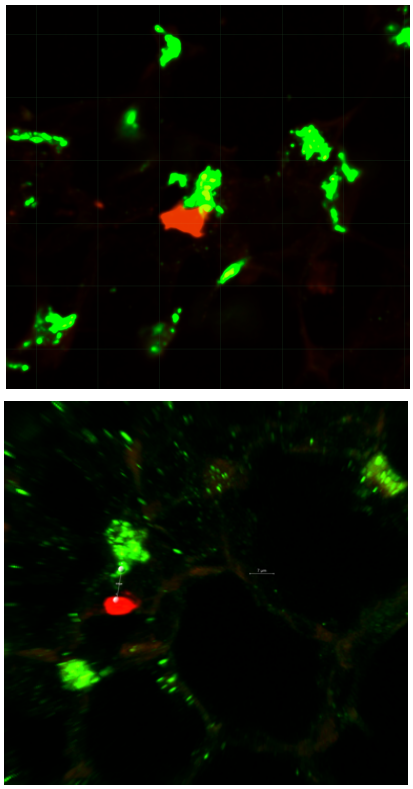
I observed that while tdTomato$^+$ cells are in close proximity to cells exposed to blood, as seen in **Figure 4-2A**, the majority are protected from circulation (~72%), while ~28% of tdTomato$^+$ cells are exposed to the IV-administered CD45 antibody, based on quantification of images using Imaris software. Flow cytometry analysis of digested lungs reveals slightly increased numbers of tdTomato$^+$ cells exposed to blood, at ~37%, yet the majority appear within the IV-protected fraction (**Figure 4-2B**). Thus, the imaged cells represent a mixed population of non-circulating and blood-exposed cells, with the majority appearing to be tissue-resident cells based on IV-administered antibody labeling.

4.4 Exploring potential cellular partners that associate with alveolar Brm cells

While observing Brm by confocal microscopy, it was apparent they were in proximity to cell-types other than clustered B cells and PCs. The main cellular components of the alveolar tissue are the type I and type II epithelial cells (TIIAEC), the stromal and endothelial cells lining the extensive vasculature of the lung, and other pulmonary immune cells, including alveolar macrophages, interstitial macrophages, dendritic cells, and tissue-resident T cells. Since the tdTomato$^+$ cells comprising Brm were found adjacent to alveolar spaces, we questioned whether these cells might preferentially associate with structural components of the alveoli including TIIAECs, endothelial cells, or alveolar macrophages present within the alveolar lumen.

TIIAECs are well-known for producing lung surfactant but are also reported to have an immunoregulatory function and to produce cytokines that may attract leukocytes (164). Similarly, the endothelium can propagate the immune response and is a key component of leukocyte trafficking in the lung (165). Alveolar macrophages (AM) are well-characterized to modulate immune responses by recruiting and activating other lymphocytes (166).

To investigate proximity of Brm to these cell types, I optimized immunofluorescent staining for the TIIAEC-specific marker pro-surfactant protein C (pSPC) (167); CD68, a pan-macrophage and mononuclear phagocyte marker (168) to identify AM in the lumen of the alveoli; and CD31, a traditional marker used to highlight the endothelium (169). I acquired large tiles of steady-state BAT lung sections stained for each marker. I then used Imaris software to measure distances between tdTomato^{+} cells and their closest neighboring TIIAEC or alveolar macrophage. I observed that on average, the distance from TIIAEC measured ~14 μM apart (**Fig 4-3)**, while the average distance from alveolar macrophages was greater (~41 μM) (**Fig. 4-4**). Of note, in this analysis, I excluded CD68+ cells that were not located on the luminal side of alveoli or did not exhibit autofluorescence, as these cells likely represent dendritic cells, interstitial macrophages, or monocytes, which all may also express CD68 (170).



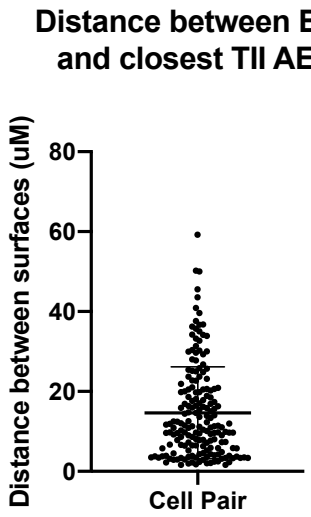
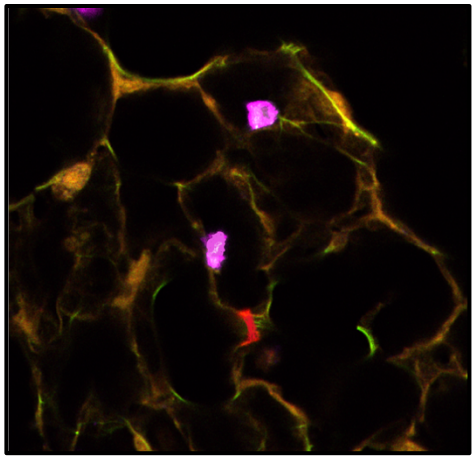


Figure 4-3: Proximity of Brm to TIIAEC.

(Left) Confocal microscopy of BAT lung d42 post-influenza X31 infection, stained with anti-pSPC to label TIIAEC [25uM thick sections]. Imaris software was used to create surfaces at consistent mean MFI values, and further to measure distances between points on two surfaces. (Right) Summary graph of measured distances between each tdTom-TIIAEC pair, from 500 x 500 x 20 μM tiles [N=3, n=2]. Bars represent mean



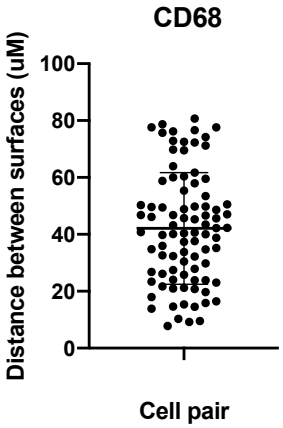


Figure 4-4: Proximity of Brm to alveolar macrophages.

(Left) Confocal microscopy of BAT lung d42 post-influenza X31 infection, stained with anti-CD68 to label macrophages [25uM thick sections]. (Right) Summary graph of measured distances between each tdTomato+ and intra-alveolar CD68+ cell pair using Imaris software, from 500 x 500 x 20 μM tiles [N=3, n=2]. Bars represent mean values ± SD.

This comparison initially implied potential preferential proximity to TIIAECs; however, I considered the possibility that this result was biased by differences in concentrations of TIIECs and AMs. Thus, to account for differences in cell density between TIIAECs and AMs, I normalized the analysis based on the total number of TIIAEC or AM per imaged field of view (by the number of cells per surface area, uM^2) which demonstrated there was, in fact, no preferential localization of Brm between either cell type (**Figure 4-5**).

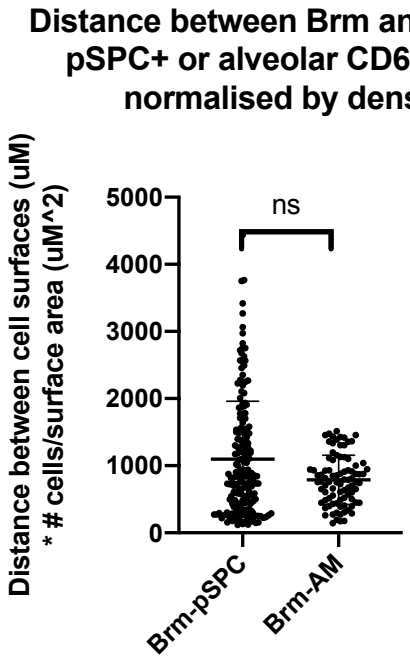
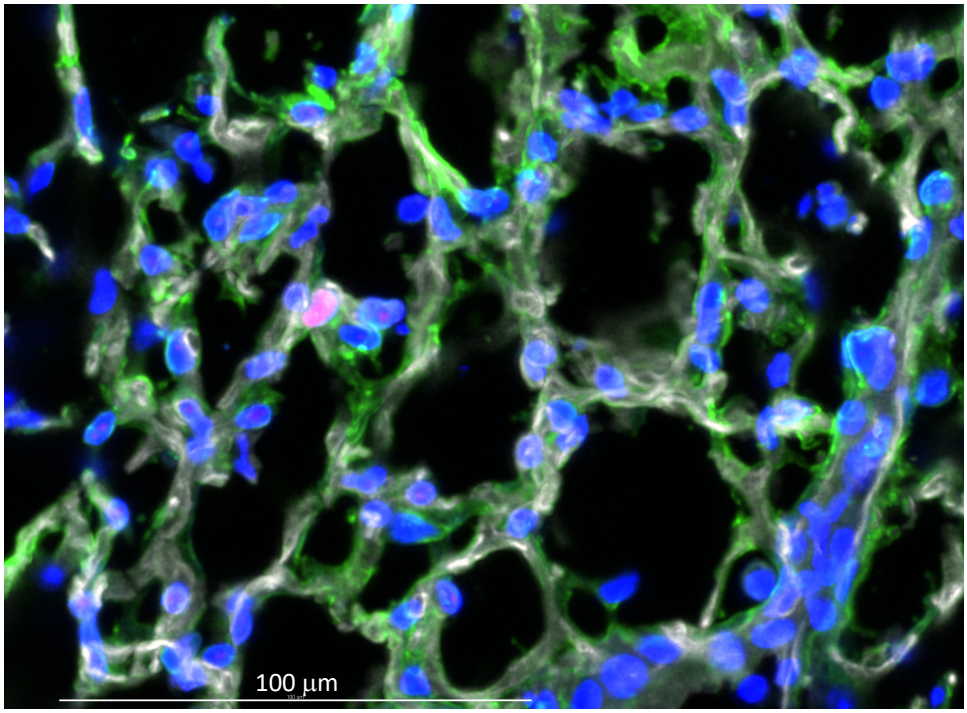


Figure 4-5 (left): Normalized distances between cell types.

Measured distances between cell types from Figures 4.3 and 4.4 were normalized by density for comparative purposes. Bars represent mean values $\pm$ SD, and p value is derived from Mann-Whitney statistical test (p=0.11).

Instead, it is possible that to exhibit the surveillance-like type behavior observed during resting-state conditions, Brm may reside or migrate between the endothelium of lung capillaries and the type I epithelium of the alveolar walls. The parenchymal space between these two strata is minimal in the lung (thicker in regions where fibrous networks are concentrated to provide mechanical stability and thin where alveolar epithelium and capillary endothelium share a common basal lamina; minimizing the thickness of the diffusion barrier to less than 1 μm) (171). Thus, leukocytes infiltrating the lung interstitium

must squeeze between these two layers of cells. While type I AEC (TIAEC) are not usually associated with retention of immune cells, I co-stained podoplanin (PDNP), a classical TIAEC marker, along with CD31, to reveal the localization of Brm between the endothelium on the basal lamina side of the interstitium, and the alveolar epithelium. Confocal imaging revealed the Brm to be indeed proximal to both cell types (**Figure 4-6**), the distances between them too short to accurately measure (<1uM). In summary, the data suggest that the niche of Brm cells is potentially dictated by interactions between the capillary networks and alveolar epithelium, likely involving contacts with fibroblasts oriented across the inter-alveolar septum (172).



AID
PDPN
CD31
DAPI

Figure 4-6: Proximity of Brm to endothelium and TIIAEC.

Confocal microscopy of BAT lung d42 post-influenza X31 infection, stained with anti-PDPN to label type I epithelium, CD31 to label endothelium, and DAPI nuclear stain. [25uM thick sections].

4.5 Investigating the role of CCR1 in Brm establishment or retention.

The complete mechanisms retaining Brm in the lung tissue after their establishment are currently unclear. Brm are known to express CD69 on their cell surface, which antagonizes the surface expression of G-protein–coupled sphingosine-1-phosphate receptor-1 (S1PR1). S1PR1 provides a critical mechanism for T cell egress from lymphoid and nonlymphoid sites by promoting trafficking toward its lipid ligand, sphingosine-1-phosphate (S1P), which is found in high concentrations in the blood and lymph, but at much lower concentrations in tissues. By inhibiting surface expression of S1PR1, CD69 can therefore impair egress and promote T cell residency in lymph nodes (106, 160, 162). Loss of S1PR1 and increased surface expression of CD69 are transcriptionally regulated in T cells by KLF2, a transcription factor that is downregulated after stimulation with cognate antigen (106).

Furthermore, in lymph nodes and spleen, the expression of ligands specific for CCR7 is a key component of T cell attraction and for lymphocyte entry. Moreover, CCR7 promotes the residency of T cells within the lymph node, as CCR7 deficiency results in the more rapid exit of T cells from LN to lymph, and overexpression of CCR7 increases the retention of T cells in LNs (173). Interestingly, treatment with FTY720, an agonist of S1PR1, results in a 60%-70% reduction of CCR7-deficient cells in lymph, compared to 90% of wildtype cells (173). This suggests that the CCR7 retention cue is in part overridden by S1PR1 signaling. The expression of KLF2 returns as the response evolves, allowing S1PR1 to be upregulated, CD69 extinguished, and thus T cells are released into the periphery. This balance between egress and retention dictates how long lymphocytes remain in LNs and spleen, and thus differentiation cues that T cells may receive during the response. It is proposed that, ahead of egress, receptors important for chemo-attractant cues become desensitized, along with

the re-sensitization of S1PR1 (173). These shifts in GPCR sensitivities allow for the attraction, retention, and egress of lymphocytes from LN and spleen by overcoming retentions cues.

For tissue-resident cells, transcriptional downregulation of S1PR1 can be a requirement for their development into tissue-resident cells, as is reported for CD8+ Trm (106). The persistent down-regulation of S1PR1 can shift the balance towards confinement by allowing retention signals to prevail. It is possible that loss of S1PR1, as indicated by CD69 expression in Brm, may enable these cells to respond continuously to tissue-retaining signals in the lung.

While CD69 is critical for establishing resident memory lymphocytes in some tissues, e.g., Trm in the kidney after LCMV infection (174), its continued expression is not always a requirement. In lung-resident memory T cells (lung-Trm), established after influenza infection, CD69 expression is important for their establishment but not required for maintenance or retention (175). Parabiosis experiments elegantly demonstrated that up to 80% of $\mathrm{CD69}^{-/-}$ Trm were retained in the lungs of CD69-deficient hosts when surgically paired to wildtype mice (175). It is possible that loss of CD69 may be compensated for by transcriptional downregulation of S1PR1, or that additional tissue-retention cues are important for the maintenance of tissue-resident lymphocytes.

Additional Gαi-coupled receptor signaling mechanisms are known to mediate Trm retention. After infection with herpes simplex virus, CCR1 and CCR5-expressing Trm normally present in the vagina are reduced upon antibody blockade of CCL5, a ligand for chemokine C-C motif receptors CCR1, CCR3, and CCR5 (176), suggesting a role for these receptors in promoting Trm cell retention. In this context, low levels of IFN-y production by Trm induced the production of CCL5 by local macrophages in a positive feedback loop. Thus, macrophages in the Trm niche are responsible for producing the chemokines required for

their retention in the vagina. In the context of B cell-specific signals that may be of interest, it is reported that intraepithelial B cells of human tonsils express CCR1 (177), which suggests this receptor may be involved in the localization or retention of B cells in proximity to the epithelium. I, therefore, hypothesized that GPC receptor-ligand chemokine pairs promote Brm retention in the lung.

To investigate whether Brm express unique GPCRs relative to splenic memory and naïve B cell counterparts, I performed bulk RNA-sequencing analysis on a Brm dataset previously generated by Dr. Andrew MacLean from our lab. For this analysis, I compared RNA expression of sorted naïve B cells ($B220^{+}$ $tdTomato^{neg}$ $Venus^{neg}$ $GL7^{neg}$) as well as memory B cells from lung (*in vivo* $CD45^{neg}$ $dTomato^{+}$ $Venus^{neg}$ $GL7^{neg}$ $CD69^{+}$ HA^{+}) and spleen ($tdTomato^{+}$ $Venus^{neg}$ $GL7^{neg}$ HA^{+}) of BAT mice six weeks post-infection. Principal component analysis of the top 500 genes selected for the highest variance (**Figure 4-7-A**) demonstrated the three populations to separate in spatially distinct regions, with apparent intragroup similarity (individual samples clustering more closely together than intergroup distances). While this indicates heterogeneous transcriptomes between the populations, correlation analysis portrays high similarity across the populations (**Figure-4-7-B**). Thus, the samples share core signatures, yet some variability also exists. To identify differentially expressed genes of interest, I analyzed the data using the DESeq2 package in R. This revealed that, like some Trm cells, CCR1 is one of the GPCRs transcriptionally upregulated in Brm (**Fig 4-7-C**) relative to naïve B and splenic memory B cells. I also observed that Brm express the CD69 marker, as previously reported, and upregulate several additional GPCRs, including CCR7, CCR6, CXCR3/4/5. As expected, I found S1PR1 to be downregulated in Brm (106, 112).

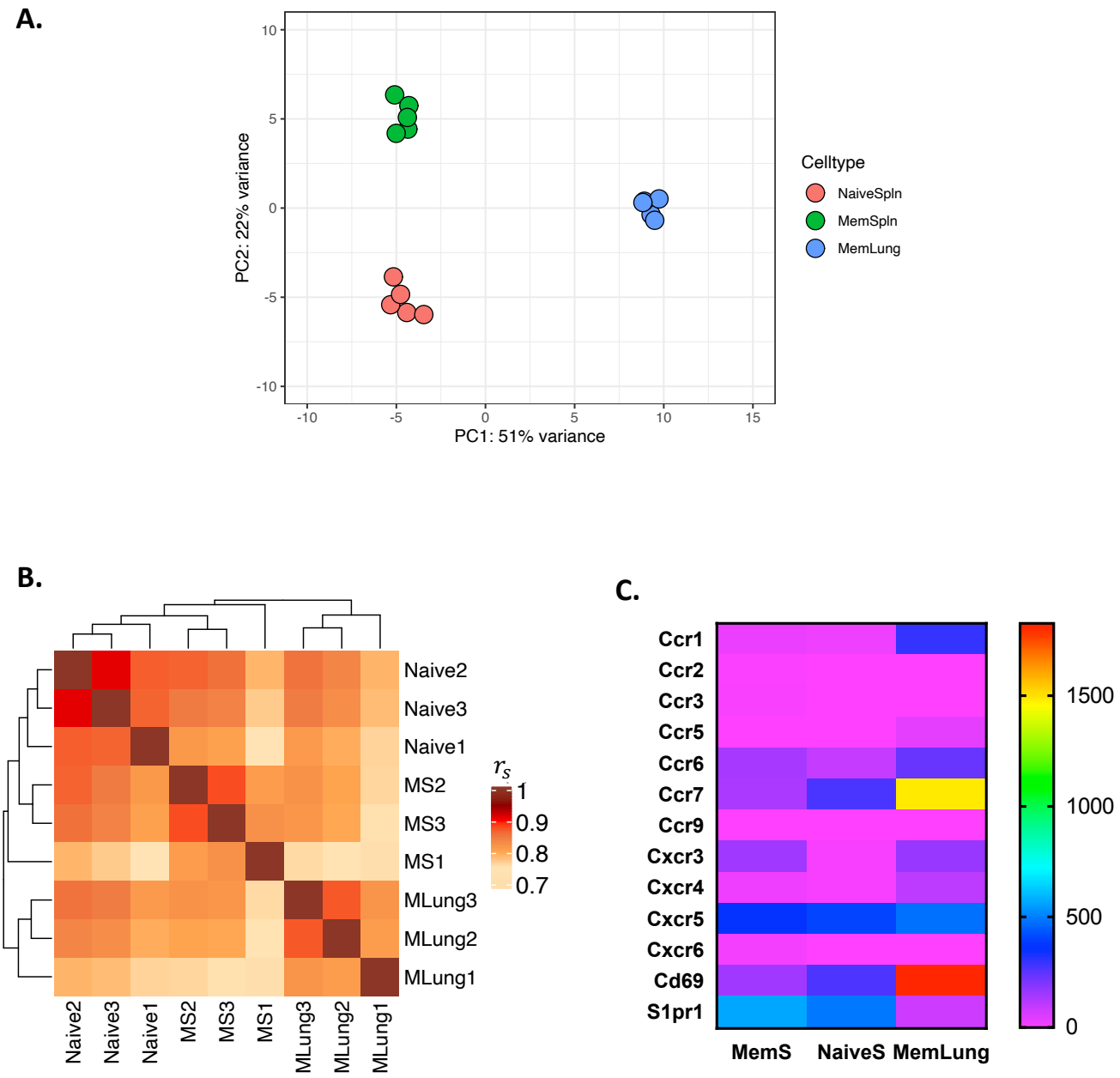


Figure 4-7: Bulk RNA-sequencing of Brm reveals changes in select GPCR expression.

A. Principal component (PC) analysis of the bulk RNA-sequencing count matrix. PC analysis was applied to the top 500 genes selected for highest row (gene) variance.

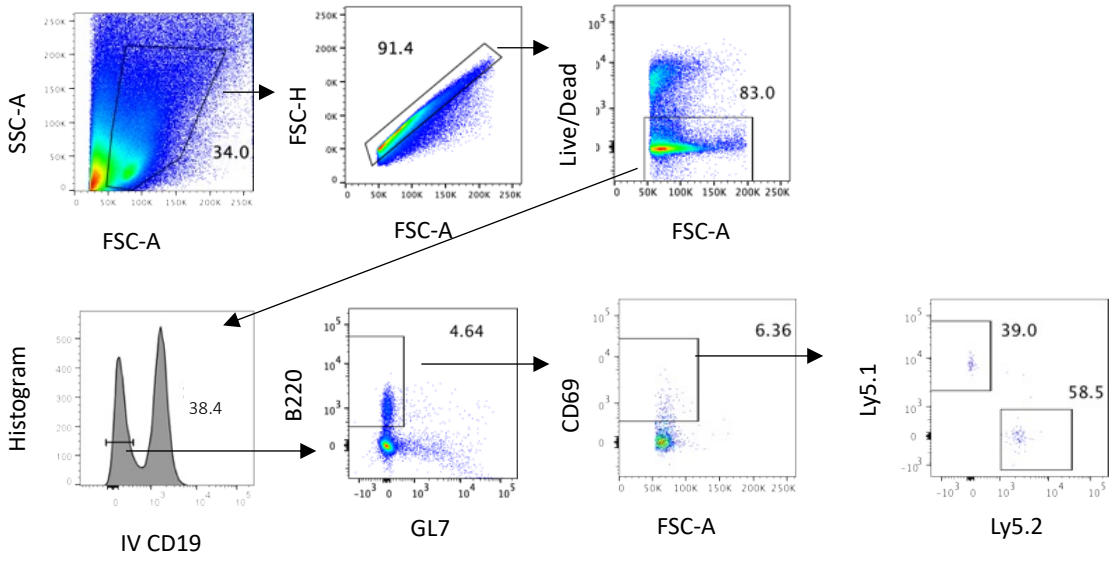
B. Dendrogram and symmetrical heatmap visualisation of bulk RNA-sequencing correlation matrix showing inter-sample Spearman coefficients (r_s). Scale bar represents the range of the correlation coefficients displayed.

C. Heatmap of select differentially expressed genes with an adjusted p-value (FDR) < 0.05, from sorted naïve B cells and HA+ memory B cells from lung and spleen derived from BAT mice (sorts performed and sequences provided by Dr. Andrew MacLean).

Due to the known role of CCL5 in mediating vaginal Trm retention, I hypothesized that its receptor CCR1 could be required for either the establishment or the retention of Brm in lung tissue during steady-state conditions. To test this, I generated mixed bone marrow chimeras with CCR1 knockout ($CCR1^{-/-}$) donor marrow and evaluated by flow cytometry whether a loss of CCR1 impacted the establishment or retention of Brm in the lung. More specifically, I mixed $CCR1^{-/-}$ bone marrow from Ly5.1 donor mice 50/50 with wildtype Ly5.2 bone marrow and transferred into irradiated Ly5.2 hosts. For comparison, I generated littermate Ly5.1 wildtype mixed with Ly5.2 wildtype (50/50) chimeric controls. Eight weeks after bone marrow transfer, I challenged the mice with X31 influenza virus. Forty days later, during the memory phase, I assessed by flow cytometry the frequency of IV^{-} $B220^{+}$ $GL7^{-}$ $CD69^{+}$ cells in the lung (the Brm fraction) deriving from either the wildtype or $CCR1^{-/-}$ populations to assess whether wildtype cells had a competitive advantage over the $CCR1^{-/-}$ cells.

Figure 4-8A shows a representative flow cytometry plot with a gating strategy for Brm cells. I found that the average frequency of Ly5.1 (CCR1 KO) Brm cells in the lung was ~50%, indicating no disadvantage compared to WT cells in forming and maintaining Brm cells. Furthermore, the ratio of CCR1$^{-/-}$:WT and WT:WT lung Brm were 0.94, and 0.82 respectively and did not significantly differ from each other (**Figure 4-8B**). While the ratios in the splenic naïve (IgD+ Fas-) and splenic GC (GL7+) compartments were slightly higher (>1) than the lung Brm, they too were not significantly different between CCR1$^{-/-}$:WT and WT:WT mice.

A.



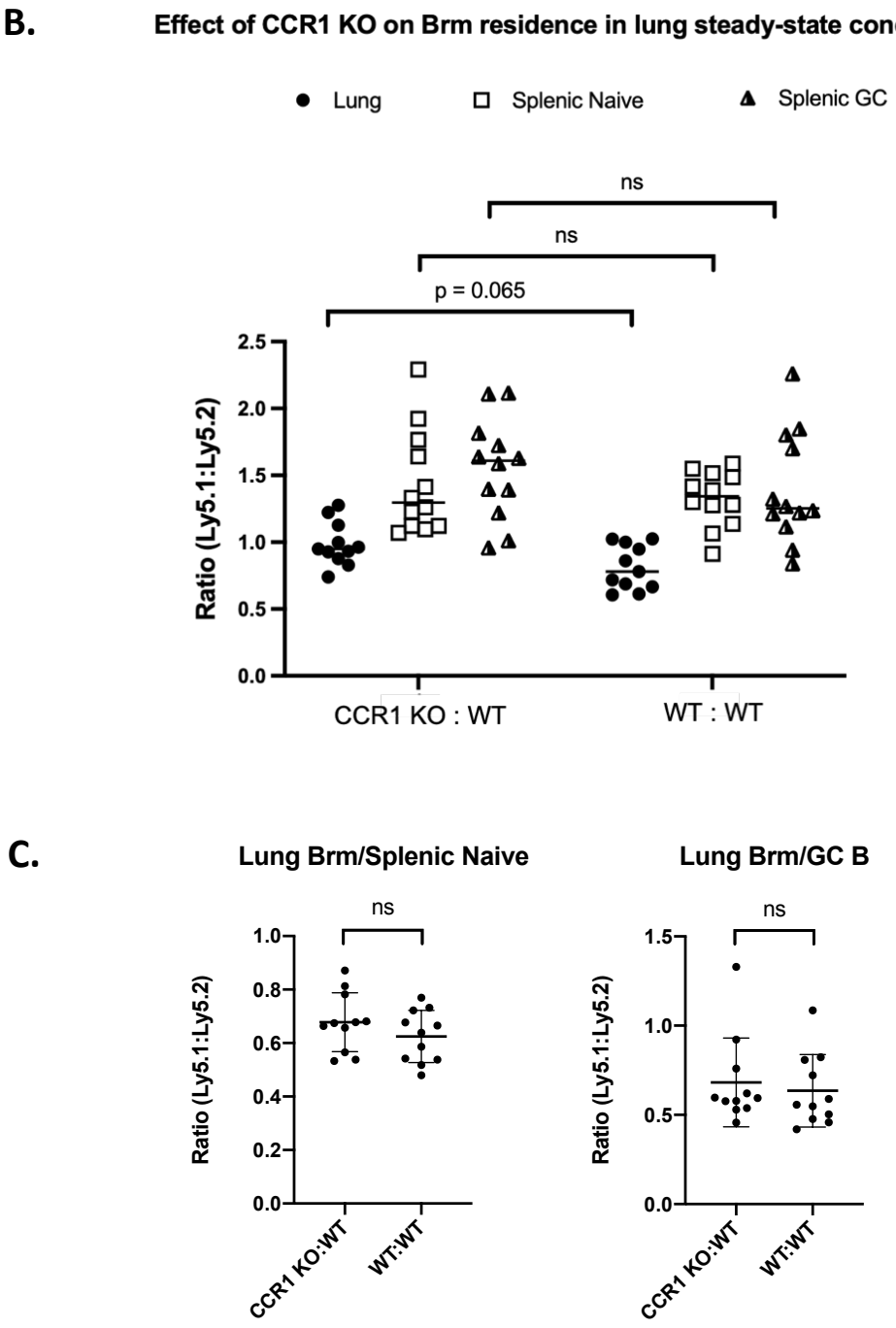


Figure 4-7: CCR1 does not affect B cell subset establishment or retention in the lung.

A. Gating strategy to identify Brm in murine lung tissue. Brm cells are identified as B220+, *in vivo* label negative, GL7-, CD69 (int/hi] cells. Donor cells were identified as Ly5.1+ cells.

B. Ratio of donor cells ($CCR1^{-/-}$ cells are Ly5.1: WT are Ly5.2; for WT:WT controls, a 50:50 mix of Ly5.1:Ly5.2 cells were transferred) in each B cell subset. Naïve B cells (splenic) are identified as B220+ IgD+ Fas- cells.; germinal centre B cells (splenic) are identified as IgD- Fas+ GL7+ cells. Bars represent mean values ± SD, and p values are derived from Mann-Whitney statistical tests.

C. Lung Brm ratios were normalised to splenic naïve or GC subsets. Bars represent mean values ± SD, and p values are derived from Mann-Whitney statistical tests.

This indicated that the distribution of B cells in all compartments, including lung Brm, splenic naïve, and splenic germinal center B cells, were not affected by CCR1-deficiency compared to WT-WT control hosts. My objective was to ascertain the potential effects of CCR1 knockout on Brm establishment. Therefore, it was important to normalize potential recruitment changes and exclude the possibility of an inherently lower capacity for $CCR1^{-/-}$ cells to develop into B cells. As such, I divided the ratios obtained within the lung tissue by those I saw within naïve B cell and GC B cells subsets in spleen tissue (**Figure 4-8C**). I observed no significant difference in the number of lung IV^{-} $B220^{+}$ $GL7^{-}$ $CD69^{+}$ cells deriving from the $CCR1^{-/-}$ donor compared to wildtype. To summarize, by comparing KO and WT in the different compartments, I found no apparent bias in favor or against $CCR1^{-/-}$ cells.

4.6 Discussion

The first objective of this chapter was to gain insights into the niche of Brm in the lung tissue. Through confocal microscopy, I found the majority of tdTomato^{+} Venus^{neg} cells dispersed across the alveoli to be protected from circulation, in line with our previous characterization of Brm by flow cytometry (157). However, a subset of alveolar Brm observed during microscopy are exposed to blood, as evidenced by the ability of IV-administered CD45 antibody to bind the cells. It is possible that IV-CD45^{+} tdTomato^{+} cells could represent a recirculating subset of lung-derived Bmem, or circulation-derived previously activated B cells from LN or spleen that became trapped in the capillary beds during perfusion of the lung prior to collection. To distinguish these two possibilities, it would be important to repeat these experiments with and without FTY720 treatment to discern if the ratio of IV$^{+/-}$ cells in the tissue shifts, depending on the presence of memory B cells in the blood. Furthermore, characterization of the IV^{+} tdTomato^{+} population could give insights as to whether they are lung-derived or LN/spleen-derived. BCR-repertoire clonal analysis from tdTomato^{+} cells isolated during the memory phase from blood, LN, spleen, and lung could potentially reveal the origin of IV^{+} tdTomato^{+} in the lung, compared to the IV^{-} tdTomato^{+} fraction. Gregoire et al. have conducted a BCR-sequencing analysis to reveal clonal overlap in the BCR repertoires of Brm and Bmem in the lung, lymph nodes, and spleen, suggesting these populations are interconnected in their generation or maintenance, however, the relationship between circulating and resident subsets remains unclear. Characterization of the IV^{+} tdTomato^{+} population by flow cytometry may be misrepresentative as one would expect a recirculating subset of lung-derived memory B cells to upregulate S1PR1 and lose expression of CD69, one of the important markers used to identify Brm. From a technical perspective, while it is important to note that IV-

administered antibodies are frequently used to distinguish blood-protected cells from those exposed, the diffusion rates of the antibody across the interstitium in the lung have not been optimized in our hands. It is possible that minor differences in the timing of administration of the *in vivo* label, as well as the vascular permeability of the lung at the time of administration and during euthanasia will impact the percentage of cells exposed to the antibody. Finally, while we perfuse the lung prior to collection according to previously established protocols, it is also known that this can leave more than 50% of circulating leukocytes in the lung tissue (178). Thus, it would be expected that a number of circulating memory B cells be retained in the tissue after collection.

My results further demonstrate that during the resting memory phase, lung Brm likely associate with the stromal compartment of the lung interstitium. I observed the alveolar Brm to be positioned primarily in close proximity to the lung endothelium and TIAEC, with no preferential localization against other Brm, TIIAEC, or AM. It is interesting to note that lung-Trm have been shown to rely on integrin-mediated adhesion to the lung parenchymal and epithelial compartments. Integrins CD49a and CD103 are often viewed as markers of Trm cells and functionally confer CD8 T cells the ability to interact with collagen IV underlying the lung epithelium, collagen I in the interstitium, and epithelial cells directly through CD103/E-cadherin binding. It is plausible that Brm may utilize similar mechanisms to patrol the inter-alveolar spaces in an integrin-dependent manner, as the lung interstitium contains high levels of collagen to maintain alveolar structure and integrity. While Brm do not exhibit CD103 expression (156), it may be informative to characterize other integrins potentially expressed by Brm that could assist with their attachment or movement within the lung interstitium. Exploring integrin expression of Brm first by qPCR and flow cytometry, then functionally by treating mice with antibody blockade (i.e., anti-CD49a) after Brm

establishment during the memory phase, may reveal insights into Brm retention and distribution in the lung. Additionally, CD103- Trm have been shown to form clusters with macrophages and CD4 T cells in the lung lamina propria (179). The CD8 Trm cells that develop after LCMV infection in the lamina propria, but not epithelia, show sign of TCR engagement (106). This suggests that cells within the described clusters may provide necessary retention signals for Trm residency in the lamina propria. It is possible that a similar niche may be a requirement for Brm retention in the lung; thus, further studies are needed to characterize the proximity of Brm against pulmonary T cells, DCs, and interstitial macrophages, as well as the potential role of BCR engagement for Brm survival and retention.

Of note, our bulk sequencing experiments do not distinguish between alveolar and iBALT-associated Brm. Granted recent reports of GL7-negative Brm expressing the same hallmark CD69 marker after influenza infection and residing within lung peribronchial iBALT (115, 116), we must acknowledge that the lung Brm population isolated for bulk sequencing analysis likely contains both alveolar and iBALT-associated Brm. Therefore, the interpretation of mechanisms retaining Brm in the lung may be confounded by unique factors mediating the alveolar versus GC-associated localization. Ongoing work will attempt to delineate niche-specific cues and what causes Brm to potentially egress ongoing iBALT reaction to alveolar space or the potentially extrafollicular origins of the alveolar-associated Brm. *In situ* hybridization techniques such as RNAScope may be useful when probing spatially for known B cell survival factors such as BAFF, in the lung interstitium, as potential mediators of Brm survival.

From mixed bone marrow chimera experiments comparing Brm numbers in CCR1$^{-/-}$:WT animals with WT:WT animals, I observed that a deficiency in CCR1 expression did not

provide any disadvantage to the number of Brm present within the lung during the resting state. Therefore, I conclude that this receptor is not required for Brm retention in the lung. However, is it possible that due to the redundancy of CCR1 with CCR5 for the CCL3 ligand, those alternate receptors compensated for a deficiency of CCR1. To better explore this possibility, ongoing experiments in the lab will take a broader approach to target multiple GPCRs simultaneously. To achieve this, I've developed a CCL3-IgFc fusion protein (and IgFc control protein) that may be administered intranasally to block both CCR1 and CCR5 receptor signaling. IgFc fusion proteins are composed of the Fc domain of IgG genetically linked to a peptide or protein of interest and are used to target receptor-ligand interactions, often functioning as antagonists to block receptor binding (180). The IgFc proteins have been purified and are currently undergoing testing for their binding efficiency *in vitro* to CCR5 over-expressing cells.

I observed from bulk-RNA sequencing that Brm also upregulate CCR7, in addition to CCR1, relative to splenic memory and naïve B cells. This hasn't yet been reported in the literature and may reflect the attraction of resting state Brm to the ligands CCL21 or CCL19. Interestingly, in mice, one variant of CCL21 (CCL21-Leu, containing a leucine at position 65) is present in non-lymphoid tissues, including the lung (181) during resting state conditions, whereas the alternate variant CCL21-Ser is expressed in lymphoid organs and lung after airway inflammation. Adoptive transfer of CCR7+/CD62L-low T cells into murine recipients demonstrated a 3-fold reduction of lung-homing T cells after desensitization of the CCR7 receptor compared to control, establishing the importance of CCR7 on T cells for homing to nonlymphoid tissues (181). Of note, both CCL21 and CCL19 are upregulated in the lung after influenza infection (182). Interestingly, the expression of both ligands appears to come from the non-hematopoietic compartment. *Plt/plt* mice (a naturally occurring strain of mutant

mice wherein the CCL19 and CCL21-Ser genes have been deleted, leaving the CCL21-Leu gene intact) reconstituted with either wildtype or *plt/plt* bone marrow exhibit a 4-10 reduction in CCL19/21 mRNA expression after infection compared to wildtype mice reconstituted with either wildtype or *plt/plt* bone marrow (182). To investigate the role of CCR7 more thoroughly in Brm homing and/or retention in the lung, it may be interesting to adoptively transfer Brm from immunized BAT mice into wildtype, wildtype treated with anti-CCL21/19 antibodies, and *plt/plt* recipients to assess the role of CCR7 ligands within the periphery (non-hematopoietic) or central immune response for both the homing and retention of Brm. Pre-treatment with CpG oligonucleotides to establish iBALT in the lung prior to transfer may be required to home Brm to the lung tissue, as hinted by experiments assessing their protective capacity (110). Along this same line of thought, *plt/plt* mice may have abnormal IBALT formation; thus, differences between wildtype and heterozygote *plt/wt* animals may serve as a more practical approach. Also, inducible knockout mice of the CCL21/19 alleles may best serve to answer these questions, yet at a higher cost.

5 Results II: The role of alveolar macrophages in regulating Brm cell activation in the lung

5.1 Introduction

Previous work in our lab demonstrates that upon rechallenge with X31 influenza, Brm cells alter their migratory capacity and quickly cluster at infected sites (157). Dr. Andrew MacLean observed alveolar Brm undergoing a burst of motility within 24 hours of reinfection, doubling their speed (>3µm/min) and displacing greater distances (from ~6.2µm during resting state to ~13.0µm during rechallenge, over the course of 30 minutes). Furthermore, the rapid increase in Brm motility is independent of antigen specificity as it also occurs after a mock rechallenge infection with virus-like particles (VLPs). These particles have many molecular characteristics of live virions but do not express any influenza virus antigens (183), thus suggesting that Brm migration can be induced through innate sensing pathways, such as the recognition of danger signals. In support of this possibility, RNA-free VLPs do not elicit a Brm response (157). Our group also observed that blocking GPCR signaling during rechallenge by administering pertussis toxin (PTx) abrogated the ability of Brm to cluster at sites of infection after rechallenge, leading to the conclusion that re-localization of BRM cells to infected sites is an active process that is likely regulated by the engagement of chemotactic receptor(s). Together, this data suggests that innate sensing pathways in cells amenable to producing GPCR-based signals are upstream of Brm mobilization after rechallenge. It became of interest to identify cellular candidates mediating Brm responses to potentially manipulate antibody production in response to recurring respiratory infections. When considering cell candidates that may be upstream of Brm responses, I focused on early responders already known to mediate influenza infection

immune responses, residing proximal to Brm in a similar niche, and which are known to produce chemokine ligands whose receptors are expressed by Brm.

Alveolar macrophages (AM) matched the above criteria and have been shown as essential for protection against morbidity induced by influenza during primary infections (184-187). AM reside in the surfactant of lung alveoli and aid viral clearance by phagocytosing infected cells and potentially blocking viral replication, preventing IAV spread (188, 189). The recognition of damage and pathogen-associated molecular patterns (DAMPs and PAMPs, respectively) by pattern recognition receptors, such as TLRs and RLRs, allows them to recognize the presence of pathogens or products of injury and respond directly to provide optimal host protection (reviewed in (190)). Alveolar macrophages isolated from mice and treated with TLR7 agonist demonstrate the same NOX2 oxidase and ROS activation profile as when infected with influenza A virus, suggesting this TLR may be involved in ssRNA recognition during influenza virus infection (191). Within infected dendritic cells, ssRNA from IAV was shown to trigger an inflammatory response characterized by cytokine (IL- β, IFN-β, IL-6 and IL-12) release in a TLR7-dependent manner (192). In porcine AM, influenza dsRNA is recognized by TLR3 (193), which induces NF-κB inflammatory signaling, and type I interferon production. Viral RNA released in the cytoplasm is also recognized by retinoic acid-inducible gene I (RIG-I), activating mitochondrial antiviral signaling protein (MAVS) and increasing ROS production (194). Furthermore, the viral matrix ion channel protein M2 induces the formation of the NOD-LRR-pyrin domain-containing inflammasome 3 (NLRP3), activating caspases and releasing IL-1β (195).

A critical challenge in the field of delineating the function of AM in mediating responses to IAV infection has been the relatively limited availability of specific mouse models that selectively target AM. Nonetheless, genetic models with partial specificity have

helped to better explore the role of AM in responses to influenza virus and to demonstrate their contribution to pathogen clearance. In CD11c-Cre/*Pparg*$^{fl/fl}$ mice, AM are missing, but adaptive immunity is otherwise normal. Under these conditions, mice displayed increased morbidity and lung failure to influenza virus, despite normal T cell responses (186). Similarly, influenza-induced pathology and morbidity were worse in *Csf2*-deficient mice, which have a global defect in macrophage development, but intact B and T cell responses (186). Depletion of alveolar macrophages via intranasal administration of clodronate liposomes (CLL) prior to influenza virus infection resulted in morbidity comparable to *Csf2*-deficient mice. CLL treatment was shown to only deplete alveolar macrophages, leaving dendritic cells intact. Importantly, the reconstitution of AM in *Csf2*-deficient mice prevented pulmonary pathology and morbidity following influenza virus infection (186). These studies highlight a specific role for AM in the protective immune response to influenza infection.

A key pathway that has been implicated in this protective process is mediated via the production of interferons (IFN) by AMs upon IAV (186). This leads to the upregulation of IFN-stimulated genes (ISGs), which inhibit cellular translation machinery and degrade ssRNA to effectively impair virus spread (reviewed in(196)). Constitutively heightened type I IFN signaling in AMs from β6-deficient mice was shown to attenuate IAV spread, pro-inflammatory cytokine production, and lung edema, resulting in protection against IAV-induced lung morbidity and mortality (197). In contrast, loss of type I IFN production by AMs during RSV infection is associated with increased viral replication and exacerbated disease, which was at least partially attributed to a reduction in the CCL2-dependent recruitment of monocyte-derived inflammatory cells into the lung (198). In line with this role as recruiters of immune cells, during infection with influenza virus, AMs increase the secretion of a series of inflammatory CC chemokines (CCL2, CCL3, CCL5, and CCL11) and interferon–responsive

chemokines (CXCL1, CXCL8, CXCL9, and CXCL10) (199), a spectrum that is characteristic of the classical activation (M1) of AMs (200). The induction of inflammatory chemokines by AMs during IAV implies the mobilization of additional cells to sites of infection. It is interesting to speculate that CCL3 and CCL5 expressed by AMs may have yet unidentified targets, such as CD8+ T cells, as seen with DC recruitment in the lymph node (201, 202). Furthermore, CXCL9 and CXCL10 are important for CXCR3-mediated recruitment of activated and memory T and B cells (203), which may indicate that AMs expressing these two ligands could have a role in the recruitment of these cells towards sites of infection in the lung.

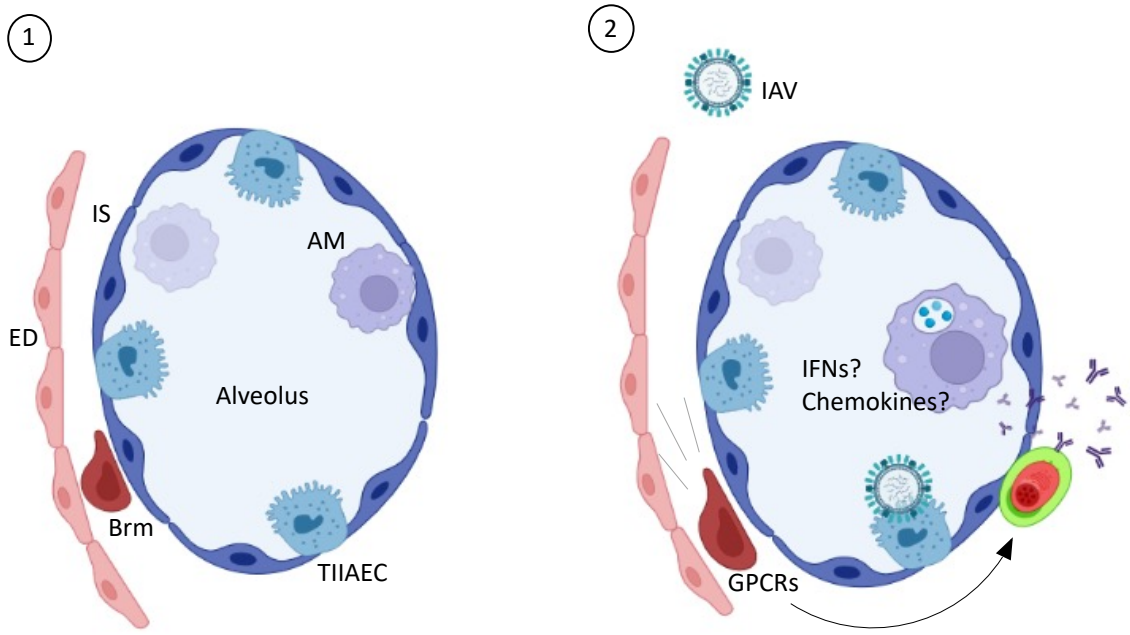


Figure 5-1 (schematic): Brm mobilize to infected sites rapidly after influenza rechallenge. 1. In resting state conditions, Brm patrol the interstitial spaces between alveoli in the lung. 2. Upon infection with influenza virus, AM phagocytose infected cells and initiate a signaling cascade that mediates Brm migration towards infected sites, where they differentiate into antibody-secreting plasma cells, providing local protection. [IS = interstitial space; ED = endothelium; AM = alveolar macrophage]

Due to the ability of AMs to respond to IAV infection and produce ligands specific for Brm receptors, I hypothesized that AMs may be upstream of Brm migration and sought to deplete AMs to assess Brm responses after infection in the absence of AMs.

Objectives:

I. Optimize identification and depletion of alveolar macrophages in mouse models.

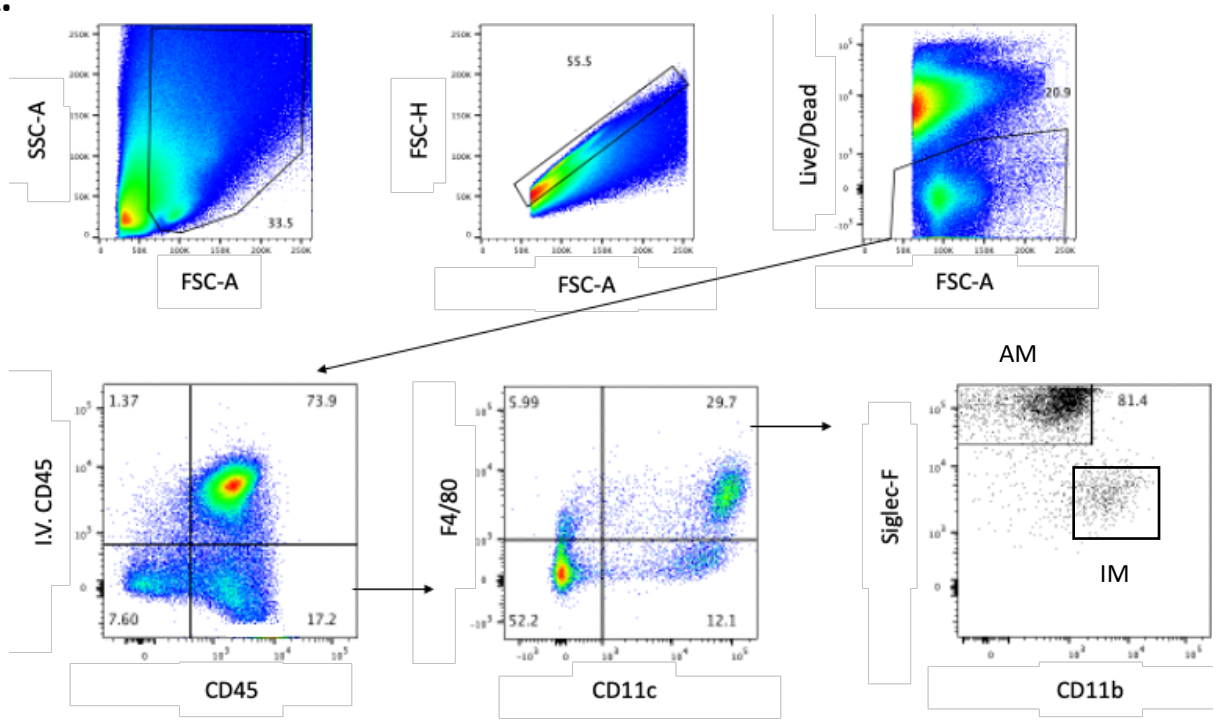
II. Identify signaling cues from alveolar macrophages that may mediate Brm migration after rechallenge.

5.2 Optimizing alveolar macrophage identification by flow cytometry

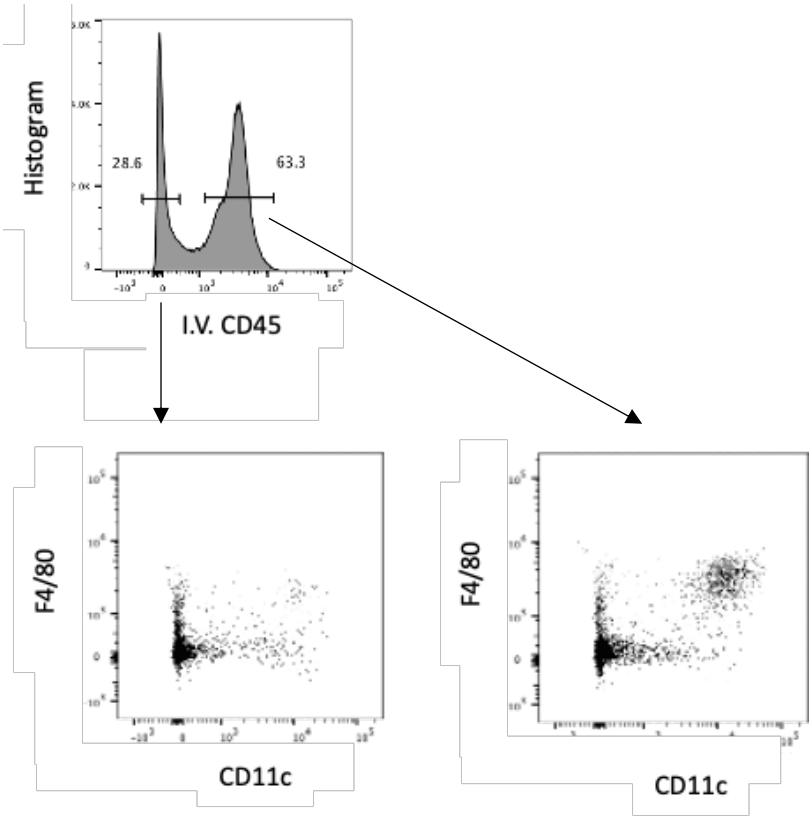
To target the AM population, I first designed a flow cytometry antibody staining panel to identify AM and other innate immune cells present in the lung, including interstitial macrophages, dendritic cells, neutrophils, and monocytes. The literature reveals that in normal mouse lungs, alveolar macrophages are identified based on the expression of Siglec F, CD11c, F4/80, the absence of CD11b, high side scatter, and high autofluorescence (204). Interstitial macrophages, on the other hand, also stain for F4/80 and CD11c but do not express Siglec F and are CD11b-high. Neutrophils express high levels of Ly6G and are CD11b+ (205). Monocytes can be distinguished from the former as Ly6G negative cells and are Ly6C high. Dendritic cells (DCs) I identified as F4/80-negative and CD11c-expressing cells. **Figure 5.2(A)** portrays the flow cytometry gating strategy to identify AM and other immune cell subsets. I originally included the use of an *in vivo* label within my panel – as AM are tissue-resident cells and protected from circulation, they should be negative for IV-administered antibodies. I observed that due to the high autofluorescence of AMs, fluorochromes FITC and PE were unsuitable for exclusively labeling AM markers as they appeared within the IV-positive and IV-intermediate populations, respectively

(representative plots are shown In **Figure 5-2(B-C)**), not matching the physiology of their localization outside of blood circulation.

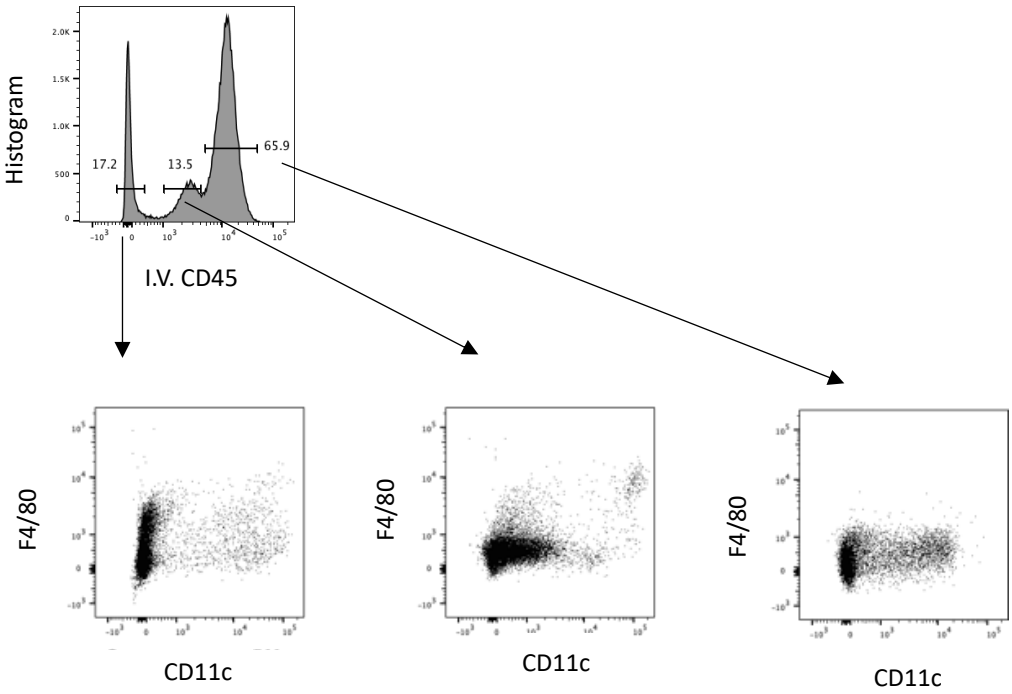
A.



B. **I.V. CD45-FITC**



C. I.V. CD45-PE



D. I.V. CD45-APC

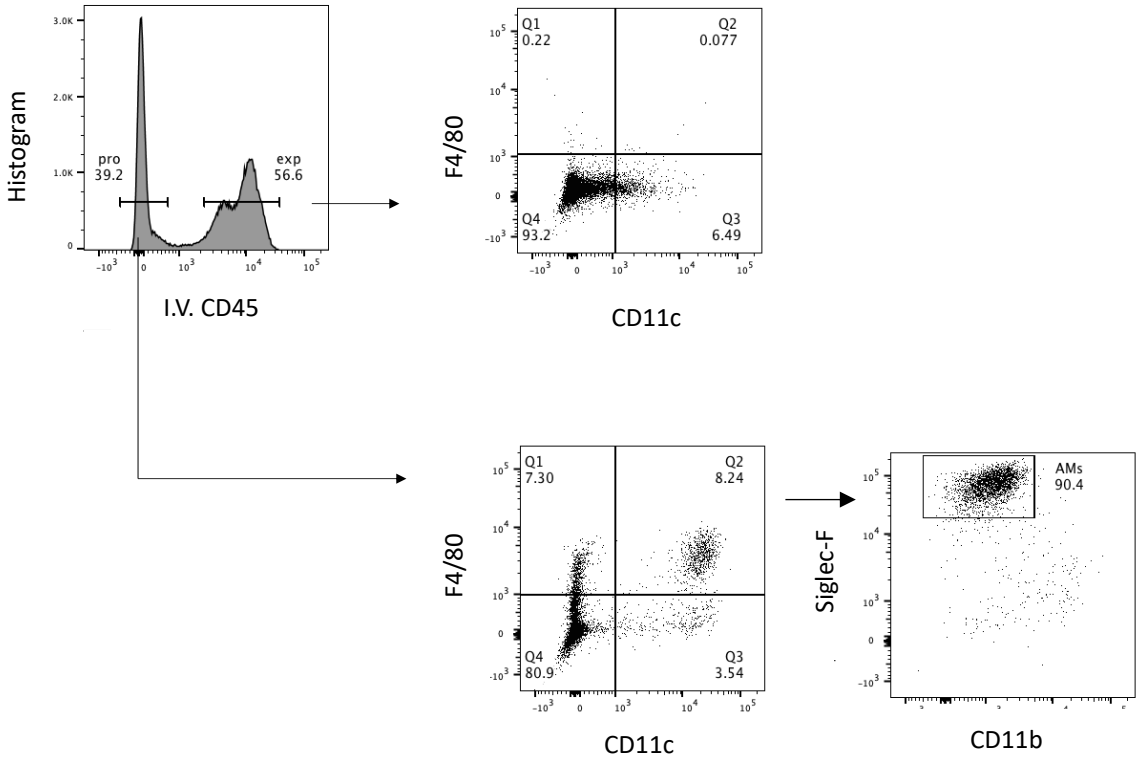


Figure 5-2 (above): Identification of AM and IM by flow cytometry.
Gating strategy to identify AM and IM in murine lung tissue. AM cells are identified as *in vivo* label negative, CD45+, F4/80+, CD11c+, CD11b-low, SiglecF+ cells. IM are CD45+, F4/80+, CD11c+, CD11b-high, SiglecF- cells**. A)** AM appear to stain with FITC-conjugated CD45 antibody due to autofluorescence. **B)** AM appear PE-intermediate due to autofluorescence in this channel (CD45-PE antibody). **C)** AM are found protected from circulation when using *in vivo* administered CD45-APC antibody.

I, therefore, restricted the use of IV-label to the APC fluorochrome (representative plot shown in **Figure 5-2D**), which exhibited the least autofluorescence. These observations are supported by literature that also identifies APC as a less autofluorescent channel for AMs compared to FITC and PE (206). It also explains why the AM population in **Figure 5-2A** appears CD11b-low, as this antibody was conjugated to a700, another channel in which low AM-autofluorescence is detected. Yet, they are still distinguishable from CD11b-high interstitial macrophage counterparts, also based on Siglec F expression.

Because AM were enriched in the lung resident population when using APC-conjugated antibodies, I only used this fluorochrome to administer *in vivo* label throughout the rest of my studies. In parallel, I assessed whether excess *in vivo* antibodies could transfer to unlabeled cells during tissue processing by mixing tissues collected from wildtype B6 animals having received an *in vivo* label and *UBC-GFP* transgenic mice (which express green fluorescent protein directed by the human ubiquitin C promoter) and identifying whether GFP+ cells became labelled with the *in vivo*-administered antibody. Between 1-8% of GFP+ cells adopted the *in-vivo* label (data not shown), excluding the possibility that transference of antibodies during processing could explain the appearance of the majority of AM within the *in vivo* labeled populations for FITC and PE antibodies.

I also identified lung monocytes (Mo), neutrophils (No), and dendritic cells (DCs), as seen in **Figure 5-3**., as I anticipated these cells may be involved in early resolution to rechallenge.

Neutrophils are known to be recruited to the lung during primary IAV infection in a CXCR2-dependent manner but are not required for viral clearance (207). Primary influenza infection also leads to the recruitment of circulating monocytes and dendritic cells into the lung in a CCR2-dependent manner (208, 209), with monocytes contributing in part to the replacement of dying alveolar macrophages and interstitial macrophages. Pulmonary CD11c-high subsets of dendritic cells are known to bridge innate and adaptive immunity by migrating to mediastinal lymph nodes after IAV infection and presenting antigen to CD4+ and CD8+ T cells (210). Certain subsets of DCs also accumulate in the lung after infection and can be replaced by circulating monocytes (211-213). The kinetics of recruitment of these cell types have been extensively studied in the context of primary infection, but less so after recall infections, therefore it was important to identify and track their presence in the lung in addition to macrophages, as potential contributors to the adaptive response observed during rechallenge. For this reason, I also optimized their staining in the lung using FACS analysis (**Figure 5-3**).

Gated on live, single, CD45+

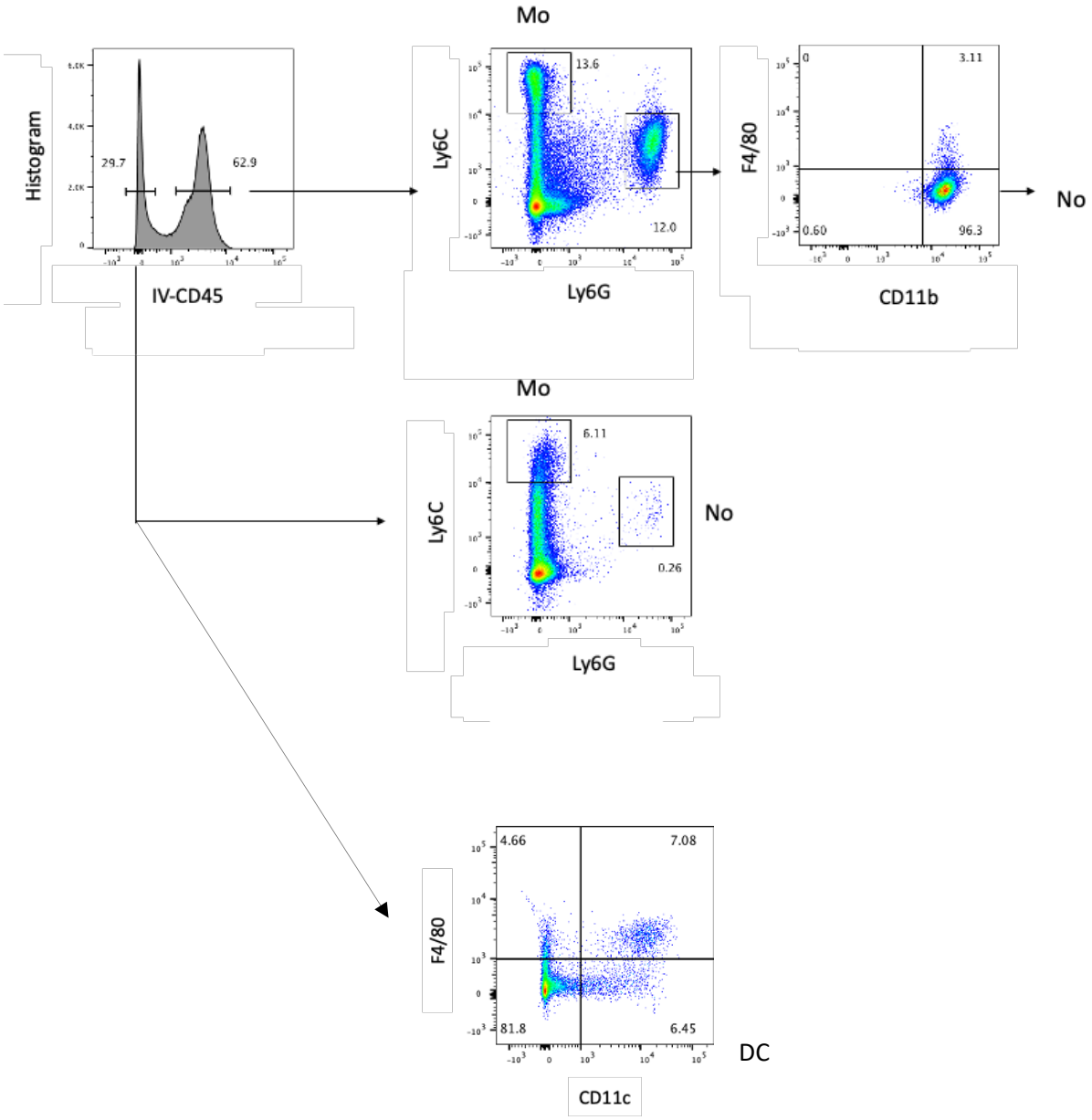


Figure 5-3: Lung immune cell composition.
Gating strategy to identify monocytes (*in vivo* CD45-, CD45+, LyG6-, Ly6C-high), neutrophils (*in vivo* CD45-, CD45+, Ly6G+, CD11b+, F4/80-), and dendritic cells (*in vivo* CD45-, CD45+, F4/80-, CD11c+) in murine lung tissue.

5.3 Alveolar macrophage depletion using clodronate liposomes causes local inflammation in the lung.

After identifying AM and other immune cell subsets in the lung by flow cytometry, I proceeded to optimize a method of AM depletion using clodronate liposomes (CLL). This would allow us to target their role during the influenza rechallenge. CLL is a common method used to selectively deplete macrophages, whereby liposome-encapsulated clodronate is transported into local macrophages by phagocytosis, and, after digestion, clodronate is released and induces cellular death. When administered intranasally or intratracheally, CLL has been used to deplete alveolar macrophages in the rat and in the mouse (214, 215). Intracellular accumulation of clodronate (dichloromethy-lene-bisphosphonate) disrupts the formation of adenosine triphosphate (ATP) within the mitochondria, generating a cytotoxic analog, thus causing cellular apoptosis (216). On its own, it does not easily cross cell membranes and has an extremely short half-life in circulation and body fluids; thus, it is encapsulated in liposomes – which are phagocytosed by macrophages. Lysosomal phospholipases within the macrophage then disrupt the phospholipid bilayers of the liposome, releasing the clodronate into the intracellular space. Intratracheal administration of CLL has a specific effect on alveolar macrophages among the different cell populations in the lung, as the liposomes are unable to cross vascular barriers formed by capillary walls (217) to impact interstitial cells. However, due to the ongoing apoptosis of AM during the course of CLL treatment, this therapy often induces low levels of local inflammation (214). To minimize potential ongoing effects of local inflammation induced from administering CLL, I split the full dose required for AM depletion into four smaller doses over the course of 1 week prior to the rechallenge. Thus, I administered CLL intranasally twice on day -6 and twice on day -3 prior to rechallenge (day 0). I was unable to

extend the doses further apart as the AM population began to recover when attempted. **Figure 5-4** shows that this regiment of CLL causes selective depletion of AM, dropping an average of 80%, from over a million cells recovered per lung to less than 200,000. In contrast, the frequencies of neutrophils and dendritic cells in the lung increased after CLL treatment, with neutrophils increasing 4 to 5-fold, from an average of ~40,000 to ~180,000, and dendritic cells doubling from ~33,000 to ~60,000. These increases in cell counts suggest a local inflammatory response due to AM apoptosis.

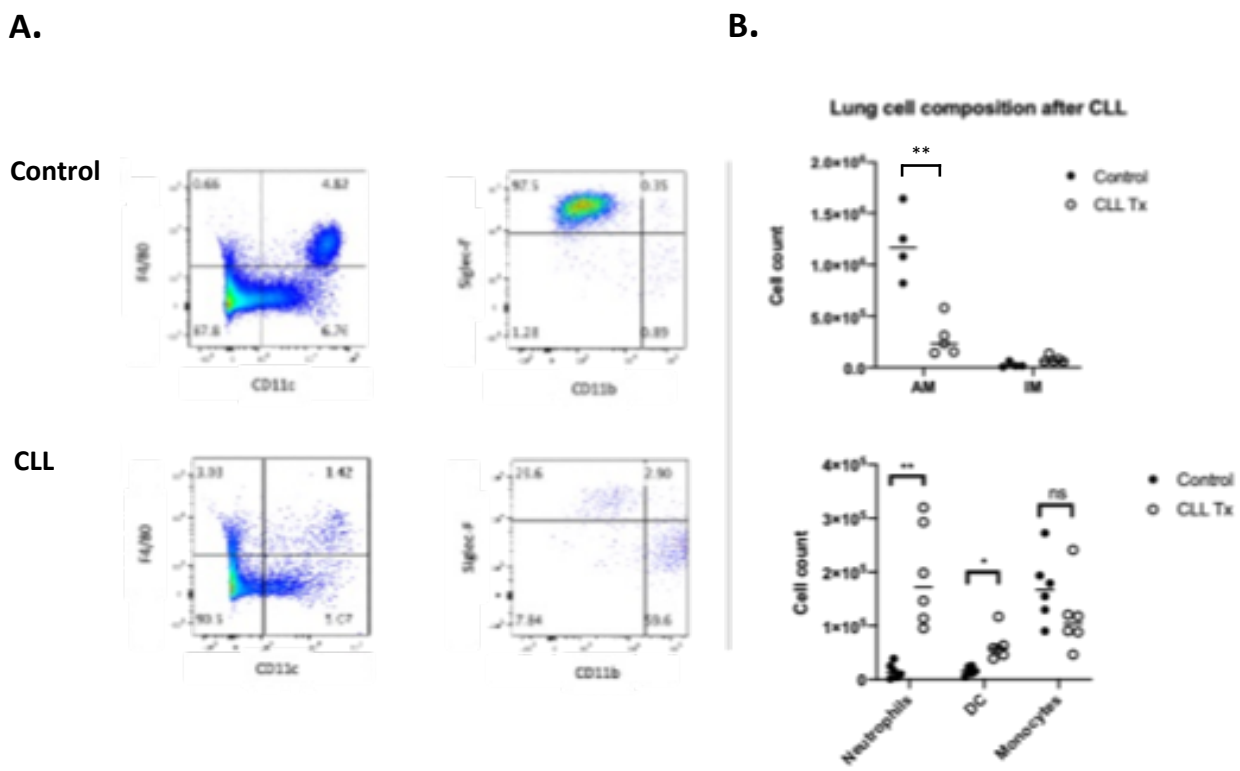


Figure 5-4: Lung immune cell composition after CLL treatment.
A. Gating strategy to identify AM in PBS-control and CLL-treated conditions (as in Figure 5.1). B. Quantification of lung cells with PBS-control and CLL-treated conditions (gating strategies as in Figure 5.2). Unpaired t-test. **p<0.01; *p<0.05. Data are pooled from 2 independent experiments, with 4-6 mice per experiment.

To attempt a longer-term AM depletion strategy that would enable Brm-tracking as with BAT reporter mice, I searched for a genetic model constituting an AM-inducible knockout strategy. *LysM*$^{Cre+}$ *Clec4a2*$^{flox/DTR}$ mice are available in our institute and have been shown to selectively deplete AMs in the lung, leaving other pulmonary subsets of myeloid cells intact (218). CLEC4A2 is expressed in several tissue-resident macrophages, including alveolar macrophages and conventional dendritic cells. The *Clec4a2*$^{flox/DTR}$ strain carries a construct containing diphtheria-toxin receptor (DTR) upstream of the *Clec4a2* gene. Importantly, while Clec4a2 is also expressed on DCs, LyzM is restricted to myeloid cells (218). Thus, LyzM^{Cre+} activity allows selective expression of the diphtheria toxin receptor (DTR) in Clec42a^{+} myeloid cells, but not Clec42a^{+} DCs (218). Upon DT injection, AM are depleted in *LysM*$^{Cre+}$ *Clec4a2*$^{flox/DTR}$ mice, leaving interstitial macrophages and monocytes intact (which express LyzM but not Clec42a) (218).

My purpose was to establish a model wherein Brm and PCs could be visualized during genetic ablation of alveolar macrophages. A simple breeding cross between BAT and *LysM*$^{Cre+}$ *Clec4a2*$^{flox/DTR}$ mice was not feasible, granted the number of gene loci involved; thus, I performed shielded irradiations of *LysM*$^{Cre+}$ *Clec4a2*$^{flox/DTR}$ recipients and reconstituted them with BAT donor bone marrow. It was necessary to shield the chest of the recipients with lead plates during irradiation to protect the alveolar macrophages residing there (a self-renewing population of cells) so that their sensitivity to diphtheria toxin-inducible knockout be retained (and not be replaced by wildtype bone-marrow derived donors). I then waited eight weeks after irradiation to infect intranasally with influenza virus to establish memory lymphocytes and waited another 35 days prior to administering DT to assess ablation of alveolar macrophages prior to rechallenge. **Figure 5-5** illustrates that depletion of alveolar macrophages using this strategy was only partially

effective. In the first replicate (panel Rep #1), an obvious population of F4/80+, CD11c+, SiglecF+ alveolar macrophages are still apparent after DT injection. Furthermore, a CD11c-low F4/80+ SiglecF+ population of macrophages appears to be enriched. In the second replicate (panel Rep #2), the alveolar macrophage population is depleted, yet the same CD11c-low F4/80+ SiglecF+ population of macrophages appears to be enriched. Potentially, these effects are due to the AMs being partially replenished by BAT monocytes after primary infection or after DT administration. Repeats of these experiments were completed separately by Dr. Andrew Maclean, with similarly mixed results.

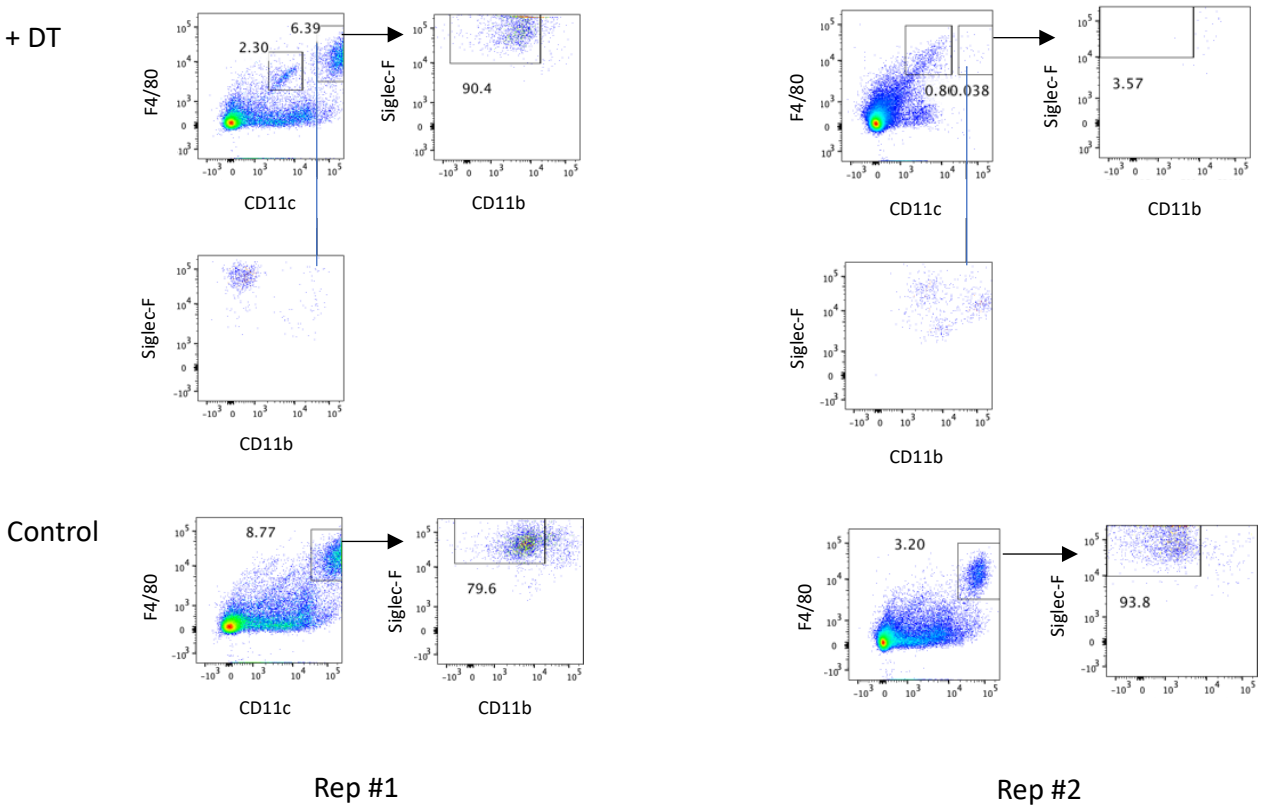


Figure 5-5: Lung macrophage composition in memory state LysMCre+ Clec4a2flox/DTR recipient/BAT donor chimeras after DT administration.
A. *LysM*$^{Cre+}$ *Clec4a2*$^{flox/DTR}$ mice underwent chest-shielded irradiations and were reconstituted with BAT donor bone marrow. 8 weeks later, they were infected with X31 influenza virus intranasally. 35 days later, they received three intraperitoneal injections of saline (control) or DT in a week. Lungs were collected and stained for pulmonary macrophages (AM cells are identified as live, singlets, CD45+, F4/80+, CD11c+, CD11b-low, SiglecF+ cells). Data is from 2 independent experiments, with 2 mice (1/treatment group) per experiment.

To avoid an uncharacterized lung macrophage population potentially interfering with the rechallenge response, we proceeded with using CLL as a method to deplete alveolar macrophages prior to rechallenge to assess their role in mediating Brm migration after rechallenge. **Appendix 2, Figure 1A-1C**, portrays experiments completed in parallel by Dr. Andrew MacLean, which reveal that after CLL treatment, Brm no longer accumulated at infected sites, nor increased their speed within 24 hours after rechallenge, as visualized via 2-photon live-imaging. AM depletion via CLL also corresponded with a greater than 50% reduction in the ratio of anti-influenza IgG present in bronchoalveolar lavage (BAL) relative to the serum by day four post-rechallenge (157). This indicates that local production of anti-virus IgG in the lung parenchyma is significantly impaired in the absence of AM during rechallenge.

5.4 Alveolar macrophages orchestrate Brm cell accumulation at infected sites via activation of CXCR3 ligands early after re-infection.

As we observed that blocking GPCR signaling during rechallenge (by administering pertussis toxin) abrogated the ability of Brm to cluster at sites of infection after rechallenge, we hypothesized that re-localization of Brm cells to infected sites is an active process that is likely regulated by the engagement of chemotactic receptor(s). Furthermore, alveolar macrophages are known to produce inflammatory CC chemokines (CCL2, CCL3, CCL5, and CCL11) and interferon–responsive chemokines (CXCL1, CXCL8, CXCL9, and CXCL10) (199) in response to IAV infection, in line with a role as recruiters of immune cells. To begin identifying potential chemokines produced by AMs in response to rechallenge that may direct Brm migration and accumulation at sites of infection, I performed qPCR of selected genes within sorted AM (gating strategy as in **Figure 5-2A**) 24 hours post-rechallenge. I initially focused on *Cxcl9* and *Cxcl10* (the ligands of CXCR3), as well as *Ccl3* and *Ccl5* (the

ligands of receptors CCR1 and CCR5), and *Ccl21/Ccl19* (the ligands of CCR7). These candidate pairs were chosen based on the receptor being expressed by the Brm population. I found no significant differences in the mRNA expression of the ligands at this time-point (**Figure 5-6**), other than *Ccl19* being downregulated approximately by half. *Ccl3* mRNA was expressed the most highly relative to all other targets; however, the levels of expression remained similar before and 24 hours after rechallenge. The high level of *Ccl3* mRNA expression relative to β-actin during the resting state requires follow-up for validation at the protein level.

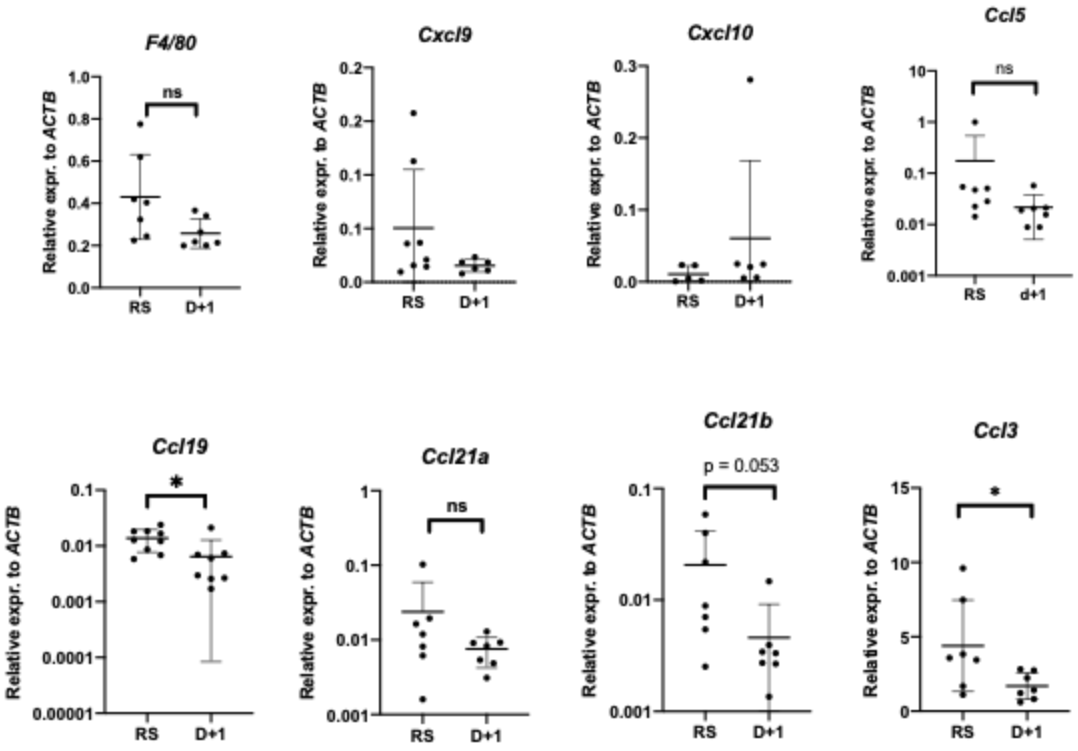


Figure 5-6: Quantitative PCR analysis of sorted AM 24 hours post-rechallenge.
10,000 AM from lungs of infected mice were sorted by FACS at resting state and 1 day post rechallenge and subjected to qPCR. AM were sorted as live i.v. label- CD45+ F4/80+ CD11c+ CD11b-low, SiglecF-high. Shown are gene expression values relative to β-actin pooled from 3 independent experiments (2-3 mice per group; replicates with housekeeping gene Ct values of greater than 25 were excluded). Mann Whitney U test performed on $2^{-\Delta Ct}$ values. *p<0.05.

As we already observed Brm accumulation at infected sites by 24 hours, it was possible that AM initiated very early signaling cues only hours after rechallenge that were no longer present by 24 hours. To better capture the potential early signals emitted by these cells mediating Brm migration, I performed bulk RNA sequencing of sorted AM at 6hrs, 12hrs, and 18hrs after reinfection (10,000 cells per sample). I applied two different count normalization methods separately, prior to differential expression (DE) analysis by DESeq2, and compared the results. The first, called trimmed mean of M values (TMM), uses the weighted trimmed mean of the log expression ratios and is appropriate for evaluating both inter- and intra- sample variance (219). The alternate method, median of the ratios (MR) for DESeq2, accounts for sequencing differences in library size and RNA composition of samples, making it a suitable method to use when comparing between samples, but does not account for differences in gene length, making it unsuitable for within-sample comparisons (220). Correlation analysis within samples (TMM-normalized counts) demonstrated that one technical replicate from the 12-hour timepoint was dissimilar to its counterparts (**Figure 5-7**). This sample also had significantly lower percent alignment to the genome relative to other samples (data not shown), as observed during sequencing quality control checks; therefore, downstream differential gene expression analysis was performed both with and without this sample for comparison. The reason for the relatively low quality of this sample is likely due to RNA degradation during isolation and sample processing. DE analysis from counts normalized using median ratios (MR) for DESeq2 revealed 282, 306, and 334 differentially expressed genes at 6hr, 12hr, and 18hr, respectively, with an adjusted p-value (FDR) < 0.05 (**Appendix 3, Table 1**).

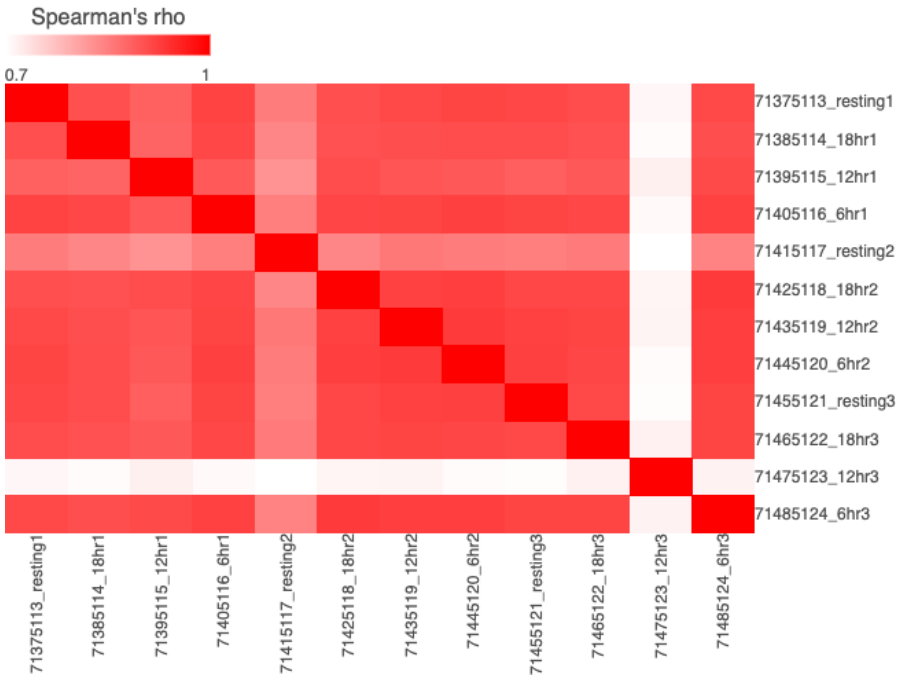


Figure 5-7: AM bulk-sequencing sample similarity.

Symmetrical heatmap visualization of bulk RNA-seq correlation matrix showing inter-sample Spearman coefficients (r_s) between AM samples sorted from lung at 6, 12, and 18 hrs post-rechallenge. Scale bar represents the range of the correlation coefficients displayed.

Interestingly, pathway analysis on MR-normalized genes (via gene set enrichment analysis, or GSEA) revealed the three timepoints to have characteristically different signatures (**Table 5-1**). At 6 hours, only pathways associated with mitochondrial translation are enriched, however at 12 hours, many more chemokine and cytokine pathways were enriched, including interferons (type I and type II), cell-cycle p53-independent DNA damage response pathways, apoptosis/programmed cell death, IL-10 and non-canonical NF-kB signaling, and GPCR signaling (to highlight a few). Remarkably, none of these gene pathways appeared enriched by 18 hours post-infection, suggesting either a very rapid and temporary response to IAV infection by the AMs, or, ensuing to the programmed cell-death of AMs at 12hrs, it could imply that the infected/responding macrophages present at 12 hours may be dying at 18hrs, and thus not included in the later sorts and RNA isolation.

6 hr

Pathway name	Entities found	Entities Total	Entities ratio	Entities pValue	Entities FDR
Defective MPI causes MPI-CDG	1	2	0	4.52E-5	1.05E-1
Mitochondrial translation elongation	88	94	0.006	2.67E-4	1.59E-1
Mitochondrial translation	94	102	0.007	3E-4	1.59E-1
Formation of tubulin folding intermediates by CCT/TriC	18	30	0.002	3.01E-4	1.59E-1
Mitochondrial translation initiation	88	96	0.006	3.43E-4	1.59E-1
Mitochondrial translation termination	88	94	0.006	6.97E-4	2.7E-1

12 hr

Pathway name	Entities found	Entities Total	Entities ratio	Entities pValue	Entities FDR
Interferon alpha/beta signaling	86	188	0.012	2.74E-14	6.36E-11
Interferon gamma signaling	109	250	0.017	9.58E-10	1.11E-6
Eukaryotic Translation Elongation	92	102	0.007	4.34E-9	2.46E-6
Peptide chain elongation	89	97	0.006	5.14E-9	2.46E-6
Regulation of expression of SLITs and ROBOs	157	183	0.012	5.31E-9	2.46E-6
Interferon Signaling	227	394	0.026	1.39E-8	5.26E-6
Viral mRNA Translation	89	114	0.008	1.59E-8	5.26E-6
SRP-dependent cotranslational protein targeting to membrane	111	119	0.008	2.29E-8	6.64E-6
Nonsense Mediated Decay (NMD) independent of the Exon Junction Complex (EJC)	94	101	0.007	2.99E-8	7.69E-6
Eukaryotic Translation Termination	92	106	0.007	9.13E-8	2E-5
Formation of a pool of free 40S subunits	101	106	0.007	9.42E-8	2E-5
Selenocysteine synthesis	93	112	0.007	1.4E-7	2.7E-5
Selenoamino acid metabolism	112	180	0.012	1.54E-7	2.74E-5
Signaling by ROBO receptors	192	235	0.016	1.84E-7	3.04E-5
Vif-mediated degradation of APOBEC3G	53	56	0.004	2.63E-7	3.82E-5
Cap-dependent Translation Initiation	119	130	0.009	6.22E-7	6.87E-5
Nonsense-Mediated Decay (NMD)	115	124	0.008	8.05E-7	7.88E-5
Nonsense Mediated Decay (NMD) enhanced by the Exon Junction Complex (EJC)	115	124	0.008	8.05E-7	7.88E-5
L13a-mediated translational silencing of Ceruloplasmin expression	111	120	0.008	8.16E-7	7.88E-5
Response of EIF2AK4 (GCN2) to amino acid deficiency	108	115	0.008	1.06E-6	9.48E-5
Vpu mediated degradation of CD4	51	53	0.004	1.1E-6	9.48E-5
Regulation of ornithine decarboxylase (ODC)	51	51	0.003	1.1E-6	9.48E-5
Regulation of activated PAK-2p34 by proteasome mediated degradation	50	50	0.003	1.17E-6	9.68E-5
Degradation of AXIN	54	57	0.004	1.67E-6	1.34E-4
Metabolism of polyamines	57	80	0.005	2.08E-6	1.58E-4
Autodegradation of the E3 ubiquitin ligase COP1	51	54	0.004	2.18E-6	1.58E-4
p53-Independent G1/S DNA damage checkpoint	52	54	0.004	2.31E-6	1.58E-4
Ubiquitin Mediated Degradation of Phosphorylated Cdc25A	52	54	0.004	2.31E-6	1.58E-4
p53-Independent DNA Damage Response	52	54	0.004	2.31E-6	1.58E-4
Hh mutants are degraded by ERAD	55	61	0.004	2.49E-6	1.65E-4
Stabilization of p53	55	59	0.004	2.64E-6	1.7E-4
Interleukin-10 signaling	63	86	0.006	3.21E-6	2.01E-4

12 hr continued...

Pathway name	Entities found	Entities Total	Entities ratio	Entities pValue	Entities FDR
Regulation of IFNG signaling	14	16	0.001	9.7E-5	2.78E-3
APC/C:Cdc20 mediated degradation of Securin	68	68	0.005	1.1E-4	3.11E-3
Programmed Cell Death	191	238	0.016	1.21E-4	3.39E-3
Defective MPI causes MPI-CDG	1	2	0	1.41E-4	3.89E-3
CLEC7A (Dectin-1) signaling	100	120	0.008	1.51E-4	4.07E-3
NIK-->noncanonical NF-kB signaling	59	61	0.004	1.57E-4	4.15E-3
Assembly of the pre-replicative complex	105	114	0.008	1.58E-4	4.15E-3
Translation initiation complex formation	58	62	0.004	1.73E-4	4.5E-3
Cellular response to starvation	157	176	0.012	1.79E-4	4.61E-3
Cytoprotection by HMOX1	118	158	0.01	2.05E-4	5.22E-3
MAPK6/MAPK4 signaling	86	106	0.007	2.41E-4	6.08E-3
APC/C:Cdh1 mediated degradation of Cdc20 and other APC/C:Cdh1 targeted proteins in late mitosis/early G1	74	74	0.005	2.46E-4	6.08E-3
Activation of the mRNA upon binding of the cap-binding complex and eIFs, and subsequent binding to 43S	59	66	0.004	2.46E-4	6.08E-3
Signaling by NOTCH4	83	92	0.006	2.54E-4	6.19E-3
Host Interactions of HIV factors	127	151	0.01	3.17E-4	7.65E-3
Apoptosis	161	192	0.013	3.52E-4	8.42E-3
OAS antiviral response	8	15	0.001	3.63E-4	8.6E-3
Host Interactions of HIV factors	127	151	0.01	3.17E-4	7.65E-3
Apoptosis	161	192	0.013	3.52E-4	8.42E-3
OAS antiviral response	8	15	0.001	3.63E-4	8.6E-3
FCERI mediated NF-kB activation	80	175	0.012	4.6E-4	1.08E-2
Signaling by GPCR	23	871	0.058	3.09E-3	8.04E-2

18 hr

Pathway name	Entities found	Entities Total	Entities ratio	Entities pValue	Entities FDR
Platelet degranulation	9	141	0.009	8.15E-5	2.87E-2
Response to elevated platelet cytosolic Ca2+	9	148	0.01	1.17E-4	2.87E-2
Platelet activation, signaling and aggregation	12	293	0.019	3.55E-4	4.7E-2
Ethanol oxidation	4	28	0.002	4.57E-4	4.7E-2
Hemostasis	22	803	0.053	4.8E-4	4.7E-2
Extracellular matrix organization	12	329	0.022	9.69E-4	7.85E-2
Peptide ligand-binding receptors	9	203	0.013	1.12E-3	7.87E-2
EGR2 and SOX10-mediated initiation of Schwann cell myelination	4	39	0.003	1.55E-3	9.45E-2
Glutathione conjugation	5	68	0.005	1.75E-3	9.47E-2

Table 5-1: Gene pathway analysis of differentially expressed genes from AM sorted at 6, 12, 18 hours after rechallenge.

Top biological pathways upregulated in mouse alveolar macrophages sorted at 6, 12, and 18 hours post-rechallenge compared with resting state alveolar macrophages, as revealed by significantly enriched corresponding gene sets in the GO database. All gene sets are significant at P <0.05 and FDR <0.25.

Inspecting the GPCR ligands enriched at 12hours more closely, I identified several chemokines differentially expressed at 12 hours (**Figure 5-8**), including *Cxcl9*, *Cxcl10*, *Ccl9*, *Ccl4*, and *Ccl2* (analysis performed with DESeq2), and interferons (α, β, γ). This suggested AM may recruit Brm towards infected alveoli via induction of CXCL9 and CXCL10, causing chemotaxis of Brm via the receptor CXCR3 for these two chemokines. **Appendix 2, Figure 1 (D-E)**, portrays experiments completed in collaboration by Dr. Andrew MacLean, which reveal that antibody blockade of CXCR3 one day prior to rechallenge with influenza virus leads to a reduction in the accumulation of Brm cells in infected sites, with only a modest 1.2-fold increase of density in these regions after re-infection (compared with >2-fold increase in the control group). Thus, the activation of the chemokine receptor CXCR3 plays an important role in mobilizing Brm cells to sites of infection.

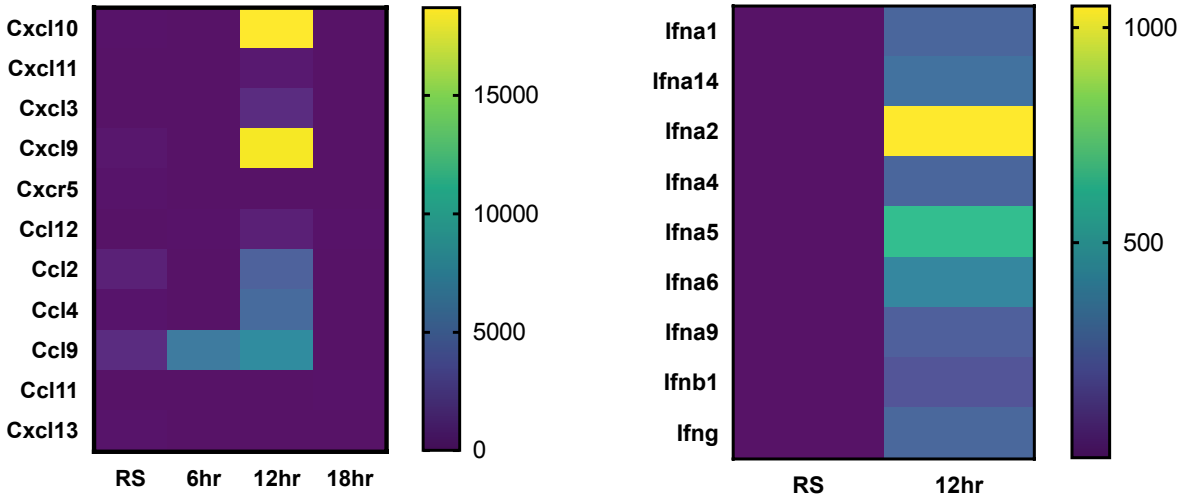


Figure 5-8: Bulk RNA-sequencing of AM at 6, 12, 18 hours post-rechallenge reveals changes in select cytokines and chemokines.

Heatmap of select differentially expressed genes with an adjusted p-value (FDR) < 0.05, from sorted alveolar macrophages at (left) resting state, 6, 12, and 18 hours post-rechallenge with X31 influenza virus, and (right) resting state and 12 hours (targets not detected at 6 or 18 hours).

5.5 Discussion

In this chapter I investigated the potential role of alveolar macrophages in mediating Brm mobilization and accumulation at infected sites during influenza rechallenge. It was important to first be able to identify AM to study them. As expected, I observed AM to be highly autofluorescent cells, in particular upon excitation by the continuous-wave 488 nm (cyan) laser (as detected within the FITC emission spectra, **Figure 5-2 B**) and the 561 nm (yellow-green) laser (as detected within the PE emission spectra, **Figure 5-2 C**). Because AM were not obviously autofluorescent within the APC channel (excited by the 633 laser and emission peak at 660nm), it suggests that longer, far-red fluorochromes are most suitable for staining and identifying these cells. While this finding has been previously reported (206), to my knowledge, it has not been considered while evaluating the effectiveness of *in-vivo* labeling lung compartments (178, 221). Future studies interested in distinguishing pulmonary macrophages within the interstitial versus circulation-exposed compartments with the use of an *in-vivo* administered antibody label could benefit from careful consideration for the choice of which conjugated fluorochromes to use.

To assess the role of alveolar macrophages in mediating Brm migration, I evaluated the efficacy and side effects of administering CLL intranasally. The technique was effective at depleting alveolar macrophages and caused infiltration and/or expansion of neutrophils and dendritic cells within the lung. This is an unwanted side effect of the treatment and may influence concurrent immune responses to influenza virus infection. Yet, as influenza virus infection is known to recruit neutrophils and dendritic cells into the lung from circulation (207, 209), their presence within the lung in advance of IAV infection may arguably promote a more rapid chemokine response to infection. At the same time, ongoing apoptosis of AM and recruitment of innate immune cells into the lung after CLL treatment suggests that

dying AM are releasing cytokines and chemokines into the alveolar space, which may interfere and/or compete with later signals induced from viral infection. Of note, the lung architecture is shown to remain intact and undamaged after intratracheal administration of CLL (222), suggesting it does not cause structural damage to the lung epithelium or vasculature. To better evaluate the potential impact of CLL on lung homeostasis, it could be useful to look for changes (e.g., transcriptomic signatures) in type I and type II epithelial cells after CLL treatment and prior to rechallenge.

It is important to note that we do not investigate the chemokines emitted by the epithelium during rechallenge response, which is a limitation of our studies. The lung epithelium is well-characterized to be infected by IAV and capable of producing several cytokines and chemokines in response to IAV infection, including CXCL10, interferons, and IL-6 (223). In fact, both the airway and alveolar epithelium are reported to rapidly secrete cytokines and chemokines that activate and attract other immune cells to the lung within 3-24 hours after IAV infection, including IL-1β, IL-6, CXCL10, TGF-β, TNF-α, IL-8 and CCL2 (reviewed in (224)). Because many of these factors are also secreted by resident and recruited immune cells, it can be difficult to delineate the specific contribution of epithelial cells versus alveolar macrophages. It is suggested that temporal effects compound the response, with epithelial cells being an early source of cytokines, but the balance shifting by 24–48hrs to recruited and resident immune cells becoming the dominant producers.

While the generation of '*LysM*$^{Cre+}$ *Clec4a2*$^{flox/DTR}$ recipient:BAT donor chimeric mice was a partially effective technique for the depletion of alveolar macrophages in rechallenge conditions, the reduced sensitivity of AM to depletion by DT administration after primary infection could be explained by the replenishment of AM by circulating monocytes from donor bone marrow, which has been shown to constitute 55% of AM by 28 days after IAV

challenge (225). In future studies, it could be possible to assess the downstream effect of alveolar macrophage depletion on Brm differentiation into PCs in non-chimeric *LysM*$^{Cre+}$ *Clec4a2*$^{flox/DTR}$ mice by assessing BAL and serum antibody levels by isotype, via ELISA, at day four post-rechallenge with and without AM. Additionally, it could be an interesting system to assess the interplay of early inflammatory cues deriving from the non-hematopoietic compartment and or/from alveolar macrophages or other pulmonary myeloid cells by reconstituting DAMP or PAMP-deficient recipients with *LysM*$^{Cre+}$ *Clec4a2*$^{flox/DTR}$ bone marrow. For example, in macrophages and cDCs, downstream of dimerized TLR3 and TLR4, the MyD88-independent/TRIF-dependent pathway leads to the expression of IFN and ISGs (reviewed in(226)). If the architecture of the lung lacks TLR3 (*TLR3*$^{-/-}$ recipients) but the myeloid lineage does not (*LysM*$^{Cre+}$ *Clec4a2*$^{flox/DTR}$ donors), one could interrogate whether viral sensing by the epithelium, AM, or DCs is essential to propagate adaptive immune responses by selectively depleting AMs after reconstitution and before challenge to isolate the DC-derived TLR3 response (and comparing against WT or *TLR3*$^{-/-}$ lung architecture).

My results exploring the AM transcriptomic response to rechallenge infection suggest that AM upregulate interferon α/β/γ mRNA and *Cxcl9*, *Cxcl10*, *Ccl2,* and *Ccl4* expression around 12 hours after rechallenging but do not sustain this signature in a prolonged fashion, as by 18hrs post-infection none of these genes are upregulated at the mRNA level, and *Cxcl9* and *Cxcl10* are not enriched by qPCR relative to resting state AM by 24 hours post-infection. Furthermore, gene set enrichment analysis demonstrates that only at the 12-hour timepoint do AM portray an interferon response, apoptotic pathway enrichment, as well as IL-10 and NF-kB signaling enrichment. The propensity of alveolar macrophages to die after IAV infection is somewhat debated in the field. Some studies

demonstrate that AM are vastly depleted (~70%) within 3 days of primary IAV infection (227, 228) and yet others show that AM persist throughout infection with an alternate, less phagocytic phenotype (229, 230). Califano et al. demonstrate that this discrepancy can be explained by the genetic background of the mice, wherein BALB/c mice exhibit extensive IFN-γ-dependent reduction in numbers of alveolar macrophages following IAV infection, whereas alveolar macrophage levels in C57BL/6 mice are maintained throughout the course of infection while upregulating CD11b expression (231). Little is known about the levels of apoptosis in alveolar macrophages in the context of reinfection with IAV, yet within 24 hours post-rechallenge, I did not notice a significant reduction in the number of AM and was able to sort the same number of cells from resting state and day+1 rechallenged lungs. Granted our bulk sequencing results suggest an apoptotic signature disappears by 18hrs, and the C57BL/6 background of my mice, it is possible that only infected AM, or those phagocytizing high levels of viral load, will die in the context of rechallenge. It is possible that these same cells are activated within hours of infection and then die or that neighboring cells exposed to lower levels of IAV are activated yet persist after infection. To answer whether AM present at infected sites in the lung are phenotypically different from those at uninfected sites, I began to optimize the use of UBC-PA-GFP mice, wherein a photoactivatable variant of *Aequorea victoria* green fluorescent protein is under the regulatory control of the human ubiquitin C (UBC) promoter. Photoactivation of tissue upon two-photon irradiation (at ~720-840 nm), enables rapid, stable fluorescent labeling of living cells with microanatomical precision (39). In combination with the use of a CFP-expressing influenza strain, which permits labelling of infected cells with the fluorescent CFP protein (CFP-S-Flu), this strategy could enable the detection, photoconversion, and isolation of cells

specifically at sites of infection. Currently, the photoconversion of alveolar macrophages is not highly efficient – ongoing work will attempt to improve this technique.

CXCL9 and CXCL10 are well-characterized to mediate the recruitment of CXCR3-expressing lymphocytes and are also well-known to be induced by IFNy. Granted that antibody blockade of CXCR3 prior to rechallenge reduced but did not abolish the propensity of Brm to accumulate at sites of infection, it is likely that additional mechanisms are important for the recruitment of Brm at sites of infection. Furthermore, as the AM-derived chemotactic signature disappears by 18 hours post-rechallenge, we propose that other recruited cells may propagate Brm activation and differentiation throughout the IAV response. Given that neutrophils, NK cells, monocytes, DCs, and T cells are all known to respond to IAV and to both reside within and infiltrate the lung tissue during influenza infection, we decided to take a broader approach and to investigate signaling events downstream of alveolar macrophages, that may be responsible for maintaining the Brm response, in the next chapter.

6 Results III: Identifying cellular mechanisms that act downstream of AM to induce Brm migration to infected sites.

6.1 Introduction

In the previous chapter, I begin to explore the role of alveolar macrophages in mediating Brm accumulation at sites of infection. Bulk RNA-sequencing reveals that interferons and *Cxcl9/10* chemokines are transcriptionally upregulated at 12 hours post-rechallenge, which may act directly on CXCR3-expressing Brm – however, this transcriptional signature is lost in alveolar macrophages by 18 hours. During primary influenza infections, innate leukocytes, including neutrophils, monocytes, and NK cells, are rapidly recruited into the lung – while there is limited literature on recruitment during secondary exposures, it is possible that these same lineages are recruited early after rechallenge and may propagate the response initiated by infected cells and alveolar macrophages, to stimulate Brm accumulation at infected sites.

Leukocyte trafficking from the circulation into the alveolar spaces of the lung occurs across alveolar capillaries lined with elongated and flattened endothelial cells. These capillaries can be smaller in diameter than leukocytes (232), leading to slow transit times and a large number of marginated immune cells capable of crossing the endothelium into the parenchyma in response to chemotactic cues released within the alveoli (reviewed in(233)).

During primary influenza infections, neutrophils mobilize into inflamed sites of the lung in a multi-step process, involving initial arrest in the capillaries and subsequent migration across the endothelium, extracellular matrix, and epithelium. Chemokines mediate recruitment at every step by forming gradients that involve glycosaminoglycan

interactions (234). Several chemokines and growth factors have been identified as mediators of neutrophil recruitment during influenza infections, including CXCL1, CXCL2, CCL3, CXCL4, and granulocyte-colony stimulating factor (G-CSF) (207, 235-238). Cells of the hematopoietic compartment, including lung alveolar macrophages and interstitial macrophages, as well as the epithelium and endothelium, are known to produce neutrophil-attractant chemokines and growth factors. Once infiltrated to sites of inflammation, neutrophils contribute to viral clearance by phagocytosing dying virus-infected epithelial cells and macrophages, producing pro-inflammatory cytokines, and releasing granular peptides such as defensins (239). Neutrophils entrapped inside inflamed pulmonary vessels can also produce neutrophil extracellular traps (NETs) in a process termed 'NETosis', which are thought to capture viral particles and thereby restrict viral dissemination (240). They may also aggravate pathology via a feedforward inflammatory circuit (241). Interestingly, human primary neutrophils isolated from peripheral blood exhibit NETosis in the presence of IgA–IAV virus immune complexes (ICs), while significantly less so after induction by IgG-ICs. This process occurs via the engagement of Fc alpha receptors (Fc-αRI) on neutrophils through a toll-like receptor-independent, NADPH oxidase complex–dependent pathway (242). However, only serum-derived monoclonal IgA-ICs can induce NETosis, not the secretory, dimeric IgA subclass (sIgA), suggesting that induction of NETosis is unlikely to occur in the airways in which sIgA is enriched but instead likely takes place primarily in the lung tissue and vasculature, to trap and inactivate viruses if they've crossed through the mucosal barrier and into the parenchyma.

Interestingly, in LPS-induced inflammation, the accumulation of neutrophils within the parenchyma and alveolar spaces is assisted by the presence of CCR2+ monocytes (243),

yet it is unclear whether they fulfil this facilitator function from the intravascular side of the pulmonary vessels or whether premigration or comigration of monocytes with neutrophils are required. Monocytes are recruited into the lung after influenza infection in a CCR2-dependent manner (228) that is also regulated by type I interferons (244). A portion of these inflammatory monocytes replace tissue-resident alveolar macrophages, while others differentiate into dendritic-like cells and exudate macrophages which both produce inflammatory chemokines, including CXCL9/10 and type I interferons, themselves (228).

Several subsets of lung dendritic cells (DC) respond during influenza infections, including the resident population of conventional DCs (cDC), newly recruited DC precursors from bone marrow, and newly differentiated DC-like cells originating from inflammatory monocytes. Dendritic cells phagocytose dying, infected epithelial cells and/or influenza virions, release inflammatory cytokines, and migrate through lymphatics to the draining and mediastinal lymph nodes, where they prime T cells. Recently, a conditional knockout mouse model of CCR2-expressing, fluorescently tagged, dendritic cells (*Clec9a*$^{Cre/+}$*Ccr2*$^{fl\text{-}eGFP/+}$ animals) demonstrated that pre-DCs are specifically recruited to infected foci of the lung from bone marrow in a CCR2-dependent manner, as ablation of CCR2 significantly reduced lung pre-DCs five days after primary infection while increasing the random distribution of remaining cells across the parenchyma (245). Interestingly, while the pulmonary epithelium produces the CCL2 ligand required for monocyte recruitment early after infection, by five days post-immunization, the primary CCL2-producing population is the monocytes, implying a positive feedback loop that attracts more monocytes and other immune cells.

Natural killer cells (NK) are also recruited to the lung during inflammation onset by influenza infection. IL-15, produced by both immune and non-immune cells of the lung, creates a chemotactic gradient that attracts NK and T lymphocytes by stimulating their

adhesion to vascular endothelium (246). Different subsets of NKs have distinct functions, either by secreting regulatory cytokines and chemokines on stimulation by IL-18 and IL-12 (CD56-high) (247) or by directly lysing infected cells via NKp44 and NKp46 receptors, which can directly bind to the glycoprotein haemagglutinin (HA) on the surface of influenza viruses (CD56-low) (248-250).

Effector and central memory T cells are also recruited to the lung during pulmonary infections and are much better characterized in the literature during recall infections due to their essential role in developing prime-boost vaccination strategies. Effector T cells infiltrate the lung between 3-5 days after recall influenza infection, where central memory T cells lag slightly behind and are found between 5-7 days after boost (251). As this time window falls much later than the immediate 24 hours after the rechallenge, it is not of immediate focus here in this chapter. Yet, lung tissue-resident memory T cells established after primary infection are indeed reactivated within 12-24 hours post rechallenge (252) and thus may contribute towards Brm responses upon rechallenge. Experiments performed in our group by Dr. Andrew MacLean demonstrate that plasma cell differentiation at infected alveoli four days after rechallenge is not dependent on CD40L, suggesting that Brm differentiation is primarily independent of T cell help (157).

Due to their reported infiltration into the lung tissue during influenza infections, I hypothesized that neutrophils, monocytes, and NK cells are downstream of alveolar macrophage-response to rechallenge but may also be involved with mediating the accumulation of Brm at infected sites by propagating interferon and cytokine signaling initiated by alveolar cells in response to influenza infection.

Objectives:

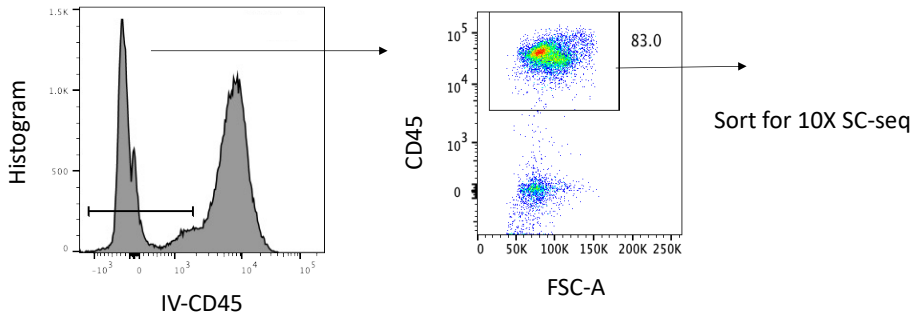
I. Identify infiltrating immune cells in the lung tissue 24 hours after rechallenge.

II. Detect signaling cues from infiltrating cells that may mediate Brm migration.

III. Determine whether the presence and transcriptional signature of infiltrating immune cells is impacted by the absence of alveolar macrophages.

6.2 Innate cells, including neutrophils, monocytes, and natural killer cells, infiltrate the lung tissue within 24 hours of rechallenge.

To understand whether recruited cells are propagating the Brm migratory response, we performed single cell RNA sequencing (scRNA-seq) on total lung hematopoietic (IV-negative, CD45+) cells, sorted from resting state (day 35 post-primary X31 influenza infection), rechallenged (day +1), and rechallenged plus CLL-treated (alveolar macrophage-depleted), wildtype mice (**Figure 6-1**). We aimed to identify inflammatory chemokines that are induced after rechallenge in an alveolar macrophage-dependent manner and which may attract Brm cells.



3 conditions

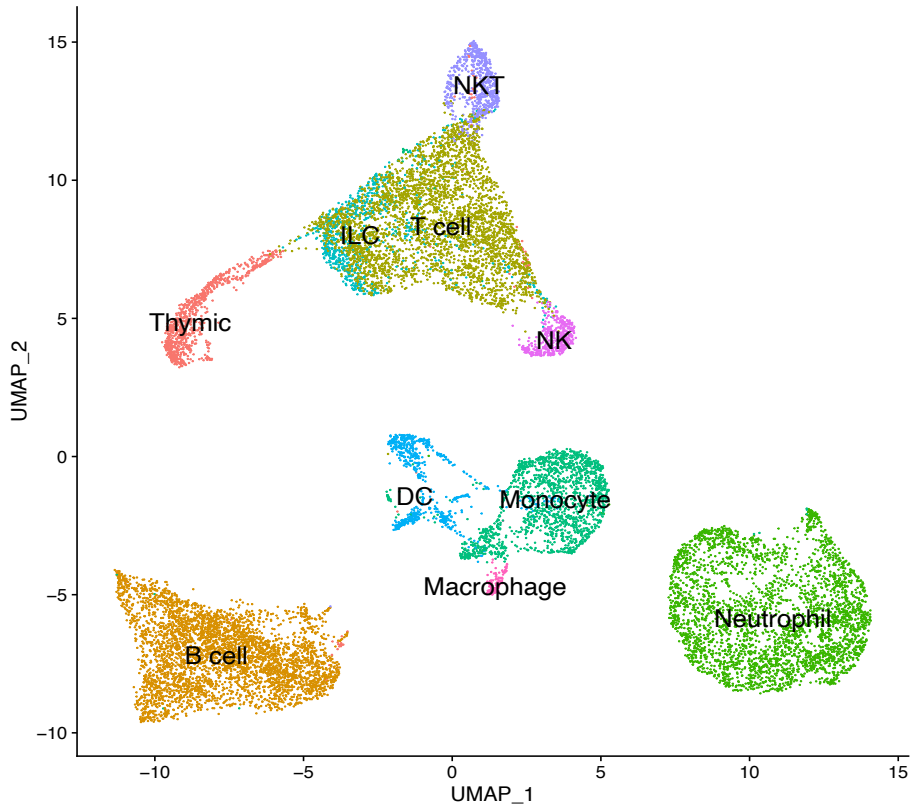
3 biological replicates	Condition_1: Not re-challenged	Condition_2: Re-challenged with the same virus	Condition_3: Treated with clodronate liposome + re-challenged	Sequencing pool
	A1 ♀(Mouse_1) C0301	B1 ♀(Mouse_2) C0302	C1 ♀(Mouse_3) C0303	Pool 1 (sorted on 8/12/2020)
	A2 ♀(Mouse_4) C0302	B2 ♀(Mouse_5) C0301	C2 ♀(Mouse_6) C0303	Pool 2 (sorted on 8/12/2020)
	A3 ♂(Mouse_7) C0301	B3 ♂(Mouse_8) C0302	C3 ♂(Mouse_9) C0303	Pool 3 (sorted on 10/12/2020)

Figure 6-1: Lung hematopoietic scRNA sequencing experimental set-up.
(Top) scRNA-seq sorting strategy of lung leukocytes (gated on live, singlets) isolated from B6 mice prior to rechallenge and 1 day post-rechallenge of PBS or CLL-treated mice. (Bottom) Animals and sample names per treatment condition. Approximately 20,000 cells per sample pool were loaded onto the 10X Genomics ChipK for sequencing.

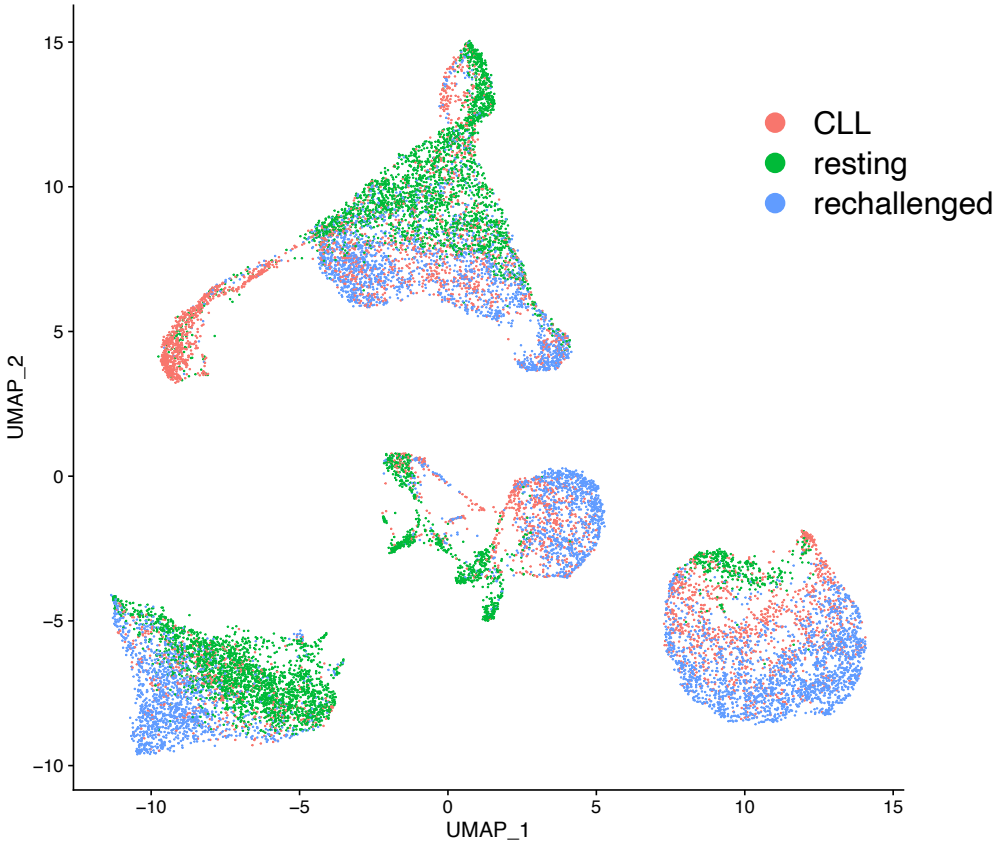
Sequence reads were mapped by our collaborators (Prof. Steve Sansom and Dr. Lada Koneva) using CellRanger multi (version 6.0.0) with the 10x mouse reference transcriptome (version 2020-A). Cells were demultiplexed using GMM-Demux (version 0.2.1.3) (Xin et al., 2020). I was provided with the output cell count and features matrix and used the world-renowned Seurat package to perform most steps of the sequencing analysis (253), along with SingleR and Celldex to annotate cells against the built-in ImmGen database reference, as has previously been described to perform lung single-cell sequencing analysis (254). After filtering out doublets and low-quality cells, as well as cells with high mitochondrial counts, and performing standard reads-normalization and scaling, I retained 16,238 cells for analysis

and estimated a principal component score of between 12-13 (via elbow plot). I identified 10 clear “main label” clusters, as visualized via the non-linear dimensional reduction technique, UMAP (**Figure 6-2A**). By keeping Seurat’s ‘FindCluster()’ resolution parameter fairly low (0.4), I did not attempt to further subset clusters of cells at this point. The use of the Celldex package compares the transcriptome of each individual cell against the normalized expression values of 830 microarray samples of pure mouse immune cells, generated by the Immunologic Genome Project (ImmGen), to annotate the identity of each cell. The ‘FindAllMarkers’ function of Seurat permits the identification of cluster biomarkers via differential expression. **Appendix 4, Table 1,** lists the top 20 markers distinguishing the clusters and used to annotate the cell identities of each cluster in parallel to the Celldex labels, as depicted in **Figure 6-2A.**

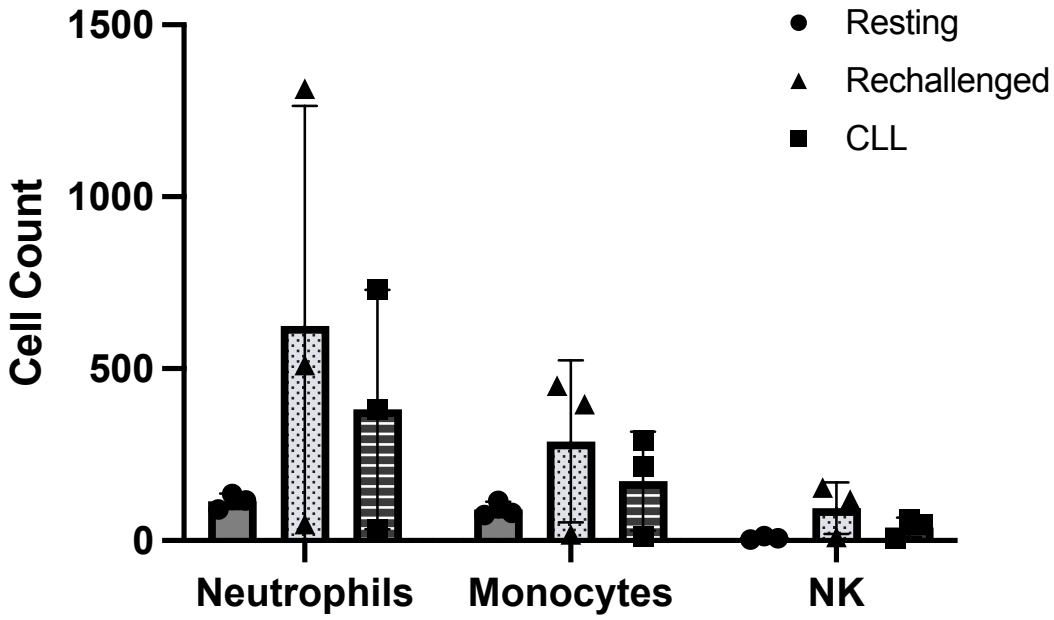
A.



B.


CLL
resting
rechallenged
UMAP_2
UMAP_1
15
10
5
0
−5
−10
−10
−5
0
5
10
15

C.


Resting
Rechallenged
CLL
Cell Count
1500
1000
500
0
Neutrophils
Monocytes
NK

D.

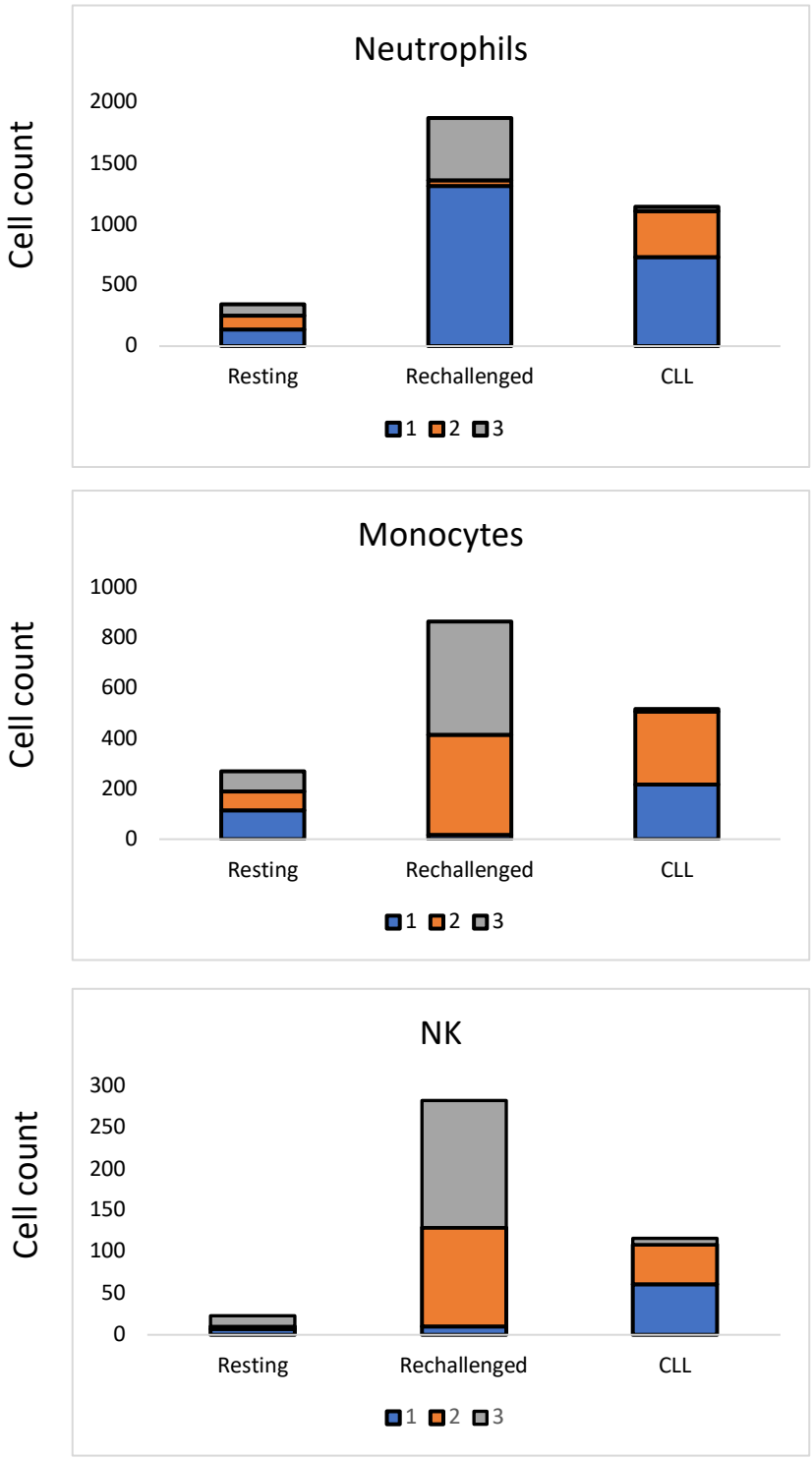


Figure 6-2: Changes in the cellular landscape of rechallenged mice in the presence and absence of alveolar macrophages.

scRNA-seq of lung leukocytes prior to rechallenge and 1 day post rechallenge of PBS or CLL-treated mice (treated as in Figure 6.1). (a) UMAP showing clusters of total cells detected under all 3 conditions combined. (b) UMAP showing total cells detected split by condition. (c) Cell counts of neutrophils, monocytes, and natural killer cells by experimental group (n=3 per group; Kruskal-Wallis one-way ANOVA). (d) Cell count data from (c) represented as individual replicate contribution to total cell count per group (split bar graph).

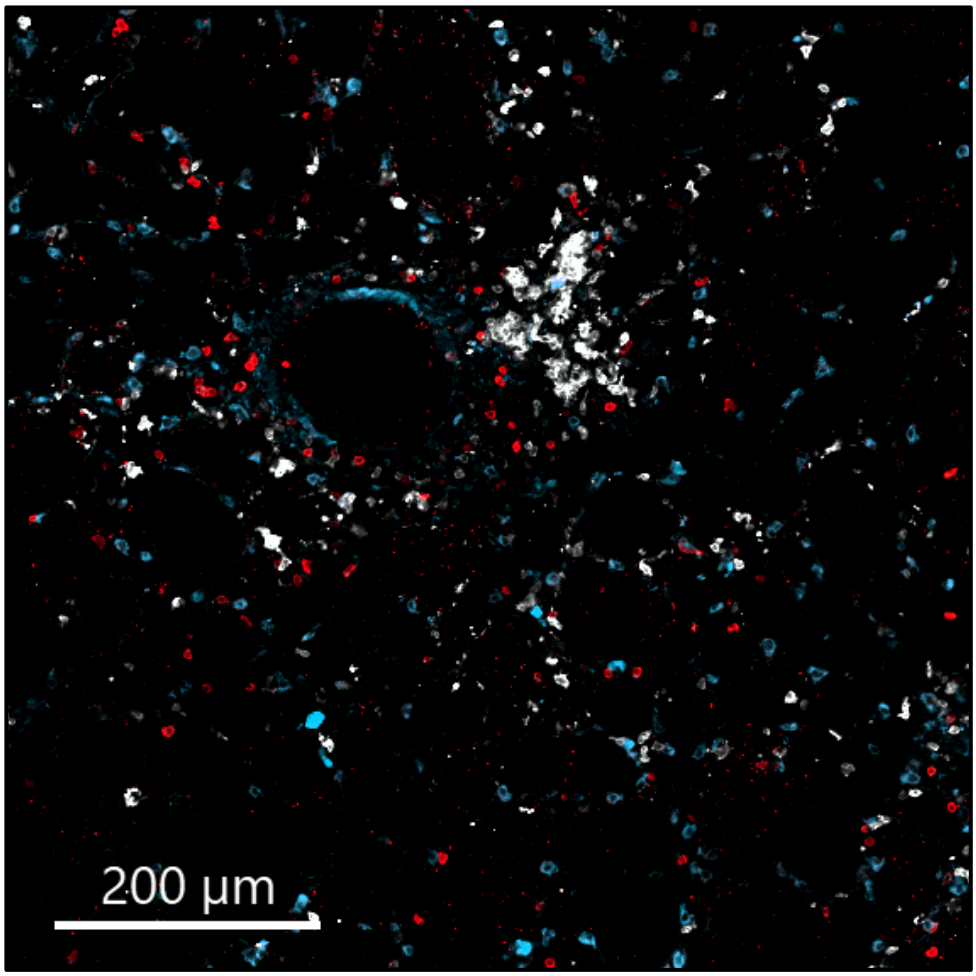
Visualization of the same UMAP plot, split by condition, illustrates that the monocyte, neutrophil, and NK clusters are dominant during rechallenged conditions and potentially reduced after the depletion of alveolar macrophages (**6-2-B**). I subclustered each of these populations to determine the cell count of individual replicates (annotated by their "sample_id" column in the matrix metadata) utilizing the data.table package in R with the following code:

```
> Mono <- subset(lung_f, idents = "Monocyte")
> Monod <- Mono@meta.data %>% as.data.table
> Monod[, .N, by = c("sample_id")]
        sample_id   N
1:          CLL_1 217
2:      resting_1 116
3: rechallenged_1  18
4: rechallenged_2 397
5:          CLL_2 290
6:      resting_2  74
7: rechallenged_3 451
8:      resting_3  81
9:          CLL_3  12
```

This portrayed considerable variability between sample replicates; thus, differences between conditions did not reach significance (**6-2-C/D**). Suppose we regard the infiltration of innate cells into the lung as a time-sensitive signaling cascade. In that case, subtle differences in collection times between replicates could result in the appearance of neutrophils over monocytes, for example. Additional work is needed to investigate the dynamics of potential cell "waves" after rechallenge infections. The thymic cluster was prevalent in one out of three samples in the CLL+rechallenge condition, most likely due to contamination of the sample during dissection and tissue collection. The number of T cells and B cells in each condition at this time point did not demonstrably differ. Yet, the shifted position on the UMAP likely reflects changes in the transcriptional programming of the cells under inflammatory conditions. To confirm the scRNA-seq analysis, I further assessed whether neutrophils and NK cells infiltrate the lung 24 hours after rechallenging via

histology. I utilized a fluorescently tagged influenza virus, CFP-S-Flu (143), to allow detection of infected areas of the lung – as the dispersion of intranasally administered solutions is not uniform across lung lobes (255, 256). CFP-S-Flu is a single-cycle fluorescent reporter strain of influenza A virus, the neuraminidase of which is encoded by the PR8 strain genes, and with a PR8 strain-derived H1 coating. The CFP fluorescent tag permits the detection of initially infected cells by the emission of CFP fluorescence. To identify neutrophils and NK cells in tissue sections, I performed immunofluorescence staining for CD177, a neutrophil-specific adhesion molecule upregulated during inflammatory conditions (257), and NKp46, an Ig-like transmembrane glycoprotein unique to NK cells (258) (**Figure 6-3A**). Confocal microscopy revealed that both NK cells and neutrophils are present in proximity to infected lung tissue within 24 hours of rechallenge (**Figure 6-3**). Neutrophils were observed to swarm within infected regions of the tissue (**Figure 6-3A**). In some cases, fine processes could be observed extending from infiltrating neutrophils, potentially indicating cells undergoing NETosis (**Figure 6-3B**), left panel). NK cells appeared in proximity to both infected cells and neutrophils.

A.



Nkp46 (NK cell) CD177 CFP-S-Flu (infected)

B.

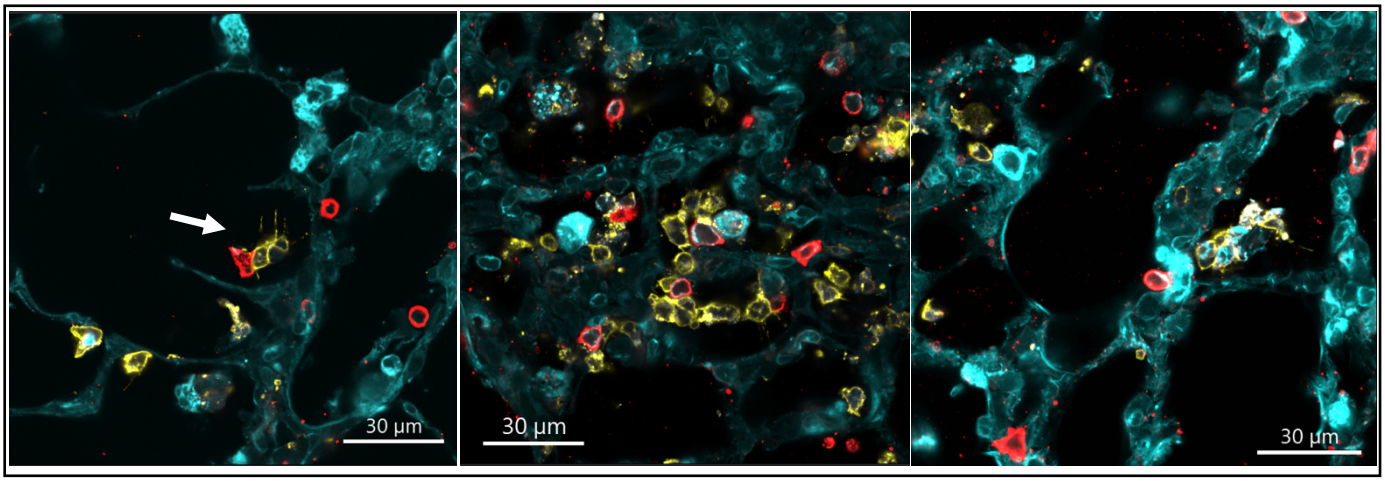


Figure 6-3: Neutrophils and NK cells are proximal to infected cells within 24 hours of rechallenge. Confocal microscopy of lung tissue sections from day +1 CFP-s-Flu-rechallenged mice, stained with anti-CD177 (white in A and yellow in B) and ant-NKp46 (red) to identify neutrophils and natural killer cells, respectively [25uM thick sections]. The white arrow points to potential NETosis.

Because the CFP-S-Flu does not replicate as the X31 virus (used for the scRNA-seq experiments) to infect neighboring cells, the localization of the NK and neutrophils observed may be unique to the single-cycle CFP-S-Flu infection. Without propagation of the influenza virus throughout the lung tissue, individual pockets of infected cells may recruit immune cells in a different pattern than expected with a larger, diffuse area of infection. Furthermore, because the surface antigens of the CFP-S-Flu are PR8-derived, rechallenge of X31 primed animals represents a heterotypic immunization. Therefore, we can conclude that neutrophils and NK cells are also recruited to the lung within 24 hours of infection in a heterotypic context (the scRNA-seq data being representative of a homotypic rechallenge).

6.3 Depletion of AM leads to selective loss of *Cxcl9* and C*xcl10* expression in neutrophils and reduced interferon-gamma transcription in natural killer cells.

Comparison of chemokine and cytokine gene expression via differential expression analysis in the CLL-treated and untreated rechallenged animals identified the reduction of *Cxcl10* and *Cxcl9* mRNA expression by neutrophils and monocytes (**Figures 6-4A, 6-5A**) after CLL treatment, which was confirmed by QPCR analysis (**Figure 6-4B**). Further analysis also showed that interferon-gamma (IFNγ), a potent inducer of CXCL10 and CXCL9, exhibited reduced mRNA expression in the lung NK of CLL-rechallenged mice (**Figures 6-4A, 6-5B**), suggesting that alveolar macrophages may be necessary for optimal activation of this pathway.

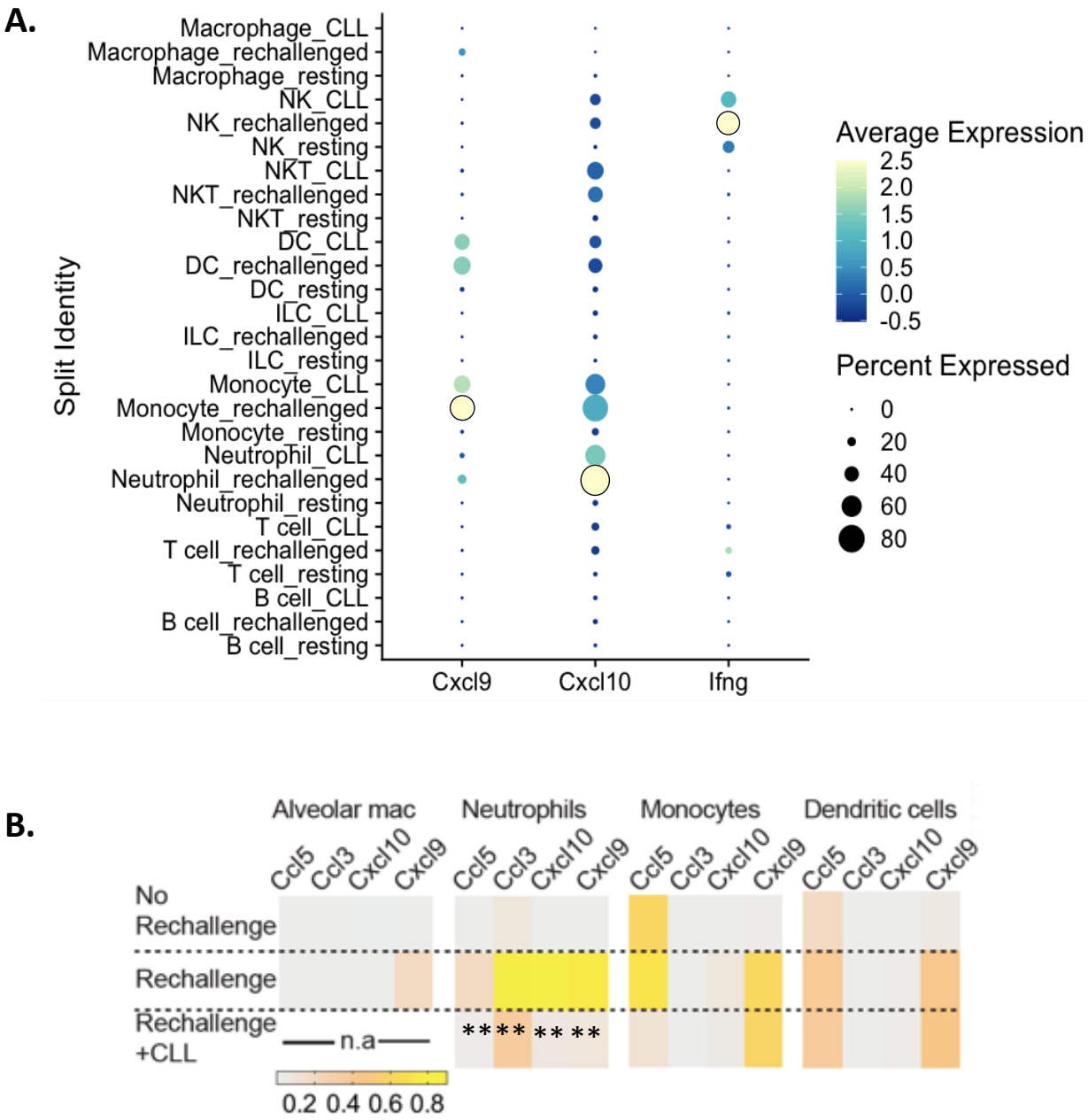


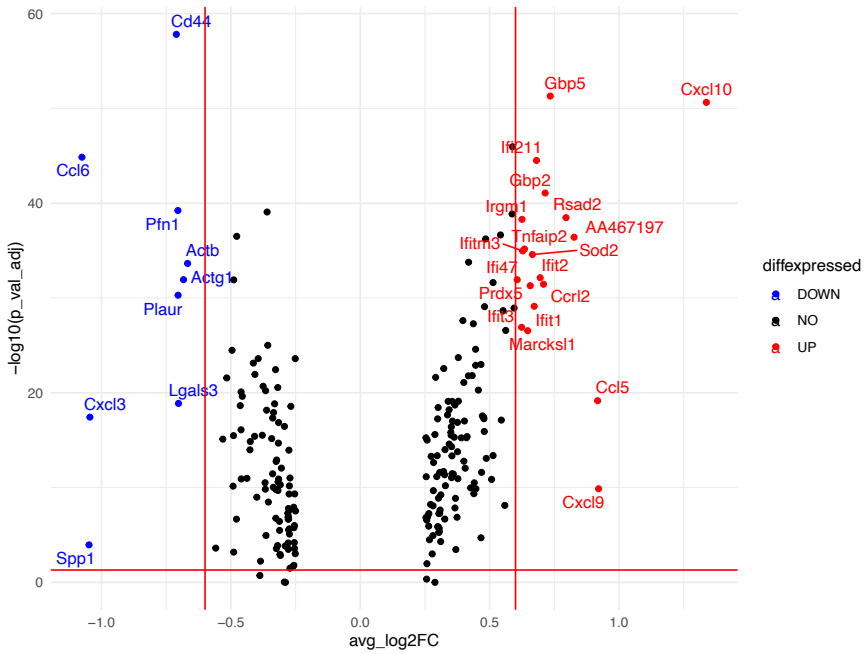
Figure 6-4: Infiltrating immune cells transcriptionally express IFNγ and CXCR3 ligands during rechallenge response in an alveolar macrophage-dependent manner.

A) Dot plot of expression of CXCR3 ligand-related genes in resting, rechallenged and rechallenged + CLL-treated lung hematopoietic cells. The size of the dots represents the fraction of the expressing cells in each cell population, and the color intensity represents the average expression level. B) Heatmap of qPCR data from the indicated cell subsets sorted from mice treated as in 'a'. Shows results of one of 2 independent experiments. The average expression from 3 biological replicates is shown. Statistical symbols indicate results of one-way ANOVA, comparison between 'Rechallenged CLL' and 'Rechallenged' groups.

Volcano plots (**Figure 6-5**) portray gene names of those with the greatest statistical significance versus magnitude of change (fold change), comparing the rechallenged condition to the rechallenged+CLL treatment group. Neutrophils (**6-5A**) exhibit 18 genes that are significantly upregulated in the rechallenge group by at least 1.5-fold compared to the alveolar macrophage-depleted group and nine down-regulated genes. Several interferon response genes, along with *Cxcl9* and *Cxcl10,* are among the most significantly differentially expressed, with *Cxcl10* being 3-fold more highly expressed in the untreated rechallenged condition compared to after alveolar macrophage depletion. Within the NK cell cluster, IFNγ, granzyme A and B exhibit significantly higher mRNA transcription (between 2-3-fold) in the rechallenged group compared to alveolar macrophage-depleted mice, suggesting reduced activation/inflammatory NK cell response in the absence of alveolar macrophages. Given the strong transcriptional induction of interferon-gamma observed in NK cells upon rechallenge, I hypothesized that neighboring cells could be directly responding to the cytokine, and in particular, those with a strong *Cxcl9/10* signature, as these two chemokines are well-characterized to be upregulated in response to interferon-gamma (IFNγ) (259, 260). I performed geneset analysis utilizing the published GSEA (Gene Set Enrichment Analysis) hallmark IFNγ response geneset (containing a list of genes upregulated in response to interferon-gamma) and obtained AUC scores for each individual cell across conditions, thereby estimating the proportion of genes in the gene-set that are highly expressed in each cell (261). Cells expressing many genes from the gene-set have higher AUC values than cells expressing fewer. **Figure 6-6** illustrates that neutrophils exhibit a much higher probability of responding to IFNγ during rechallenge conditions than at resting state, as well as compared to B cells. Depletion of alveolar macrophages by CLL treatment results in a lower predicted probability for the cells to respond to interferon-gamma.

A.

Neutrophils



B.

Natural killer cells

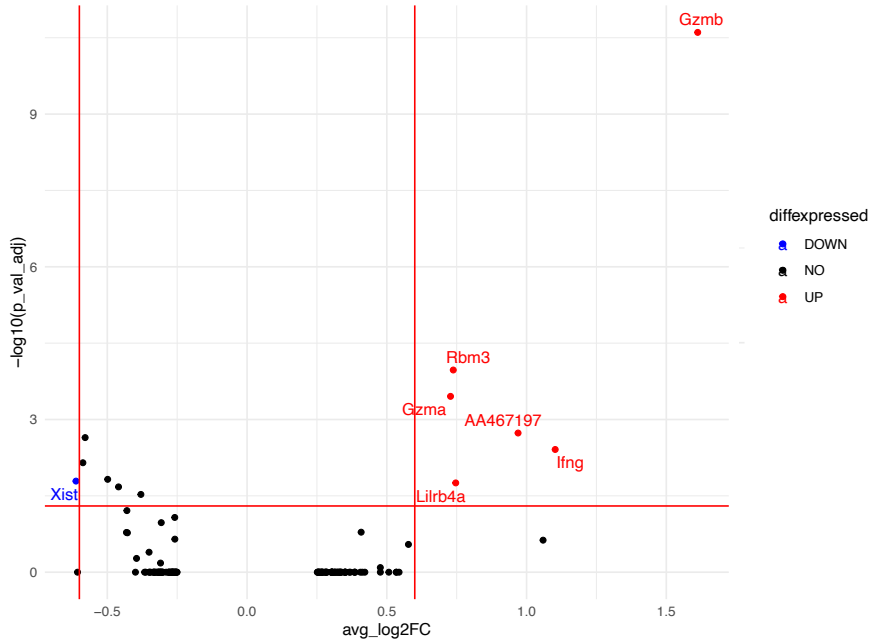


Figure 6-5: Neutrophils and natural killer cells exhibit distinct transcriptional profiles during rechallenge in the absence of alveolar macrophages.
Volcano plot of differentially expressed genes for neutrophils a) and NK cells b), comparing the rechallenged condition to the rechallenged + CLL condition. The -log10 (p values) represents the level of significance of each gene while log2 fold change represents the difference between the levels of expression for each gene. The red lines indicate a threshold of p=0.05 (x-axis), and fold-change of 1.5 (y-axis).

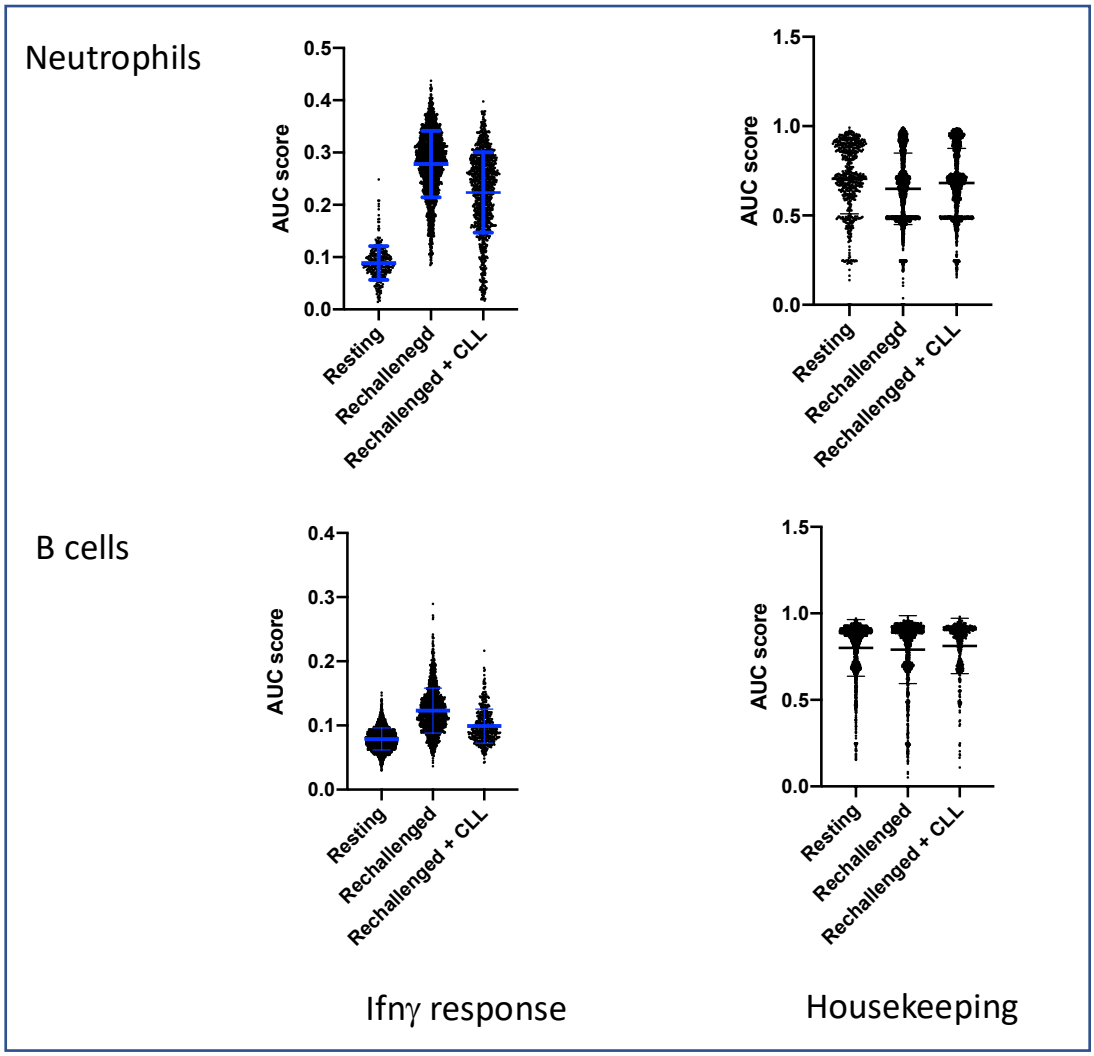


Figure 6-6: Neutrophils respond to interferon gamma during rechallenge.
Violin plots showing the expression of the GSEA "Interferon gamma response" geneset in the cells from each of the three conditions (AUCell analysis). Housekeeping genes are included as a comparison across conditions.

Housekeeping genes across conditions do not exhibit demonstrable differences in AUC scores. Thus, B cells may respond directly to IFNγ to a limited extent, yet less so than neutrophils, at 24 hours post-rechallenge. Antibody blockade experiments performed in collaboration by Dr. Andrew MacLean led to a reduction in the accumulation of BRM cells in infected sites and a modest 1.2-fold increase of density in these regions after re-infection (compared to a >2-fold increase in the control group) when IFNγ was neutralized (**Appendix 2, Figure 1F**).

6.4 Discussion

In this chapter we identify signaling cues derived 24 hours post-rechallenge from infiltrating immune cells that mediate Brm response to infection. Live-imaging studies demonstrate that Brm cells quickly increase their migration capacity and relocate to sites of infection after rechallenge, where they differentiate into antibody -secreting PCs within four days (157). Localization to sites of infection is independent of recruitment of recirculating B cells or antigen specificity but is dependent on the presence of alveolar macrophages and innate signals. Here, single cell RNA-seq and QPCR analysis of rechallenged lungs revealed a likely role for alveolar macrophages in orchestrating this process, in part by promoting local production of IFNγ by infiltrating NK cells, subsequently leading to induction of inflammatory chemokines, including *Cxcl9* and *Cxcl10*, particularly prominently from neutrophils. This, in turn, promoted the CXCR3-dependent accumulation of Brm cells within sites of infection, where they quickly differentiated into PCs. We propose that IFNγ deriving significantly from infiltrating NK cells induces the expression of the CXCR3 ligands, yet the mechanisms driving NK cell recruitment and activation are still untested (**Figure 6-7**).

RNA-sequencing of alveolar macrophages at 12 hours post-infection indicated that type I interferons as well as interleukin-a (IL1-a) are transcriptionally upregulated in response to rechallenge, highlighting these cytokines as potential mediators of innate cell activation, recruitment and/or IFNγ-expression (**Appendix 3 Figure 1**, related to Figure 5-8). Interestingly, upregulation of IL-18, IL-12, or IL-15, known synergistic activators of NK cell-derived IFNγ (262), were not observed in any hematopoietic population at the 24hr timepoints by single cell sequencing analysis (as illustrated by FeaturePlots in **Appendix 4, Figure 1a**). However, post-translational modification of these particular cytokines and thus their activation state should not be ruled out, for example, by the proteolytic processing of

pro-IL-18 into biologically active IL-18 by caspase-1 enzyme during viral infection and its subsequent cellular release (263). In fact, the strongest IL-18 transcriptional signature was observed during the resting state in the small macrophage cluster (**Appendix 4, Figure 1b**), suggesting these cells may constitutively express the inactive form of IL-18 and release it upon exposure to flu infection and/or cell death signals.

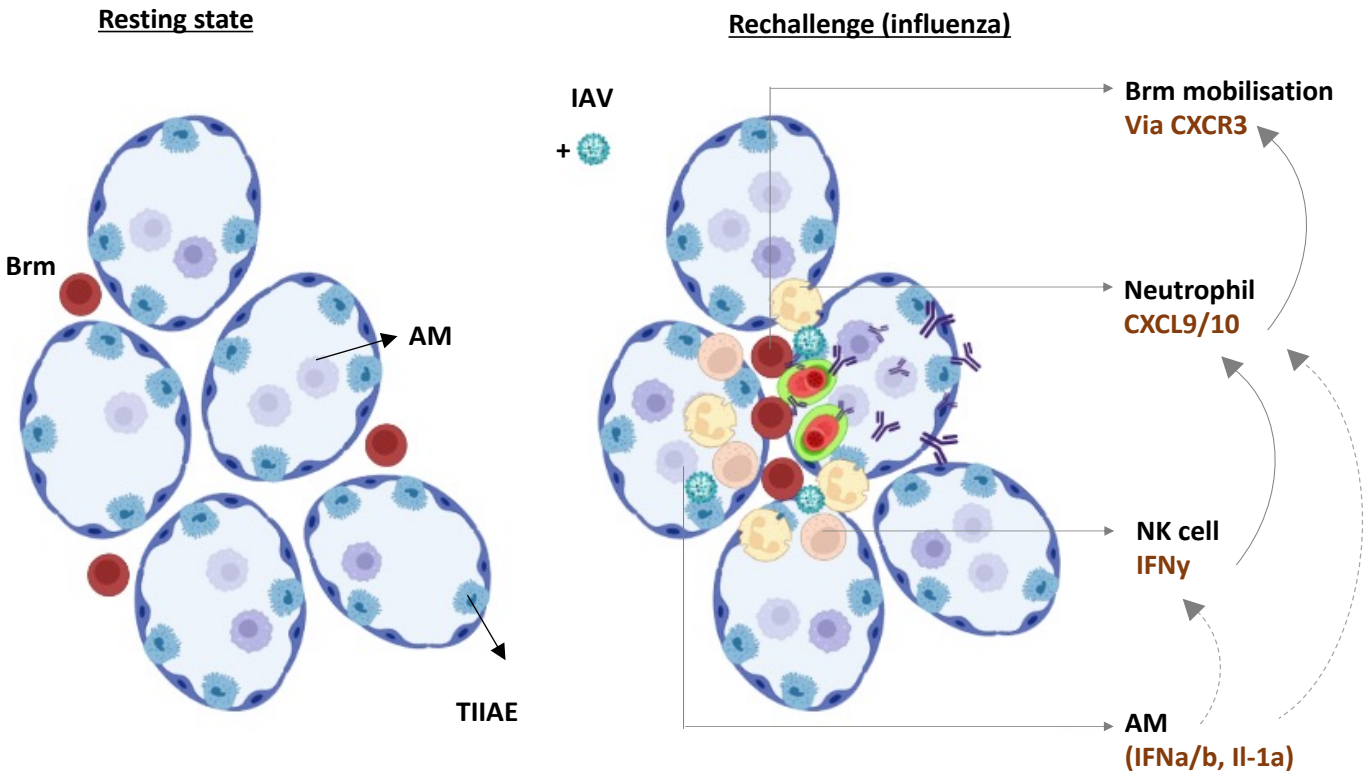


Figure 6.7 (above): Summary schematic of chemokine mediated Brm mobilization during influenza rechallenge. Upon re-exposure to X31 influenza virus, resting state Brm dispersed throughout lung alveoli migrate in response to CXCR3 ligands. Alveolar macrophages initiate the inflammatory response causing neutrophil and NK cell recruitment and induction of IFNγ expression. In turn, this induces CXCL9 and CXCL10 expression predominantly in neutrophils, attracting Brm to infected sites where they differentiate into antibody-producing plasma cells. Dashed lines indicate currently untested hypotheses.

Interestingly, observed IL-18 binding protein (IL18bp) mRNA expression by alveolar macrophages, an inhibitor of IL-18 activity, at 12 hours after rechallenge (**Appendix 3, Figure**

1, related to Figure 5-8) suggests that these cells are potentially responding to an excess of IL-18-derived IFNγ-release, as IL-18bp is known to competitively inhibit the IL-18 receptor and prevent IL-18-dependent IFNγ production (264). Yet, it is also possible that type I interferons secreted by alveolar macrophages may directly induce NK cell proliferation and IFNγ production. Type I IFN is essential for the survival, expansion, and maturation of NK cells: interferon alpha receptor knockout mice (IFNAR-/-) have very low reported levels of peripheral NK cells (265), and NK cells with specific IFNAR deletion show diminished expansion and protection against MCMV infection and exhibit more apoptosis compared with wild-type NK cells (266). Additionally, type I IFN has been shown to activate NK cells to produce IFNγ through signal transducer and activator of transcription (STAT)4, in addition to inducing cytotoxic effects through STAT1, yet their effectiveness in performing such functions may heavily depend on the costimulatory action of cytokines including IL-15 (267).

Interleukin alpha (IL1-a) produced by alveolar macrophages may contribute to neutrophil recruitment. During chronic peritonitis induced by hydrocarbon oil, IL1-a and IL1 receptor (IL1-R) signaling promote the migration of neutrophils to the peritoneal cavity in a CXC chemokine receptor-2 (CXCR2)-dependent manner (268). In other models of peritonitis, in which cell lysates were injected into the peritoneal cavity of mice, IL-1α-deficient cell lysates show reduced recruitment of neutrophils as compared to mice treated with cell extracts from WT mice (269). The source of IL-1α in WT mice was mainly necrotic cells, and the surrounding mesothelial cells responded in an IL-1R1-Myd88 signaling dependent manner by further secretion of CXCL1. Furthermore, cell lysates derived from the heart, lung, kidney, or liver recruit neutrophils into Matrigel plugs in an IL-1α dependent manner (270).

While our work establishes an important role for CXCR3 in regulating Brm mobilization and activation, other inflammatory chemokine receptors may also contribute to this effect. This possibility is supported by our observation that depletion of alveolar macrophages prevented Brm cell mobilization more effectively than blocking CXCR3. Moreover, we found that alveolar macrophage depletion was also associated with reduced expression of *Ccl5* and *Ccl3*, transcripts encoding inflammatory chemokines which engage the chemotactic receptor CCR1, which is expressed on Brm cells. The role of chemoattractant CCL3 has been described in neutrophil recruitment and suggested that influenza virus recognition via TLRs in the lung induces chemotactic factors that facilitate neutrophil migration into the infected lung – accordingly, along with the reduced neutrophil levels, CCL3 is reduced in the airways of Myd88 −/− mice after influenza infection (271). The development of CCL3-IgFc fusion proteins, as described in chapter 4, may aid in delineating the role of CCL3-CCR1 chemotaxis in Brm mobilization by blocking the CCR1 and CCR5 receptors.

It remains possible that other cell types, including non-hematopoietic populations that line the lung parenchyma and that have not been included in our single cell RNA analysis, contribute to the inflammatory response that ultimately directs Brm responses. Numerous *in vitro* studies of primary influenza infections demonstrate that epithelial cells release IFNβ, IL-1, IL-6, CCL5, and CXCL10 expression within 6 hours of infection (272, 273). Future work assessing the CD45- fraction of pulmonary cells during rechallenge is needed to obtain a complete picture of the initial cues released by infected cells and immune cell recruitment into the lung tissue.

Mechanistically, there are few studies connecting intracellular innate-stimulated signaling to the adaptive, humoral, immune response – but granted its established role in

sensing viral components, cytosolic danger signals, and mediating cytokine release, the inflammasome poses as a likely candidate. During primary influenza infections, the NLRP3 inflammasome has been shown to be activated *in vivo* in alveolar macrophages and DCs within the alveolar space after challenge in a type I IFN-independent manner (274). Starting at two days post infection, IL-1β secretion was evident in the BAL in WT mice infected with influenza virus. However, mice deficient in NLRP3, ASC, or caspase-1, failed to secrete IL-1β or IL-18 into the alveolar space in response to influenza infection. Bone marrow chimeric mice in which only the hematopoietic (WT→caspase-1−/−) or the stromal cells (caspase-1−/−→WT) expressed caspase-1, revealed that inflammasome activation *in vivo* occurs both within the hematopoietic compartment and the stromal compartment, yet, in contrast to the BAL fluid, IL-1β secretion in the lung tissue was found to be independent of NLRP3. Importantly, two weeks post primary infection, nasal IgA responses are dependent on ASC, caspase-1, IL-1R, and MyD88, as deficient animals exhibited significantly reduced levels of the antibody by nasal swab. Ongoing experiments seek to test the production of IFNγ and differentiation of plasma cell isotypes after rechallenge in NLRP3 inflammasome inhibitor-treated animals to identify the potential role of the inflammasome in mediating Brm response and humoral immunity during rechallenge.

7 Concluding remarks and limitations of study

The chapters of this thesis explore the presence and responses of pulmonary resident memory B cells in alveolar spaces. We find that their establishment is independent of CCR1, yet CXCR3-dependent cues are required for peak rechallenge mobilization responses to influenza virus. The ligands of CXCR3 are produced by neutrophils and monocytes at 24 hours post-rechallenge, likely induced by interferon-γ originating from natural killer and/or CD8+ T cells.

During the writing of this thesis, two novel studies were published on pulmonary Brm – both looking at those present within the germinal centers of iBALT structures (as opposed to the alveolar space interstitium). Utilizing an HA probe, Tan et al. do not observe Brm within the alveolar spaces of the lung and find B cells present in the alveolar spaces to be labeled by IV-CD45 (115). Our analysis suggests that there is a mixed population of AID-labeled B cells present in the lung after cardiac perfusion: those exposed to circulation (deriving from blood), and a subset of interstitial, IV-label protected Brm. These discrepancies may reflect poor technical validation of the kinetics of antibody diffusion across the lung capillaries or two unique populations. Irrespectively, future live tissue imaging of Brm responses should persistently include an IV label to distinguish between subsets responding to rechallenge. Additionally, a full characterization of the lung memory B cell repertoire against multiple influenza antigens (including nucleoprotein, neuraminidase, matrix proteins, as well as hemagglutinin) ought to be completed prior to concluding the localization of influenza-specific memory B cells. The use of the AID-Cre Rosa26-stop-tdTomato reporter mouse model raises important questions about the gene regulation of AID. Widely regarded as a marker of GC-derived B cells, AID is also known to be upregulated prior to the GC reaction (275), and public databases report it to be transcriptionally

expressed in peritoneal-derived B1b cells (276). It can be induced by T cell-independent mechanisms, including TLR-BCR cross-linking (277). While its function is essential for CSR and SH, its transcription does not necessarily signify activity – as it is tightly regulated post-transcriptionally by microRNAs, post-translationally by phosphorylation, and interacts with several cofactors (reviewed in (277)). Detailed characterization of the expression of AID in all pulmonary B cells is crucial to the interpretation of memory B cell subsets. Additional attention must be made to the potential (mis)regulation of AID expression via the estrogen receptor (ER) – HoxC4 transcription factor axis (278) if utilizing inducible Cre-ERT2 models, wherein tamoxifen can have both antagonistic or agonistic effects on ER activity (279).

While experiments by our group and others demonstrate the ability of Brm to develop from GC-derived B cells, attention must be paid to the potential contribution of extrafollicular B cells to the memory compartment. B1b cells can produce antigen-specific IgG+ PCs in response to pneumococcal polysaccharide – thus demonstrating a capacity to class-switch and contribute to the adaptive immune response in some instances (280). Thus far, an extrafollicular origin for Brm has not been explored – considering CD40L can be delivered outside of GCs (where Allie et al. propose a likely GC origin for Brm based on the requirement of CD40L for their establishment (112)). Indeed, Gregoire et al. observe a cluster of splenic Bmem to harbor a B1 phenotype (expressing tyrosine kinase Lck, Nfatc1, Ms4a6c, and Zbtb32) that clonally overlaps with lung Bmem subsets based on BCR-sequencing, raising interesting questions about their origin. Furthermore, the appearance of plasma cells in BAT mice four days after rechallenge in the absence of CD40L (157) does not necessarily exclude a role for T cell help to Brm during rechallenge. CD40-independent T cell help from CD4+ T cells is reported to prime CD8+ cytotoxic T cells (281). To assess this, wildtype or CD40-deficient mice were adoptively transferred with clonotypic HA-specific

CD8+ T cells, with or without HA-specific clonotypic CD4+ T cells. The animals were then infected one day later intraperitoneally with recombinant vaccinia virus encoding HA or were left untreated. Four days after infection, a significant CD4-dependent enhancement of HA-specific CD8+ T cell expansion was observed in the CD40−/− mice (281). *In vitro* stimulation of human B cells by CD40L-deficient T cells induced reduced but modest PC differentiation compared to CD40L+ T cells (282), suggesting that T cell-derived help other than CD40L may potentially help reactivate Brm. Future experiments highlighting pulmonary T cells and Brm in the early hours after infection may provide new insights into T cell Brm activation. In turn, depletion of T cell subsets, including memory T cells and lung Trm, could further address this point.

Interestingly, both Tan et al. and Gregoire et al. identify the establishment of CCR6+ and CXCR3+ subsets of Brm (115, 116) after influenza infection, and both demonstrate through mixed bone marrow chimeras that neither of these chemokines is required for their establishment in the lung. However, the authors of both studies find reduced numbers of Brm from CCR6-deficient animals and, furthermore, a defect in the antibody response upon rechallenge. Tan et al. illustrate that CCR6-/- animals fail to expand NP-specific CD138+ ASCs to the same extent as wildtype animals, and Gregoire et al. find that this deficiency is specific only to the IgA subset of PCs (where IgG and IgM numbers are unchanged), wherein CCR6-/- animals have a 10-fold decrease in IgA PCs four days after rechallenge. However, CCR6+/CXCR3- Brm exhibit far less antigen specificity compared to CXCR3+ Brm, as cultured CXCR3+ Brm bind extensively to NP, HA, and NA, whereas CXCR3- cells showed minimal binding. Gregoire et al. suggest that the CXCR6+/CXCR3- population exists as a bystander group of cells generated from IL-4 stimulation deriving from Tfh cells and are not *bona fide* Brm like the influenzas-specific CXCR3+ subset. Interestingly, they observe that CXCR3+ Brm

are localized in the periphery of B cell clusters where CCR6+ Brm are distributed throughout. Barker et al., in contrast, also report B cells dispersed in the interstitium of the lung in experienced mice during the memory phase, four weeks after challenge with pneumococcus (113). Based on our observations of CXCR3 being necessary for Brm mobilization after rechallenging, perhaps the distribution of CXCR3+ Brm within B cells clusters observed by Gregoire et al. is non-random and reflects their exit from GCs into the alveolar spaces. Presumably, the CXCR3+ subset has experienced many more rounds of SHM than the CXCR3-, as they have greater specificity and are possibly pushed out as they expand from the center of a GC to the periphery. It is possible that only at the periphery do they gain CXCR3 expression – induced by residual IFNγ from surrounding stroma (that perhaps still has low levels resultant from the primary response) (283). Alternatively, IFNγ present in the local tissue during the primary GC response could induce CXCR3 expression on developing Bmem, and these subsets are drawn to CXCL9/10 present within the periphery. It is unclear whether the CCR6+/CXCR3- population would be present in the alveolar spaces or whether rechallenge with VLPs (no influenza) only activates the CCR6+/CXCR3- subset of Brm, in a non-specific manner. To answer these questions, an inducible AID-Cre-ERT2 combined with a floxed CXCR3 (*loxP)* knockout mouse could be helpful – while also introducing a floxed tdTomato or EGFP reporter in the Rosa26 locus (this would require embryonic stem cell manipulation). However, administration of tamoxifen could simultaneously induce CXCR3 knockout while enabling Bmem identification, thus enabling the investigator to assess whether alveolar Brm are present in the absence of CXCR3.

Curiously, as CXCR3-deficiency does not affect the total number of influenza-specific plasma cells in the lung four days after rechallenge (116), it is possible that localization of Brm throughout the lung tissue (outside of defined clusters) may not be essential for

humoral protection upon rechallenge. However, whether the localization of PC differentiation occurred differently in the absence of CXCR3 has yet to be answered. Likewise, whether the presence of plasma cells at the same site of the antigen is necessary for equivalent protection against recurring immune challenges (as opposed to diffused antibodies), needs to be further characterized.

Little is known about the requirement of antigen for Brm maintenance. Allie et al. demonstrate through parabiosis experiments that local antigen (administered to the lungs) is needed for Brm recruitment and establishment in the lung. However, these analyses were not extended to Brm maintenance (112). The most informative data is attained by putting together the findings of Adachi et al. and Gregoire et al. (2015 and 2022, respectively). Adachi et al. do not look specifically at resident memory B cells but find that the subsets of total lung memory B cells are sensitive to ongoing GC reactions, which in turn depend on the presence of viral antigen (111). More specifically, influenza antigen is found at least 30 days after primary infection (later time points were not evaluated) in the lung but not in the spleen or mediastinal lymph nodes. Importantly, depleting GCs during the memory phase (via the conditional depletion of Bcl-6, utilizing Bcl-6flox/flox Rosa26Cre-ERT2/+ mice) results in the specific reduction in the numbers of cross-reactive B cells among lung memory compartments after tamoxifen treatment, whereas strain-specific memory B cells remain intact. This suggests that cross-protective memory B cells in the lung may require antigen for their maintenance. Gregoire et al. build on these findings and observe that two subsets of lung memory B cells formed after primary influenza infection, CCR6+CXCR3- and CCR6+CXCR3+ have quite different antigen specificities (116). The CXCR3+ subset is enriched with specificity for influenza antigens that robustly respond upon secondary challenge by secreting protective antibodies. In contrast, the CXCR3- subset has no evident specificity for

influenza antigens and limited effector capacity (plasma cell differentiation). Some care should be taken to consider technical limitations for lower affinity BCRs (they still may be antigen specific, but the affinity below the technical threshold). Nonetheless, the CXCR3- subset preferentially binds immune complexes, despite the observed lack of specificity for influenza antigens. This phenomenon would increase antigen density in the proximity of antigen-specific lung memory B cells. It is likely that persistent antigen contributes to ongoing Brm formation, but specific viral antigen is not required to maintain HA-specific Brm established from the primary exposure. As previously described, Maruyama et al. demonstrate that BCR activity is important for memory B cell maintenance, but antigen specificity is not (96). It is unresolved whether this is due to a B-cell-autonomous 'maintenance' signal or whether it reflects low-affinity interactions of the BCR with (self-) antigens in the environment. This fits into Gregoire et al.'s suggestion that immune complexes retained by "bystander" memory B cells in the lung may act as a reservoir of antigen for display. To test Brm dependence on antigen in our context, firstly, it is important to detect how long influenza antigen persists in the lung after primary infection, for example, by RT-PCR or immunoassay detection of NP and HA antigens. It would be interesting to see whether the longevity of Brm observed in our lab (approximately six months) correlates with antigen detection. Secondly, it would be interesting to utilize a similar genetic switch as Maruyama et al., to change the BCR of Brm after their establishment to non-immunizing antigen specificity. If previously HA-specific Brm perish after BCR switch – this would strongly suggest they depend on influenza antigen for maintenance. Much has yet to be explored regarding Brm populations arising from different immunizing antigens, which may compete for the same niche. It would be interesting to perform simultaneous heterotypic primary immunizations and observe whether equal

numbers of antigen specific Brm are established and maintained relative to a single immunization.

This discussion critically highlights the potential differences in modes of immunization and the types of immune responses they elicit. The magnitude of the exposure to a respiratory challenge could sway a locally mediated response to one inducing peripheral GCs to respond and/or a systemic response. The intranasal influenza immunizations we administer upon rechallenge have quite high viral titers, and likely are not reflective of most naturally-occurring transmission of influenza, as the provided dose of $1x10^6$ PFU is lethal if administered during a primary exposure (284). Dose-dependent studies show that during primary infection, the initial viral load of X31 influenza can significantly impact the infiltration and/or expansion of innate cells into the lung tissue of mice and mRNA expression of inflammatory cytokines (285). Presumably, similar differences may occur during secondary infections. One could speculate that low viral copies present in an area outside of GCs or iBALT may only require local memory (Brm and Trm) to respond, whereas higher viral loads may propagate the immune response and signal to more distal sites, thereby activating Brm and Trm present within these constrained structures. This assumes that chemokine and cytokine gradients stimulate leukocyte migration and/or activation from an area of a higher concentration circumferentially.

Furthermore, it is important to consider the use of the single-cycle PR8 strain-derived CFP-S-Flu during some rechallenge experiments for imaging purposes. Despite being non-pathogenic and incapable of propagating the infection throughout the lung tissue, CFP-S-Flu induces the robust establishment of HA- and NP-specific cytotoxic T-cells in the lung and neutralizing HA-specific antibodies at high doses (143). In the context of heterotypic challenge, viral titers of the heterologous virus X31 in the lungs of S-FLU-vaccinated mice are

reduced by >two orders of magnitude, whereas homologous virus is reduced by ~three orders of magnitude (143). These findings demonstrate that CFP-S-Flu induces adaptive immune responses comparable to the replicative strains. The lack of actively reproducing virus after rechallenging with CFP-S-Flu may change the foci of infection in that its dispersion is likely more punctate as a single-cycle infection than a potentially dispersive X31 infection. This could result in a concentrated chemokine gradient causing Brm activation and mobilization toward a specific site, which may not occur with widespread infection already encompassing areas of Brm residence. However, live, replicative influenza infections and intranasal immunizations are typically non-uniformly distributed throughout the lung (255, 286, 287); therefore, the mechanisms dictating observed Brm accumulation at specific sites of infection during CFP-S-Flu could still apply during natural infection and intranasally administered influenza vaccines. To address this, it would be helpful to rechallenge with a replicative fluorescently tagged strain of influenza virus and assess the dispersion of the fluorescent tag (indicative of viral propagation) and the Brm response to a naturally replicating virus. It would be interesting to assess whether the rapid activation of local Brm in a secondary response is enough to restrict the viral infection to a particular site (of the original infection).

The protection offered by lung Brm has been studied to a limited extent by Allie et al. in the context of heterotypic flu infections. Mice intranasally primed with the PR8 strain of influenza exhibit less weight loss and lower viral titers in BAL 5 days after rechallenging with the X31 strain relative to intraperitoneally primed mice (112). By day 8, the weight between IP and IN-primed animals is the same (fully recovered); while there is no data on viral titers at day 8, one can presume it follows the weight-loss pattern and is equivalent or similar to IN-primed animals. At first glance, this suggests lung Brm directly provide a more

rapid antibody response than systemic and circulating humoral immunity. However, this ignores the likely contribution of lung-resident memory T cells only present in the intranasally-primed animals and other potential sources of local protection, including trained immunity within lung macrophages, for example. While intranasally primed animals have greater numbers of plasma cells by day 4 of rechallenge relative to intraperitoneally primed animals, the proportional contribution of diverse resident cell populations to protection is still unclear. A way of better delineating the Brm contribution to protection more directly would be to comprehensively quantify and characterize antibodies present in the lung tissue and BAL of intranasally primed versus intraperitoneally primed animals over time. This would directly answer the question of whether the presence of Brm is associated with greater neutralizing and cross-protective antibodies in the lung (considering the ability of antibodies to diffuse across tissues). Presumably, they do, based on the greater number of PCs, but it is important to measure protection more directly.

Onodera et al. perform such definitive experiments with a "memory-like B cell" population isolated from the lungs of mice primed by influenza infection. They observe that adoptive transfer of CD4+ T cells and lung memory-like B-cell populations generate sixfold more IgG- and IgA-secreting plasma cells in the lungs of recipient *scid* mice compared with splenic counterparts. In addition, anti-HA IgG and IgA antibody titers in BAL are elevated in the mice reconstituted with the lung B-cell population after CpG treatment but not in those given the splenic B cell population. Together, these data indicate that HA-binding IgM/D−CD38+ lung B cells can generate large amounts of antibodies at the site of virus replication to confer protection more effectively than splenic counterparts. The latter adoptive transfer experiments tease out some complications of other contributing immune cells by isolating the protection granted by Brm in the presence of CD4+ T cells.

Intriguingly, the recruitment of memory B cells to infected tissue and the secretion of virus specific IgG2 antibodies is impaired in chimeric mice that lack CXCR3 only on B cells after secondary challenge with HSV (288). Additionally, five weeks after immunization with PR8, CXCR3-B cell knockout (KO) mice have lower numbers of IgA+ Brm, PCs, and antibodies in the lung (289). Following homologous virus challenge, recovery of body weight of CXCR3-B cell KO mice is slow and impaired compared to control mice, indicating that loss of CXCR3 on B cells affects the protective function during secondary challenge independently of T cell action.

However, there are important limitations to Onodera et al.'s protection study. Firstly, all HA-binding IgM/D−CD38+ B cells were adoptively transferred – while this plausibly includes Brm, it is not a "clean" population and certainly not comparable to the IV label-/GL7-/CD69+ populations we and others currently demarcate as Brm. Secondly, it excludes IgM+ Brm cells – which we and others observe can be a significant fraction of memory B cells (50-90% in some cases (290, 291)). Finally, local inflammation is provided to the site of lung B cell homing (via intranasally administered CpG) but not to the site of splenic B cell homing.

In summary, to assess Brm protection, I would adoptively transfer the Brm population of interest (IV label-/GL7-/CD38+/CD69+/HA+); the same population (+/- CD69) from mediastinal lymph nodes; the same population from spleen (+/- CD69), from memory phase X31-primed animals into inflammation-primed recipients (both lung and systemic) and confirm equivalent grafting. Then, I would challenge with a) a homotypic influenza virus; b) a heterotypic influenza virus; c) a series of non-influenza respiratory challenges, including viruses (e.g., coronavirus), bacteria (e.g., pneumococcus), and allergens (e.g., house dust mites). As readouts (over time), I would assess body weight and condition,

antigen titers, antibody concentrations, reactivity, and neutralizing capacity. I would also enumerate and characterise PCs after challenge.

The volume of influenza immunization we administer is also likely not reflective of naturally inhaled liquid droplets. If we directly translate the volume by body weight (30uL per a 30g male mouse) to human standards (an average of 80kg, for example) – this would correspond to about 80mL of volume being inhaled intranasally. The total surface area of the mouse and human lungs are 82 cm^2 and 70m^2, respectively (256, 292), which corresponds to an estimated equivalent of 12uL/1 cm administered in the mouse, and 166uL/1 cm in the human. Although much of the administered dose is likely to be absorbed by the nasal passages before reaching the alveoli, clinical studies report that larger, heavier droplets are more likely to descend directly into the alveolar spaces within the lower respiratory tract compared to aerosolized, lighter droplets which accumulate in the nasal passages and upper respiratory tract (URT) (293). Accordingly, the rechallenge dose we administer potentially reflects a severe exposure to the influenza virus within the alveolar space, and consequently the observed immune responses may not always occur during natural transmission.

Studies in mice utilizing non-absorbable, radioactive tracers (99mTc-labeled sulphide-colloid) show that intranasal instillation of volumes between 25-50μl result in 30-40% accumulation of the substance in the nasal passages, with 60% recovery in lung tissue (294). This highlights the potential role of nasal-associated lymphoid tissues (NALT) as part of the observed immune response throughout our studies. In mice, NALTs in the nose consist of paired lymphoid tissues located at the entrance of the nasopharyngeal ducts. NALTs in the URT are highly organized lymphoid structures covered by ciliated epithelium, which also contain microfold (M) cells that facilitate antigen transport from the nasal cavity

to the underlying lymphoid tissues (295). The lymphoid tissues of the URT are an initiation site for cytotoxic T lymphocyte (CTL) immunity to inhaled antigens, and influenza-specific plasma cells are found in NALT after primary infection (296). IgG and IgA-specific memory B cells are found in NALT 8-12 weeks after primary infection, yet whether these cells are circulating or resident has not been established (85). Interestingly, chemical inhibition of CXCR3 during influenza infection prevents typical memory T cell recruitment to NALT (297), suggesting that if CXCR3+ Brm are found within NALT, they may respond similarly to those observed in the alveoli and contribute significantly to rechallenge responses.

The bigger question raised by these observations is whether Brm with cross-protective activity, capable of responding to VLPs, may also be detrimental in certain circumstances and contribute to autoimmune disease. It is interesting that viral infections of the lung are a risk factor in the development and exacerbation of asthma. Community-based longitudinal studies in the UK have found that 80% of children requiring hospitalization after an acute asthma attack had a viral infection at the time of entry (298). Exacerbation of asthma has been documented after RSV, rhinoviruses, influenza, adenoviruses, and coronaviruses (299), yet, the link between infection and asthma is poorly understood. Aeroallergen sensitization is rarely documented as being the sole cause, implying that inflammation from viral infection and allergens may act interdependently to disrupt lung function. Interestingly, a recent clinical trial has found CD27+ IgA+ memory B cells to be increased in patients with small airway dysfunction (SAD), a feature of asthma (300). These cells were further correlated with exacerbation, impaired asthma control, and reduced quality of life. As this study could only assess circulating memory B cells in the blood and did not provide mechanistic insight into how IgA+ memory B cells may exacerbate asthma, further characterization of tissue-resident subsets in this context is much needed. Murine

models of asthma, including sensitization from house-dust mites (HDM-sensitization), have previously been shown to increase the total number of pulmonary germinal center B cells, PCs, and IL-10+ B cells (301) and could be utilized to better understand whether Brm populations contribute significantly to atopic diseases (perhaps via initial priming with influenza, followed by dust mite exposure during the resting phase). The role of Brm in other contexts of small airway inflammation, such as chronic obstructive pulmonary disease (COPD), also remains to be explored.

Our studies reveal a rapid, local antibody response after rechallenging due to the establishment of a Brm pool in the lung during primary infection. This strongly suggests that immunization strategies directed towards stimulating this population may be beneficial for protection against recurring respiratory viruses. Future research investigating the role of Brm in the context of chronic inflammation in parallel with intranasal vaccination strategies may reveal novel mechanisms of inducing protection against pulmonary pathologies.

A broadly protective flu vaccine has been a goal for decades, constrained by the "moving target" that is the hemagglutinin protein. Granted its critical role in viral entry to host cells, HA has historically been the primary target of most vaccines. However, the HA head is especially prone to evolve, making it challenging to predict seasonal mutations within circulating strains. Subsequent strategies aimed to develop vaccines against conserved parts of the virus, such as the hemagglutinin stalk, which typically changes less than the head.

Unfortunately, the stalk does not induce as strong an immune response, and antibody titers generated through stalk immunization are often too low to prevent infection (302). Recent vaccination strategies involve sequential immunizations using chimeric HA (cHA) immunogens, featuring an identical stalk domain but a divergent globular head

domain – essentially skewing the antibody response towards to "familiar" stalk domain. The advantage of immunity to the stalk grows by delivering a second vaccination with the same stalk and another unfamiliar head. These vaccines elicit humoral immune responses directed toward the HA stalk, which are broad and capable of providing heterologous protection against diverse influenza viruses. Unfortunately, phase 1 clinical trials of such cHA immunogens revealed that neither second nor third vaccine doses could boost anti-stalk antibodies and concentrations waned over time (303-305).

Despite these discouraging findings, the haemagglutinin stalk domain remains an attractive target since the reactive antibodies induced by the haemagglutinin stalk were broadly protective in serum passive transfer experiments (304, 305). Broadly protective antibodies directed toward the HA stalk domain confer protection *in vivo* by promoting Fcγ-receptor (FcγR) interactions (302). Fc:FcγR engagement can trigger Fc-dependent effector functions, such as ADCC or antibody-dependent cellular phagocytosis (ADCP) mediated by natural killer (NK) cells, neutrophils, and alveolar macrophages. Uncovering the mechanisms which underlie the protective efficacy of broadly protective antibodies will be crucial to design next-generation universal influenza vaccines capable of engaging these pathways and maximizing vaccine-induced immunity (302).

This is where lung Brm become interesting – they categorically exhibit more cross-protective immunity than systemic counterparts and even retain immune complexes in the lung (110, 112, 116). This augments the possibility of Fc:FcγR engagements, making them an exciting population to establish via immunization. We also observe the infiltration of neutrophils and NK cells after rechallenging and propose a role for alveolar macrophages in mediating early responses – it would be interesting to evaluate whether the same kinetics exist after intramuscular priming.

Intranasal flu vaccines exist for children – primarily marketed as "needle-free!" (FluMist Quadrivalent, AstraZeneca). But is there a fundamentally biological reason for establishing anamnestic immunity through intranasal vaccination? By establishing resident memory B and T cells, GCs in the local NALT and BALT of the airway passages, and more broadly protective humoral immunity, further investigation into the protection offered by intranasal immunization strategies is certainly warranted.

Of course, with greater cross-reactivity comes a greater risk of autoimmunity. Autoreactive B cells are negatively selected against during central and peripheral tolerance (checkpoints in the bone marrow and SLOs, respectively) (306). Autoreactive B cells that escape central and early peripheral tolerance mechanisms can enter GC reactions. Additionally, non-autoreactive B cells can acquire *de novo* autoreactivity during GC-induced SHM. Accordingly, several GC checkpoint mechanisms exist (e.g., follicular exclusion, T regulatory cells, Fas-mediated apoptosis) (306). However, these checkpoints are less established and poorly understood in tertiary lymphoid structures such as iBALT and within extrafollicular response pathways. Lacking physical separation from inflammatory environments, TLOs are awash in pro-inflammatory signalling from tissue-resident innate immune and stromal components and cell-death associated danger signalling accompanying direct autoimmune attack (reviewed in (307)). Autoimmune B cells can drive the pro-inflammatory environment through autoantibody and cytokine production and respond to that inflammation by becoming even more potent presenters of autoantigen. Indeed, dysregulated TLO formation is noted in various human autoimmune disorders, including Sjogren's syndrome, myasthenia gravis, multiple sclerosis, rheumatoid arthritis, and SLE (reviewed in (307)).

Given these ectopic structures' prominent role in autoimmunity, TLOs may be pathogenic through the unopposed generation and amplification of site-specific autoreactive B cells. This is a concern for any therapy aimed at establishing lung Brm. Extrafollicular and iBALT origins of Brm have certainly not been ruled out, and EF Brm activation dominates during the rechallenge responses observed in this thesis. Future work could measure Brm autoreactivity, for example, through single-cell Brm cultures (induced to differentiate into PCs) and collecting supernatant containing antibodies for testing against antigen arrays. Flow cytometry approaches (B cell binding assays to fluorochrome-tagged peptides) and single-cell BCR cloning and expression as recombinant IgG monoclonal antibodies could also be helpful for Brm autoreactivity testing.

Furthermore, the potential role of Brm in mediating asthmatic airway inflammation remains to be explored. B cells are increased in the blood and bronchial mucosa of clinical patients undergoing an asthma attack (308). Several research groups have tracked the influx of B cells into the allergic lungs (308). The role of B cells in allergic asthma has traditionally been linked to the production of IgE antibodies, which mediate mast cell degranulation. However, the transfer of B cells isolated from mice dermally sensitized to toluene diisocyanate (TDI) into naïve wild-type mice, B lymphocyte knockout mice, or SCID mice leads to acute asthma-like phenotype after an airway challenge with TDI within three days, independent of IgE (309). The transferred B-lymphocytes home to large airways 24 hours after TDI challenge. Thus, B cells can provoke asthmatic responses in the lung. To evaluate Brm contribution to asthmatic airway inflammation, it would first be interesting to see if they are established and reactive in experimental models of inhaled allergens, such as *Aspergillus fumigatus* (a murine inhalation model to mimic human fungal asthma) (308). Sensitization to *A. fumigatus* via intranasal administration of *A. fumigatus* antigens causes

airway hyperresponsiveness, pulmonary inflammation, epithelial changes, and collagen deposition upon aerosol inhalation challenge with live *A. fumigatus* conidia.

Moreover, it would be interesting to test whether priming with the influenza virus establishes Brm with cross-reactivity to *A. fumigatus*. Our data demonstrate that Brm reactivity is not antigen-dependent but requires the presence of RNA (within VLPs). Whether BCR cross-linking to other types of pattern recognition receptors (in the presence of fungal PAMPs, for example) can stimulate Brm to respond remains to be studied.

In summary, the broader cross-protection offered by Brm presents a unique opportunity to develop universal vaccination strategies. However, caution is advised to simultaneously evaluate the potential for higher rates of tolerance escape within the extrafollicular spaces, and Brm-dependent airway hypersensitivities.

8 References

1. Fang Y, Xu C, Fu Y-X, Holers VM, Molina H. Expression of Complement Receptors 1 and 2 on Follicular Dendritic Cells Is Necessary for the Generation of a Strong Antigen-Specific IgG Response. The Journal of Immunology. 1998;160(11):5273.
2. Brockman MA VA, Zhu J, Carroll MC, Knipe DM. . Optimal long-term humoral responses to replication-defective herpes simplex virus require CD21/CD35 complement receptor expression on stromal cells. J Immunol. 1998(0022-538X (Print)).
3. Schroeder HW, Jr., Cavacini L. Structure and function of immunoglobulins. J Allergy Clin. 2010(1097-6825 (Electronic)).
4. Lu LL, Suscovich TJ, Fortune SM, Alter G. Beyond binding: antibody effector functions in infectious diseases. 2018(1474-1741 (Electronic)).
5. Lutz C, Ledermann B, Kosco-Vilbois MH, Ochsenbein AF, Zinkernagel RM, Köhler G, et al. IgD can largely substitute for loss of IgM function in B cells. Nature. 1998;393(6687):797-801.
6. Mostov KE FM, Blobel G. T. The receptor for transepithelial transport of IgA and IgM contains multiple immunoglobulin-like domains. Nature. 1984(0028-0836 (Print)).
7. Bruhns P, Iannascoli B, England P, Mancardi DA, Fernandez N, Jorieux S, et al. Specificity and affinity of human Fcγ receptors and their polymorphic variants for human IgG subclasses. Blood. 2009;113(16):3716-25.
8. Stapleton NM, Andersen JT, Stemerding AM, Bjarnarson SP, Verheul RC, Gerritsen J, et al. Competition for FcRn-mediated transport gives rise to short half-life of human IgG3 and offers therapeutic potential. Nature Communications. 2011;2(1):599.

9. Aalberse RC vdGR, van Leeuwen J. Serologic aspects of IgG4 antibodies. I. Prolonged immunization results in an IgG4-restricted response. J Immunol. 1983(0022-1767 (Print)).
10. Janeway CA Jr TP, Walport M, et al. The production of IgE. Immunobiology: The Immune System in Health and Disease. 2001(New York: Garland Science).
11. Kataoka T. MT, Honjo, T. Repetitive sequences in class-switch recombination regions of immunoglobulin heavy chain genes. 1981(0092-8674 (Print)).
12. Depoil D FS, Treanor BL, Weber M, Harwood NE, Marchbank KL, Tybulewicz VL, Batista FD. CD19 is essential for B cell activation by promoting B cell receptor-antigen microcluster formation in response to membrane-bound ligand. Nat Immunol. 2008(1529-2916 (Electronic)).
13. Treanor B, Depoil D., Gonzalez-Granja, A., Barral, P., Weber, M., Dushek, O., Bruckbauer A., Batista, F. D. The membrane skeleton controls diffusion dynamics and signaling through the B cell receptor. Immunity. 2010(1097-4180 (Electronic)).
14. Roozendaal R MT, Pitcher LA, Gonzalez SF, Verschoor A, Mebius RE, von Andrian UH, Carroll MC. Conduits mediate transport of low-molecular-weight antigen to lymph node follicles. Immunity. 2009(1097-4180 (Electronic)).
15. Pape KA CD, Itano AA, Jenkins MK. The humoral immune response is initiated in lymph nodes by B cells that acquire soluble antigen directly in the follicles. Immunity. 2007(1074-7613 (Print)).
16. Junt T, Moseman EA, Iannacone M, Massberg S, Lang PA, Boes M, et al. Subcapsular sinus macrophages in lymph nodes clear lymph-borne viruses and present them to antiviral B cells. Nature. 2007;450(7166):110-4.
17. Phan TG, Grigorova I, Okada T, Cyster JG. Subcapsular encounter and complement-dependent transport of immune complexes by lymph node B cells. Nature Immunology. 2007;8(9):992-1000.
18. Carrasco YR, Batista FD. B Cells Acquire Particulate Antigen in a Macrophage-Rich Area at the Boundary between the Follicle and the Subcapsular Sinus of the Lymph Node. Immunity. 2007;27(1):160-71.
19. Suzuki K, Grigorova I, Phan TG, Kelly LM, Cyster JG. Visualizing B cell capture of cognate antigen from follicular dendritic cells. Journal of Experimental Medicine. 2009;206(7):1485-93.
20. Cinamon G, Zachariah MA, Lam OM, Foss FW, Cyster JG. Follicular shuttling of marginal zone B cells facilitates antigen transport. Nature Immunology. 2008;9(1):54-62.
21. Pirgova G, Chauveau A, MacLean AJ, Cyster JG, Arnon TI. Marginal zone SIGN-R1+ macrophages are essential for the maturation of germinal center B cells in the spleen. Proceedings of the National Academy of Sciences. 2020;117(22):12295-305.
22. Bergtold A DD, Gavhane A, Clynes R. Cell surface recycling of internalized antigen permits dendritic cell priming of B cells. Immunity. 2005(1074-7613 (Print)).
23. Reif K, Ekland EH, Ohl L, Nakano H, Lipp M, Förster R, et al. Balanced responsiveness to chemoattractants from adjacent zones determines B-cell position. Nature. 2002;416(6876):94-9.
24. Cinamon G MM, Lesneski MJ, Xu Y, Low C, Lu T, Proia RL, Cyster JG. Sphingosine 1-phosphate receptor 1 promotes B cell localization in the splenic marginal zone. Nat Immunol. 2004(1529-2908 (Print)).
25. Green JA SK, Cho B, Willison LD, Palmer D, Allen CD, Schmidt TH, Xu Y, Proia RL, Coughlin SR, Cyster JG. The sphingosine 1-phosphate receptor $S1P_2$ maintains the homeostasis of germinal center B cells and promotes niche confinement. Nat Immunol. 2011(12(7):672-80 (Electronic)).
26. Renshaw BR, Fanslow WC, 3rd, Armitage RJ, Campbell KA, Liggitt D, Wright B, et al. Humoral immune responses in CD40 ligand-deficient mice. Journal of Experimental Medicine. 1994;180(5):1889-900.
27. Maliszewski CR GK, Fanslow WC, Armitage R, Spriggs MK, Sato TA. Recombinant CD40 ligand stimulation of murine B cell growth and differentiation: cooperative effects of cytokines. Eur J Immunol. 1993(0014-2980 (Print)).

28. Coffey F, Alabyev B, Manser T. Initial Clonal Expansion of Germinal Center B Cells Takes Place at the Perimeter of Follicles. Immunity. 2009;30(4):599-609.
29. Gatto D, Paus D, Basten A, Mackay CR, Brink R. Guidance of B Cells by the Orphan G Protein-Coupled Receptor EBI2 Shapes Humoral Immune Responses. Immunity. 2009;31(2):259-69.
30. Crotty S. Follicular helper CD4 T cells (TFH). (1545-3278 (Electronic)).
31. Allen CD AK, Low C, Lesley R, Tamamura H, Fujii N, Cyster JG. Germinal center dark and light zone organization is mediated by CXCR4 and CXCR5. Nat Immunol. 2004(1529-2908 (Print)).
32. Kepler TB, Perelson AS. Cyclic re-entry of germinal center B cells and the efficiency of affinity maturation. Immunology Today. 1993;14(8):412-5.
33. Ye BH, Cattoretti G, Shen Q, Zhang J, Hawe N, Waard Rd, et al. The BCL-6 proto-oncogene controls germinal-centre formation and Th2-type inflammation. Nature Genetics. 1997;16(2):161-70.
34. Dominguez-Sola D, Victora GD, Ying CY, Phan RT, Saito M, Nussenzweig MC, et al. The proto-oncogene MYC is required for selection in the germinal center and cyclic reentry. Nature Immunology. 2012;13(11):1083-91.
35. Tunyaplin C, Shaffer AL, Angelin-Duclos CD, Yu X, Staudt LM, Calame KL. Direct Repression of prdm1 by Bcl-6 Inhibits Plasmacytic Differentiation. The Journal of Immunology. 2004;173(2):1158.
36. Saito M NU, Piovan E, Basso K, Sumazin P, Schneider C, Crespo M, Shen Q, Bhagat G, Califano A, Chadburn A, Pasqualucci L, Dalla-Favera R. BCL6 suppression of BCL2 via Miz1 and its disruption in diffuse large B cell lymphoma. Proc Natl Acad Sci U S A. 2009(1091-6490 (Electronic)).
37. Phan RT, Dalla-Favera R. The BCL6 proto-oncogene suppresses p53 expression in germinal-centre B cells. Nature. 2004;432(7017):635-9.
38. Victora GD, Nussenzweig MC. Germinal Centers. Annual Review of Immunology. 2022;40(1):413-42.
39. Victora GD, Schwickert TA, Fooksman DR, Kamphorst AO, Meyer-Hermann M, Dustin ML, et al. Germinal Center Dynamics Revealed by Multiphoton Microscopy with a Photoactivatable Fluorescent Reporter. Cell. 2010;143(4):592-605.
40. Gitlin Alexander D, von Boehmer L, Gazumyan A, Shulman Z, Oliveira Thiago Y, Nussenzweig Michel C. Independent Roles of Switching and Hypermutation in the Development and Persistence of B Lymphocyte Memory. Immunity. 2016;44(4):769-81.
41. Suan D, Kräutler NJ, Maag JLV, Butt D, Bourne K, Hermes JR, et al. CCR6 Defines Memory B Cell Precursors in Mouse and Human Germinal Centers, Revealing Light-Zone Location and Predominant Low Antigen Affinity. Immunity. 2017;47(6):1142-53.e4.
42. Laidlaw BJ, Schmidt TH, Green JA, Allen CDC, Okada T, Cyster JG. The Eph-related tyrosine kinase ligand Ephrin-B1 marks germinal center and memory precursor B cells. Journal of Experimental Medicine. 2017;214(3):639-49.
43. Smith KGC, Light A, O'Reilly LA, Ang S-M, Strasser A, Tarlinton D. bcl-2 Transgene Expression Inhibits Apoptosis in the Germinal Center and Reveals Differences in the Selection of Memory B Cells and Bone Marrow Antibody-Forming Cells. Journal of Experimental Medicine. 2000;191(3):475-84.
44. Laidlaw BJ, Cyster JG. Transcriptional regulation of memory B cell differentiation. Nature Reviews Immunology. 2021;21(4):209-20.
45. Ersching J, Efeyan A, Mesin L, Jacobsen JT, Pasqual G, Grabiner BC, et al. Germinal Center Selection and Affinity Maturation Require Dynamic Regulation of mTORC1 Kinase. Immunity. 2017;46(6):1045-58.e6.
46. Inoue T, Shinnakasu R, Kawai C, Ise W, Kawakami E, Sax N, et al. Exit from germinal center to become quiescent memory B cells depends on metabolic reprograming and provision of a survival signal. Journal of Experimental Medicine. 2020;218(1):e20200866.

47. Inoue T, Moran I, Shinnakasu R, Phan TG, Kurosaki T. Generation of memory B cells and their reactivation. Immunological Reviews. 2018;283(1):138-49.
48. Viant C, Weymar GHJ, Escolano A, Chen S, Hartweger H, Cipolla M, et al. Antibody Affinity Shapes the Choice between Memory and Germinal Center B Cell Fates. 2020(1097-4172 (Electronic)).
49. Elsner RA, Shlomchik MJ. Germinal Center and Extrafollicular B Cell Responses in Vaccination, Immunity, and Autoimmunity. 2020(1097-4180 (Electronic)).
50. Inamine A TY, Baba N, Miyake K, Tokuhisa T, Takemori T, Abe R. Two waves of memory B-cell generation in the primary immune response. Two waves of memory B-cell generation in the primary immune response. Int Immunol. 2005(0953-8178 (Print)).
51. Thucydides. The Peloponnesian War. 430 BC (translated 1910 AC);2.51.6.
52. Pardieck IN, van der Sluis TC, van der Gracht ETI, Veerkamp DMB, Behr FM, van Duikeren S, et al. A third vaccination with a single T cell epitope confers protection in a murine model of SARS-CoV-2 infection. Nature Communications. 2022;13(1):3966.
53. Zhao J, Zhao J, Mangalam AK, Channappanavar R, Fett C, Meyerholz DK, et al. Airway Memory CD4(+) T Cells Mediate Protective Immunity against Emerging Respiratory Coronaviruses. Immunity. 2016(1097-4180 (Electronic)).
54. Koutsakos M, Illing PT, Nguyen THO, Mifsud NA, Crawford JC, Rizzetto S, et al. Human CD8+ T cell cross-reactivity across influenza A, B and C viruses. Nature Immunology. 2019;20(5):613-25.
55. Welten SPM, Oderbolz J, Yilmaz V, Bidgood SR, Gould V, Mercer J, et al. Influenza- and MCMV-induced memory CD8 T cells control respiratory vaccinia virus infection despite residence in distinct anatomical niches. Mucosal Immunology. 2021;14(3):728-42.
56. Amanna IJ, Carlson NE, Slifka MK. Duration of Humoral Immunity to Common Viral and Vaccine Antigens. New England Journal of Medicine. 2007;357(19):1903-15.
57. Landsverk OJB, Snir O, Casado RB, Richter L, Mold JE, Réu P, et al. Antibody-secreting plasma cells persist for decades in human intestine. Journal of Experimental Medicine. 2017;214(2):309-17.
58. Manz RA, Thiel A, Radbruch A. Lifetime of plasma cells in the bone marrow. Nature. 1997;388(6638):133-4.
59. Auner HW, Beham-Schmid C, Dillon N, Sabbattini P. The life span of short-lived plasma cells is partly determined by a block on activation of apoptotic caspases acting in combination with endoplasmic reticulum stress. Blood. 2010;116(18):3445-55.
60. Savage HP, Yenson VM, Sawhney SS, Mousseau BJ, Lund FE, Baumgarth N. Blimp-1–dependent and –independent natural antibody production by B-1 and B-1–derived plasma cells. Journal of Experimental Medicine. 2017;214(9):2777-94.
61. Sciammas R, Shaffer AL, Schatz JH, Zhao H, Staudt LM, Singh H. Graded Expression of Interferon Regulatory Factor-4 Coordinates Isotype Switching with Plasma Cell Differentiation. Immunity. 2006;25(2):225-36.
62. Nutt SL, Fairfax KA, Kallies A. BLIMP1 guides the fate of effector B and T cells. Nature Reviews Immunology. 2007;7(12):923-7.
63. Minnich M, Tagoh H, Bönelt P, Axelsson E, Fischer M, Cebolla B, et al. Multifunctional role of the transcription factor Blimp-1 in coordinating plasma cell differentiation. Nature Immunology. 2016;17(3):331-43.
64. Benner R HW, Haaijman JJ. The bone marrow: the major source of serum immunoglobulins, but still a neglected site of antibody formation. Clin Exp Immunol. 1981(0009-9104 (Print)).
65. Kabashima K, Haynes NM, Xu Y, Nutt SL, Allende ML, Proia RL, et al. Plasma cell S1P1 expression determines secondary lymphoid organ retention versus bone marrow tropism. Journal of Experimental Medicine. 2006;203(12):2683-90.
66. Hargreaves DC, Hyman PL, Lu TT, Ngo VN, Bidgol A, Suzuki G, et al. A coordinated change in chemokine responsiveness guides plasma cell movements. J Exp Med. 2001;194(1):45-56.

67. Belnoue E, Pihlgren M, McGaha TL, Tougne C, Rochat A-F, Bossen C, et al. APRIL is critical for plasmablast survival in the bone marrow and poorly expressed by early-life bone marrow stromal cells. Blood. 2008;111(5):2755-64.
68. Tomayko MM SN, Anderson SM, Shlomchik MJ. Cutting edge: Hierarchy of maturity of murine memory B cell subsets. Cutting edge: Hierarchy of maturity of murine memory B cell subsets. J Immunol. 2010(1550-6606 (Electronic)).
69. Tomayko MM AS, Brayton CE, Sadanand S, Steinel NC, Behrens TW, Shlomchik MJ. Systematic comparison of gene expression between murine memory and naive B cells demonstrates that memory B cells have unique signaling capabilities. J Immunol. 2008(0022-1767 (Print)).
70. Zuccarino-Catania GV, Sadanand S, Weisel FJ, Tomayko MM, Meng H, Kleinstein SH, et al. CD80 and PD-L2 define functionally distinct memory B cell subsets that are independent of antibody isotype. Nature Immunology. 2014;15(7):631-7.
71. Krishnamurty AT, Thouvenel CD, Portugal S, Keitany GJ, Kim KS, Holder A, et al. Somatically Hypermutated Plasmodium-Specific IgM(+) Memory B Cells Are Rapid, Plastic, Early Responders upon Malaria Rechallenge. Immunity. 2016(1097-4180 (Electronic)).
72. Klein U, Rajewsky K.,Küppers, R. Human immunoglobulin (Ig)M+IgD+ peripheral blood B cells expressing the CD27 cell surface antigen carry somatically mutated variable region genes: CD27 as a general marker for somatically mutated (memory) B cells. J Exp Med. 1998(0022-1007 (Print)).
73. Berkowska MA DG, Bikos V, Grosserichter-Wagener C, Stamatopoulos K, Cerutti A, He B, Biermann K, Lange JF, van der Burg M, van Dongen JJ, van Zelm MC. Human memory B cells originate from three distinct germinal center-dependent and -independent maturation pathways. Blood. 2011(1528-0020 (Electronic)).
74. Ehrhardt GtRA, Hijikata A, Kitamura H, Ohara O, Wang J-Y, Cooper MD. Discriminating gene expression profiles of memory B cell subpopulations. Journal of Experimental Medicine. 2008;205(8):1807-17.
75. Weiss GE CP, Li S, Walsh LA, Moir S, Traore B, Kayentao K, Ongoiba A, Doumbo OK, Pierce SK. The Functional Requirement for CD69 in Establishment of Resident Memory CD8+ T Cells Varies with Tissue Location. J Immunol. 2009(1550-6606 (Electronic)).
76. Moir S HJ, Malaspina A, Wang W, DiPoto AC, O'Shea MA, Roby G, Kottilil S, Arthos J, Proschan MA, Chun TW, Fauci AS. Evidence for HIV-associated B cell exhaustion in a dysfunctional memory B cell compartment in HIV-infected viremic individuals. J Exp Med. 2008(1540-9538 (Electronic)).
77. Yeo L, Lom H, Juarez M, Snow M, Buckley CD, Filer A, et al. Expression of FcRL4 defines a pro-inflammatory, RANKL-producing B cell subset in rheumatoid arthritis. Annals of the Rheumatic Diseases. 2015;74(5):928.
78. Ehrhardt GR HJ, Gartland L, Leu CM, Zhang S, Davis RS, Cooper MD. Expression of the immunoregulatory molecule FcRH4 defines a distinctive tissue-based population of memory B cells. J Exp Med. 2005(0022-1007 (Print)).
79. Liu Y, McDaniel JA-O, Khan S, Campisi P, Propst EJ, Holler T, et al. Antibodies Encoded by FCRL4-Bearing Memory B Cells Preferentially Recognize Commensal Microbial Antigens. J Immunol. 2018(1550-6606 (Electronic)).
80. Knox JJ, Myles A, Cancro MA-O. T-bet(+) memory B cells: Generation, function, and fate. Immunol Rev. 2019(1600-065X (Electronic)).
81. Peng SL, Szabo SJ, Glimcher LH. T-bet regulates IgG class switching and pathogenic autoantibody production. Proceedings of the National Academy of Sciences. 2002;99(8):5545-50.
82. Johnson JL, Rosenthal RL, Knox JJ, Myles A, Naradikian MS, Madej J, et al. The Transcription Factor T-bet Resolves Memory B Cell Subsets with Distinct Tissue Distributions and Antibody Specificities in Mice and Humans. Immunity. 2020;52(5):842-55.e6.

83. Giesecke C, Frölich D, Reiter K, Mei HE, Wirries I, Kuhly R, et al. Tissue Distribution and Dependence of Responsiveness of Human Antigen-Specific Memory B Cells. The Journal of Immunology. 2014;192(7):3091.
84. Moyron-Quiroz JE, Rangel-Moreno J, Hartson L, Kusser K, Tighe MP, Klonowski KD, et al. Persistence and Responsiveness of Immunologic Memory in the Absence of Secondary Lymphoid Organs. Immunity. 2006;25(4):643-54.
85. Joo Hye M, He Y, Sangster Mark Y. Broad dispersion and lung localization of virus-specific memory B cells induced by influenza pneumonia. Proceedings of the National Academy of Sciences. 2008;105(9):3485-90.
86. Anderson SM, Tomayko MM, Ahuja A, Haberman AM, Shlomchik MJ. New markers for murine memory B cells that define mutated and unmutated subsets. Journal of Experimental Medicine. 2007;204(9):2103-14.
87. Elgueta R, Marks E, Nowak E, Menezes S, Benson M, Raman VS, et al. CCR6-dependent positioning of memory B cells is essential for their ability to mount a recall response to antigen. J Immunol. 2015(1550-6606 (Electronic)).
88. Henneken M DT, Burmester GR, Berek C. Differential expression of chemokine receptors on peripheral blood B cells from patients with rheumatoid arthritis and systemic lupus erythematosus. Arthritis Res Ther. 2005(1478-6362 (Electronic)).
89. Csencsits KL JM, Pascual DW. Nasal-associated lymphoid tissue: phenotypic and functional evidence for the primary role of peripheral node addressin in naive lymphocyte adhesion to high endothelial venules in a mucosal site. J Immunol. 1999(0022-1767 (Print)).
90. Roy MP, Kim CH, Butcher EC. Cytokine Control of Memory B Cell Homing Machinery. The Journal of Immunology. 2002;169(4):1676.
91. Girard J-P, Moussion C, Förster R. HEVs, lymphatics and homeostatic immune cell trafficking in lymph nodes. Nature Reviews Immunology. 2012;12(11):762-73.
92. Pappu R SS, Cornelissen I, Pereira JP, Regard JB, Xu Y, Camerer E, Zheng YW, Huang Y, Cyster JG, Coughlin SR. Promotion of lymphocyte egress into blood and lymph by distinct sources of sphingosine-1-phosphate. Science. 2007(316(5822):295-8 (Electronic)).
93. Müller-Winkler J, Mitter R, Rappe JCF, Vanes L, Schweighoffer E, Mohammadi H, et al. Critical requirement for BCR, BAFF, and BAFFR in memory B cell survival. Journal of Experimental Medicine. 2020;218(2):e20191393.
94. Ackermann JA, Nys J, Schweighoffer E, McCleary S, Smithers N, Tybulewicz VLJ. Syk Tyrosine Kinase Is Critical for B Cell Antibody Responses and Memory B Cell Survival. The Journal of Immunology. 2015;194(10):4650.
95. Hikida M, Casola S, Takahashi N, Kaji T, Takemori T, Rajewsky K, et al. PLC-γ2 is essential for formation and maintenance of memory B cells. Journal of Experimental Medicine. 2009;206(3):681-9.
96. Maruyama M, Lam K-P, Rajewsky K. Memory B-cell persistence is independent of persisting immunizing antigen. Nature. 2000;407(6804):636-42.
97. Jones DD, Wilmore JR, Allman D. Cellular Dynamics of Memory B Cell Populations: IgM+ and IgG+ Memory B Cells Persist Indefinitely as Quiescent Cells. The Journal of Immunology. 2015;195(10):4753.
98. Hebeis BJ, Klenovsek K, Rohwer P, Ritter U, Schneider A, Mach M, et al. Activation of Virus-specific Memory B Cells in the Absence of T Cell Help. Journal of Experimental Medicine. 2004;199(4):593-602.
99. Weisel FJ AU, Schneider AM, Horlitz JU, van Rooijen N, Korner H, Mach M, Winkler TH. Unique requirements for reactivation of virus-specific memory B lymphocytes. J Immunol. 2010(1550-6606 (Electronic)).
100. Moran I, Nguyen A, Khoo WH, Butt D, Bourne K, Young C, et al. Memory B cells are reactivated in subcapsular proliferative foci of lymph nodes. Nature Communications. 2018;9(1):3372.

101. Asrir A, Aloulou M, Gador M, Pérals C, Fazilleau N. Interconnected subsets of memory follicular helper T cells have different effector functions. Nature Communications. 2017;8(1):847.
102. Gebhardt T, Wakim LM, Eidsmo L, Reading PC, Heath WR, Carbone FR. Memory T cells in nonlymphoid tissue that provide enhanced local immunity during infection with herpes simplex virus. Nature Immunology. 2009;10(5):524-30.
103. Jiang X, Clark RA, Liu L, Wagers AJ, Fuhlbrigge RC, Kupper TS. Skin infection generates non-migratory memory CD8+ TRM cells providing global skin immunity. Nature. 2012;483(7388):227-31.
104. Shin H, Iwasaki A. A vaccine strategy that protects against genital herpes by establishing local memory T cells. Nature. 2012;491(7424):463-7.
105. Casey KA FK, Schenkel JM, Moran A, Abt MC, Beura LK, Lucas PJ, Artis D, Wherry EJ, Hogquist K, Vezys V, Masopust D. Antigen-independent differentiation and maintenance of effector-like resident memory T cells in tissues. J Immunol. 2012(1550-6606 (Electronic)).
106. Skon CN, Lee J-Y, Anderson KG, Masopust D, Hogquist KA, Jameson SC. Transcriptional downregulation of S1pr1 is required for the establishment of resident memory CD8+ T cells. Nature Immunology. 2013;14(12):1285-93.
107. Steinert Elizabeth M, Schenkel Jason M, Fraser Kathryn A, Beura Lalit K, Manlove Luke S, Igyártó Botond Z, et al. Quantifying Memory CD8 T Cells Reveals Regionalization of Immunosurveillance. Cell. 2015;161(4):737-49.
108. Allie SR, Randall TD. Resident Memory B Cells. Viral Immunol. 2020(1557-8976 (Electronic)).
109. Tokunaga R, Zhang W, Naseem M, Puccini A, Berger MD, Soni S, et al. CXCL9, CXCL10, CXCL11/CXCR3 axis for immune activation - A target for novel cancer therapy. Cancer Treat Rev. 2018(1532-1967 (Electronic)).
110. Onodera T, Takahashi Y, Yokoi Y, Ato M, Kodama Y, Hachimura S, et al. Memory B cells in the lung participate in protective humoral immune responses to pulmonary influenza virus reinfection. Proceedings of the National Academy of Sciences. 2012;109(7):2485-90.
111. Adachi Y, Onodera T, Yamada Y, Daio R, Tsuiji M, Inoue T, et al. Distinct germinal center selection at local sites shapes memory B cell response to viral escape. Journal of Experimental Medicine. 2015;212(10):1709-23.
112. Allie SR, Bradley JE, Mudunuru U, Schultz MD, Graf BA, Lund FE, et al. The establishment of resident memory B cells in the lung requires local antigen encounter. Nature Immunology. 2019;20(1):97-108.
113. Barker KA, Etesami NS, Shenoy AT, Arafa EI, Lyon de Ana C, Smith NMS, et al. Lung-resident memory B cells protect against bacterial pneumonia. The Journal of Clinical Investigation. 2021;131(11).
114. Weisel NM, Weisel FJ, Farber DL, Borghesi LA, Shen Y, Ma W, et al. Comprehensive analyses of B-cell compartments across the human body reveal novel subsets and a gut-resident memory phenotype. Blood. 2020;136(24):2774-85.
115. Tan H-X, Juno Jennifer A, Esterbauer R, Kelly Hannah G, Wragg Kathleen M, Konstandopoulos P, et al. Lung-resident memory B cells established after pulmonary influenza infection display distinct transcriptional and phenotypic profiles. Science Immunology. 2021;7(67):eabf5314.
116. Gregoire C, Spinelli L, Villazala-Merino S, Gil L, Holgado MP, Moussa M, et al. Viral infection engenders bona fide and bystander subsets of lung-resident memory B cells through a permissive mechanism. Immunity. 2022.
117. Thornton EE LM, Bose O, Sen D, Sheppard D, Locksley R, Huang X, Krummel MF. Spatiotemporally separated antigen uptake by alveolar dendritic cells and airway presentation to T cells in the lung. J Exp Med. 2012(1540-9538 (Electronic)).

118. Piet B, de Bree GJ, Smids-Dierdorp BS, van der Loos CM, Remmerswaal EBM, von der Thüsen JH, et al. CD8+ T cells with an intraepithelial phenotype upregulate cytotoxic function upon influenza infection in human lung. The Journal of Clinical Investigation. 2011;121(6):2254-63.
119. Fleige H RS, Moschovakis GL, Bölter J, Willenzon S, Sutter G, Häussler S, Kalinke U, Prinz I, Förster R. IL-17-induced CXCL12 recruits B cells and induces follicle formation in BALT in the absence of differentiated FDCs. J Exp Med. 2014(1540-9538 (Electronic)).
120. Baluk P, Adams A, Phillips K, Feng J, Hong YK, Brown MB, et al. Preferential lymphatic growth in bronchus-associated lymphoid tissue in sustained lung inflammation. Am J Pathol. 2014(1525-2191 (Electronic)).
121. Moyron-Quiroz JE, Rangel-Moreno J, Kusser K, Hartson L, Sprague F, Goodrich S, et al. Role of inducible bronchus associated lymphoid tissue (iBALT) in respiratory immunity. Nature Medicine. 2004;10(9):927-34.
122. Taubenberger JK, Morens DM. The Pathology of Influenza Virus Infections. Annual Review of Pathology: Mechanisms of Disease. 2008;3(1):499-522.
123. Thompson WW, Shay DK, Weintraub E, Brammer L, Cox N, Anderson LJ, et al. Mortality Associated With Influenza and Respiratory Syncytial Virus in the United States. JAMA. 2003;289(2):179-86.
124. Cox NJ, Subbarao K. Global Epidemiology of Influenza: Past and Present. Annual Review of Medicine. 2000;51(1):407-21.
125. Shope RE. SWINE INFLUENZA : I. EXPERIMENTAL TRANSMISSION AND PATHOLOGY. Journal of Experimental Medicine. 1931;54(3):349-59.
126. Smith W, Andrewes CH, Laidlaw PP. A VIRUS OBTAINED FROM INFLUENZA PATIENTS. The Lancet. 1933;222(5732):66-8.
127. Shope RE. THE INFECTION OF FERRETS WITH SWINE INFLUENZA VIRUS. Journal of Experimental Medicine. 1934;60(1):49-61.
128. Shope RE. THE INFECTION OF MICE WITH SWINE INFLUENZA VIRUS. Journal of Experimental Medicine. 1935;62(4):561-72.
129. Andrewes CH, Laidlaw PP, Smith W. The Susceptibility of Mice to the Viruses of Human and S wine Influenza. Lancet. 1934:859-62.
130. Chiu C EA, Wrammert J, Ahmed R. B cell responses to influenza infection and vaccination. Curr Top Microbiol Immunol. 2015(0070-217X (Print)).
131. Li G-M, Chiu C, Wrammert J, McCausland M, Andrews SF, Zheng N-Y, et al. Pandemic H1N1 influenza vaccine induces a recall response in humans that favors broadly cross-reactive memory B cells. Proceedings of the National Academy of Sciences. 2012;109(23):9047-52.
132. Nachbagauer R, Choi A, Hirsh A, Margine I, Iida S, Barrera A, et al. Defining the antibody cross-reactome directed against the influenza virus surface glycoproteins. Nature Immunology. 2017;18(4):464-73.
133. Miyauchi K, Adachi Y, Tonouchi K, Yajima T, Harada Y, Fukuyama H, et al. Influenza virus infection expands the breadth of antibody responses through IL-4 signalling in B cells. Nature Communications. 2021;12(1):3789.
134. Vidarsson G, Dekkers G, Rispens T. IgG subclasses and allotypes: from structure to effector functions. (1664-3224 (Print)).
135. Li Z-N, Lin S-C, Carney Paul J, Li J, Liu F, Lu X, et al. IgM, IgG, and IgA Antibody Responses to Influenza A(H1N1)pdm09 Hemagglutinin in Infected Persons during the First Wave of the 2009 Pandemic in the United States. Clinical and Vaccine Immunology. 2014;21(8):1054-60.
136. Krammer F. The human antibody response to influenza A virus infection and vaccination. Nature Reviews Immunology. 2019;19(6):383-97.
137. Gould VMW, Francis JN, Anderson KJ, Georges B, Cope AV, Tregoning JS. Nasal IgA Provides Protection against Human Influenza Challenge in Volunteers with Low Serum Influenza Antibody Titre. Frontiers in Microbiology. 2017;8.

138. Sano K, Saito S, Suzuki TA-O, Kotani O, Ainai A, van Riet E, et al. An influenza HA stalk reactive polymeric IgA antibody exhibits anti-viral function regulated by binary interaction between HA and the antibody. (1932-6203 (Electronic)).
139. Mbawuike IN PS, Acuna CL, Switzer KC, Zhang Y, Harriman GR. Mucosal immunity to influenza without IgA: an IgA knockout mouse model. J Immunol. 1999(0022-1767 (Print)).
140. Couch RB. Prevention and Treatment of Influenza. New England Journal of Medicine. 2000;343(24):1778-87.
141. Ohinata Y SM, Shigeta M, Yamanaka K, Saitou M. A comprehensive, non-invasive visualization of primordial germ cell development in mice by the Prdm1-mVenus and Dppa3-ECFP double transgenic reporter. Reproduction. 2008(1741-7899 (Electronic)).
142. Kilbourne ED. Future influenza vaccines and the use of genetic recombinants. Bulletin of the World Health Organization. 1969;41(3):643-5.
143. Powell TJ, Silk JD, Sharps J, Fodor E, Townsend ARM. Pseudotyped influenza A virus as a vaccine for the induction of heterotypic immunity. Journal of virology. 2012;86(24):13397-406.
144. Powell TJ, Rijal P, McEwen-Smith RM, Byun H, Hardwick M, Schimanski LM, et al. A single cycle influenza virus coated in H7 haemagglutinin generates neutralizing antibody responses to haemagglutinin and neuraminidase glycoproteins and protection from heterotypic challenge. Journal of General Virology. 2019;100(3):431-45.
145. Nagasawa T. Microenvironmental niches in the bone marrow required for B-cell development. Nature Reviews Immunology. 2006;6(2):107-16.
146. Nagasawa T, Hirota S, Tachibana K, Takakura N, Nishikawa S-i, Kitamura Y, et al. Defects of B-cell lymphopoiesis and bone-marrow myelopoiesis in mice lacking the CXC chemokine PBSF/SDF-1. Nature. 1996;382(6592):635-8.
147. Hargreaves DC, Hyman PL, Lu TT, Ngo VN, Bidgol A, Suzuki G, et al. A Coordinated Change in Chemokine Responsiveness Guides Plasma Cell Movements. Journal of Experimental Medicine. 2001;194(1):45-56.
148. Opferman JT, Letai A, Beard C, Sorcinelli MD, Ong CC, Korsmeyer SJ. Development and maintenance of B and T lymphocytes requires antiapoptotic MCL-1. Nature. 2003;426(6967):671-6.
149. Fooksman DR ST, Victora GD, Dustin ML, Nussenzweig MC, Skokos D. Development and migration of plasma cells in the mouse lymph node. Immunity. 2010(1097-4180 (Electronic)).
150. Allen CDC, Ansel KM, Low C, Lesley R, Tamamura H, Fujii N, et al. Germinal center dark and light zone organization is mediated by CXCR4 and CXCR5. Nature Immunology. 2004;5(9):943-52.
151. Bannard O HR, Allen CD, An J, Nagasawa T, Cyster JG. Germinal center centroblasts transition to a centrocyte phenotype according to a timed program and depend on the dark zone for effective selection. Immunity. 2013(1097-4180 (Electronic)).
152. Wang X, Cho B, Suzuki K, Xu Y, Green JA, An J, et al. Follicular dendritic cells help establish follicle identity and promote B cell retention in germinal centers. Journal of Experimental Medicine. 2011;208(12):2497-510.
153. Allen CDC, Cyster JG. Follicular dendritic cell networks of primary follicles and germinal centers: Phenotype and function. Seminars in Immunology. 2008;20(1):14-25.
154. Aiba Y, Kometani K, Hamadate M, Moriyama S, Sakaue-Sawano A, Tomura M, et al. Preferential localization of IgG memory B cells adjacent to contracted germinal centers. Proceedings of the National Academy of Sciences. 2010;107(27):12192-7.
155. Blink EJ, Light A, Kallies A, Nutt SL, Hodgkin PD, Tarlinton DM. Early appearance of germinal center–derived memory B cells and plasma cells in blood after primary immunization. Journal of Experimental Medicine. 2005;201(4):545-54.

156. Allie SR, Bradley JE, Mudunuru U, Schultz MD, Graf BA, Lund FE, et al. The establishment of resident memory B cells in the lung requires local antigen encounter. (1529-2916 (Electronic)).
157. MacLean AJ, Richmond N, Koneva L, Attar M, Medina CAP, Thornton EE, et al. Secondary influenza challenge triggers resident memory B cell migration and rapid relocation to boost antibody secretion at infected sites. Immunity. 2022;55(4):718-33.e8.
158. Lu X, Tumpey TM, Morken T, Zaki SR, Cox NJ, Katz JM. A mouse model for the evaluation of pathogenesis and immunity to influenza A (H5N1) viruses isolated from humans. Journal of virology. 1999;73(7):5903-11.
159. Quan FS, Steinhauer D, Huang C, Ross TM, Compans RW, Kang S-M. A bivalent influenza VLP vaccine confers complete inhibition of virus replication in lungs. Vaccine. 2008;26(26):3352-61.
160. Matloubian M., Lo CG CG, Lesneski Matthew J, Xu Ying, Brinkmann Volker, Allende Maria L., Proia Richard L, Cyster Jason G. Lymphocyte egress from thymus and peripheral lymphoid organs is dependent on S1P receptor 1. 2004(1476-4687 (Electronic)).
161. Pham THM, Okada T, Matloubian M, Lo CG, Cyster JG. S1P1 Receptor Signaling Overrides Retention Mediated by Gai-Coupled Receptors to Promote T Cell Egress. Immunity. 2008;28(1):122-33.
162. Rosen H, Sanna MG, Cahalan SM, Gonzalez-Cabrera PJ. Tipping the gatekeeper: S1P regulation of endothelial barrier function. Trends in Immunology. 2007;28(3):102-7.
163. Masopust D, Soerens AG. Tissue-Resident T Cells and Other Resident Leukocytes. Annual Review of Immunology. 2019;37(1):521-46.
164. Fehrenbach H. Alveolar epithelial type II cell: defender of the alveolus revisited. Respiratory Research. 2001;2(1):33.
165. Doerschuk CM. Leukocyte trafficking in alveoli and airway passages. Respiratory Research. 2000;1(3):4.
166. Kopf M, Schneider C, Nobs SP. The development and function of lung-resident macrophages and dendritic cells. Nat Immunol. 2015;16(1):36-44.
167. Mulugeta S, Beers MF. Surfactant protein C: Its unique properties and emerging immunomodulatory role in the lung. Microbes and Infection. 2006;8(8):2317-23.
168. Chistiakov DA, Killingsworth MC, Myasoedova VA, Orekhov AN, Bobryshev YV. CD68/macrosialin: not just a histochemical marker. Laboratory Investigation. 2017;97(1):4-13.
169. van Mourik JA, Leeksma OC, Reinders JH, De Groot PG, Zandbergen-Spaargaren J. Vascular endothelial cells synthesize a plasma membrane protein indistinguishable from the platelet membrane glycoprotein IIa. Journal of Biological Chemistry. 1985;260(20):11300-6.
170. Zaynagetdinov R ST, Kendall PL, Segal BH, Weller KP, Tighe RM, Blackwell TS. Identification of myeloid cell subsets in murine lungs using flow cytometry. Am J Respir Cell Mol Biol. 2013(1535-4989 (Electronic)).
171. Pinkerton KE, Gehr P, Castañeda A, Crapo JD. Chapter 9 - Architecture and Cellular Composition of the Air–Blood Tissue Barrier. In: Parent RA, editor. Comparative Biology of the Normal Lung (Second Edition). San Diego: Academic Press; 2015. p. 105-17.
172. Knudsen L, Ochs M. The micromechanics of lung alveoli: structure and function of surfactant and tissue components. Histochemistry and cell biology. 2018;150(6):661-76.
173. Pham THM, Okada T, Matloubian M, Lo CG, Cyster JG. S1P1 Receptor Signaling Overrides Retention Mediated by Gαi-Coupled Receptors to Promote T Cell Egress. Immunity. 2008;28(1):122-33.
174. Takamura S, Yagi H, Hakata Y, Motozono C, McMaster SR, Masumoto T, et al. Specific niches for lung-resident memory CD8+ T cells at the site of tissue regeneration enable CD69-independent maintenance. Journal of Experimental Medicine. 2016;213(13):3057-73.

175. Walsh DA, Borges da Silva H, Beura LK, Peng C, Hamilton SE, Masopust D, et al. The Functional Requirement for CD69 in Establishment of Resident Memory CD8+ T Cells Varies with Tissue Location. The Journal of Immunology. 2019;203(4):946.
176. Iijima N, Iwasaki A. T cell memory. A local macrophage chemokine network sustains protective tissue-resident memory CD4 T cells. (1095-9203 (Electronic)).
177. Anderson MW, Zhao S, Ai WZ, Tibshirani R, Levy R, Lossos IS, et al. C-C chemokine receptor 1 expression in human hematolymphoid neoplasia. American journal of clinical pathology. 2010;133(3):473-83.
178. Patel BV, Tatham KC, Wilson MR, O'Dea KP, Takata M. In vivo compartmental analysis of leukocytes in mouse lungs. American journal of physiology Lung cellular and molecular physiology. 2015;309(7):L639-L52.
179. Bergsbaken T, Bevan MJ. Proinflammatory microenvironments within the intestine regulate the differentiation of tissue-resident CD8$^+$ T cells responding to infection. Nature immunology. 2015;16(4):406-14.
180. Czajkowsky DM, Hu J, Shao Z, Pleass RJ. Fc-fusion proteins: new developments and future perspectives. EMBO molecular medicine. 2012;4(10):1015-28.
181. Lo JC, Chin RK, Lee Y, Kang H-S, Wang Y, Weinstock JV, et al. Differential regulation of CCL21 in lymphoid/nonlymphoid tissues for effectively attracting T cells to peripheral tissues. The Journal of clinical investigation. 2003;112(10):1495-505.
182. Rangel-Moreno J, Moyron-Quiroz Juan E, Hartson L, Kusser K, Randall Troy D. Pulmonary expression of CXC chemokine ligand 13, CC chemokine ligand 19, and CC chemokine ligand 21 is essential for local immunity to influenza. Proceedings of the National Academy of Sciences. 2007;104(25):10577-82.
183. Bachmann MF, Jennings GT. Vaccine delivery: a matter of size, geometry, kinetics and molecular patterns. Nature Reviews Immunology. 2010;10(11):787-96.
184. Cardani A, Boulton A, Kim TS, Braciale TJ. Alveolar Macrophages Prevent Lethal Influenza Pneumonia By Inhibiting Infection Of Type-1 Alveolar Epithelial Cells. PLOS Pathogens. 2017;13(1): e1006140(1553-7374 (Electronic)).
185. Kim HM, Lee Y-W, Lee K-J, Kim HS, Cho SW, van Rooijen N, et al. Alveolar Macrophages Are Indispensable for Controlling Influenza Viruses in Lungs of Pigs. Journal of Virology. 2008;82(9):4265.
186. Schneider C, Nobs SP, Heer AK, Kurrer M, Klinke G, van Rooijen N, et al. Alveolar macrophages are essential for protection from respiratory failure and associated morbidity following influenza virus infection. PLOS Pathogens. 2014;10(4)(1553-7374 (Electronic)).
187. Purnama C, Ng, S. L., Tetlak, P., Setiagani, Y. A., Kandasamy, M., Baalasubramanian, S., Karjalainen, K., & Ruedl, C. Transient ablation of alveolar macrophages leads to massive pathology of influenza infection without affecting cellular adaptive immunity. European journal of immunology. 2014;44(7)(1521-4141 (Electronic)).
188. Londrigan SL, Short KR, Ma J, Gillespie L, Rockman SP, Brooks AG, et al. Infection of Mouse Macrophages by Seasonal Influenza Viruses Can Be Restricted at the Level of Virus Entry and at a Late Stage in the Virus Life Cycle. Journal of virology. 2015;89(24):12319-29.
189. Cline TD, Karlsson EA, Seufzer BJ, Schultz-Cherry S. The Hemagglutinin Protein of Highly Pathogenic H5N1 Influenza Viruses Overcomes an Early Block in the Replication Cycle To Promote Productive Replication in Macrophages. Journal of Virology. 2013;87(3):1411.
190. Zhang X, Mosser DM. Macrophage activation by endogenous danger signals. The Journal of Pathology. 2008;214(2):161-78.
191. To EE BB, Hendricks KS, Vlahos R, Selemidis S. Influenza A virus and TLR7 activation potentiate NOX2 oxidase-dependent ROS production in macrophages. Free Radic Res. 2014(1029-2470 (Electronic)).

192. Diebold Sandra S, Kaisho T, Hemmi H, Akira S, Reis e Sousa C. Innate Antiviral Responses by Means of TLR7-Mediated Recognition of Single-Stranded RNA. Science. 2004;303(5663):1529-31.
193. Zhang J, Miao J, Hou J, Lu C. The effects of H3N2 swine influenza virus infection on TLRs and RLRs signaling pathways in porcine alveolar macrophages. (1743-422X (Electronic)).
194. Wang R, Zhu Y, Lin X, Ren C, Zhao J, Wang F, et al. Influenza M2 protein regulates MAVS-mediated signaling pathway through interacting with MAVS and increasing ROS production. (1554-8635 (Electronic)).
195. Ichinohe T PI, Iwasaki A. Influenza virus activates inflammasomes via its intracellular M2 ion channel. Nat Immunol. 2010(1529-2916 (Electronic)).
196. Sadler AJ, Williams BR. Interferon-inducible antiviral effectors. Nature Reviews Immunology. 2008;559–568(1474-1741 (Electronic)).
197. Meliopoulos VA, Van de Velde LA, Van de Velde NC, Karlsson EA, Neale G, Vogel P, et al. An Epithelial Integrin Regulates the Amplitude of Protective Lung Interferon Responses against Multiple Respiratory Pathogens. PLOS Pathogens. 2016;12(8)(1553-7374 (Electronic)).
198. Goritzka M, Makris S, Kausar F, Durant LR, Pereira C, Kumagai Y, et al. Alveolar macrophage-derived type I interferons orchestrate innate immunity to RSV through recruitment of antiviral monocytes. 2015(1540-9538 (Electronic)).
199. Zhou J, Law HKW, Cheung CY, Ng IHY, Peiris JSM, Lau YL. Differential Expression of Chemokines and Their Receptors in Adult and Neonatal Macrophages Infected with Human or Avian Influenza Viruses. The Journal of Infectious Diseases. 2006;194(1):61-70.
200. Mantovani A, Sica A, Sozzani S, Allavena P, Vecchi A, Locati M. The chemokine system in diverse forms of macrophage activation and polarization. Trends in Immunology. 2004;25(12):677-86.
201. Honey K. CCL3 and CCL4 actively recruit CD8+ T cells. Nature Reviews Immunology. 2006;6(6):427.
202. Araujo JM, Gomez AC, Aguilar A, Salgado R, Balko JM, Bravo L, et al. Effect of CCL5 expression in the recruitment of immune cells in triple negative breast cancer. Scientific reports. 2018;8(1):4899.
203. Rabin RL, Alston MA, Sircus JC, Knollmann-Ritschel B, Moratz C, Ngo D, et al. CXCR3 Is Induced Early on the Pathway of CD4+ T Cell Differentiation and Bridges Central and Peripheral Functions. The Journal of Immunology. 2003;171(6):2812.
204. Misharin AV, Morales-Nebreda L, Mutlu GM, Budinger GRS, Perlman H. Flow cytometric analysis of macrophages and dendritic cell subsets in the mouse lung. American journal of respiratory cell and molecular biology. 2013;49(4):503-10.
205. Rose S, Misharin A, Perlman H. A novel Ly6C/Ly6G-based strategy to analyze the mouse splenic myeloid compartment. Cytometry Part A : the journal of the International Society for Analytical Cytology. 2012;81(4):343-50.
206. Baharom F, Thomas S, Rankin G, Lepzien R, Pourazar J, Behndig AF, et al. Dendritic Cells and Monocytes with Distinct Inflammatory Responses Reside in Lung Mucosa of Healthy Humans. The Journal of Immunology. 2016;196(11):4498.
207. Wareing MD SA, Inglis CA, Dias PB, Sarawar SR. CXCR2 is required for neutrophil recruitment to the lung during influenza virus infection, but is not essential for viral clearance. VIral Immunol. 2007(0882-8245 (Print)).
208. Ellis GT, Davidson S, Crotta S, Branzk N, Papayannopoulos V, Wack A. TRAIL+ monocytes and monocyte-related cells cause lung damage and thereby increase susceptibility to influenza–Streptococcus pneumoniae coinfection. EMBO reports. 2015;16(9):1203-18.
209. Cabeza-Cabrerizo MA-OX, Minutti CA-O, da Costa MA-O, Cardoso AA-O, Jenkins RA-O, Kulikauskaite J, et al. Recruitment of dendritic cell progenitors to foci of influenza A virus infection sustains immunity. (2470-9468 (Electronic)).

210. GeurtsvanKessel CH, Willart MAM, van Rijt LS, Muskens F, Kool M, Baas C, et al. Clearance of influenza virus from the lung depends on migratory langerin+CD11b− but not plasmacytoid dendritic cells. Journal of Experimental Medicine. 2008;205(7):1621-34.
211. León B L-BM, Ardavín C. Monocyte-derived dendritic cells formed at the infection site control the induction of protective T helper 1 responses against Leishmania. Immunity. 2007(1074-7613 (Print)).
212. Lin KL SY, Nakano H, Ramsburg E, Gunn MD. CCR2+ monocyte-derived dendritic cells and exudate macrophages produce influenza-induced pulmonary immune pathology and mortality. J Immunol. 2008(0022-1767 (Print)).
213. Nakano H, Lin KL, Yanagita M, Charbonneau C, Cook DN, Kakiuchi T, et al. Blood-derived inflammatory dendritic cells in lymph nodes stimulate acute T helper type 1 immune responses. Nature Immunology. 2009;10(4):394-402.
214. Berg JT, Lee ST, Thepen T, Lee CY, Tsan MF. Depletion of alveolar macrophages by liposome-encapsulated dichloromethylene diphosphonate. Journal of Applied Physiology. 1993;74(6):2812-9.
215. Broug-Holub E, Toews GB, van Iwaarden JF, Strieter RM, Kunkel SL, Paine R, 3rd, et al. Alveolar macrophages are required for protective pulmonary defenses in murine Klebsiella pneumonia: elimination of alveolar macrophages increases neutrophil recruitment but decreases bacterial clearance and survival. Infection and immunity. 1997;65(4):1139-46.
216. Markell R, Saviola G, Barker EA, Conway JD, Dujardin C. What Do We Know About Clodronate Now? A Medical and Veterinary Perspective. Journal of Equine Veterinary Science. 2020;88:102874.
217. Rooijen NV, Sanders A. Liposome mediated depletion of macrophages: mechanism of action, preparation of liposomes and applications. Journal of Immunological Methods. 1994;174(1):83-93.
218. Park I, Goddard ME, Cole JE, Zanin N, Lyytikäinen L-P, Lehtimäki T, et al. C-type lectin receptor CLEC4A2 promotes tissue adaptation of macrophages and protects against atherosclerosis. Nature Communications. 2022;13(1):215.
219. Robinson MD, Oshlack A. A scaling normalization method for differential expression analysis of RNA-seq data. Genome Biology. 2010;11(3):R25.
220. Anders S, Huber W. Differential expression analysis for sequence count data. Genome Biology. 2010;11(10):R106.
221. Anderson KG, Mayer-Barber K, Sung H, Beura L, James BR, Taylor JJ, et al. Intravascular staining for discrimination of vascular and tissue leukocytes. Nature Protocols. 2014;9(1):209-22.
222. Venosa A, Katzen J, Tomer Y, Kopp M, Jamil S, Russo SJ, et al. Epithelial Expression of an Interstitial Lung Disease-Associated Mutation in Surfactant Protein-C Modulates Recruitment and Activation of Key Myeloid Cell Populations in Mice. J Immunol. 2019;202(9):2760-71.
223. Wang J, Nikrad MP, Phang T, Gao B, Alford T, Ito Y, et al. Innate immune response to influenza A virus in differentiated human alveolar type II cells. American journal of respiratory cell and molecular biology. 2011;45(3):582-91.
224. Denney L, Ho L-P. The role of respiratory epithelium in host defence against influenza virus infection. Biomedical journal. 2018;41(4):218-33.
225. Aegerter H, Kulikauskaite J, Crotta S, Patel H, Kelly G, Hessel EM, et al. Influenza-induced monocyte-derived alveolar macrophages confer prolonged antibacterial protection. Nature immunology. 2020;21(2):145-57.
226. Sartorius R, Trovato M, Manco R, D'Apice L, De Berardinis P. Exploiting viral sensing mediated by Toll-like receptors to design innovative vaccines. npj Vaccines. 2021;6(1):127.
227. Ghoneim HE, Thomas PG, McCullers JA. Depletion of alveolar macrophages during influenza infection facilitates bacterial superinfections. Journal of immunology (Baltimore, Md : 1950). 2013;191(3):1250-9.

228. Lin KL, Suzuki Y, Nakano H, Ramsburg E, Gunn MD. CCR2+ Monocyte-Derived Dendritic Cells and Exudate Macrophages Produce Influenza-Induced Pulmonary Immune Pathology and Mortality. The Journal of Immunology. 2008;180(4):2562.
229. Sun K, Metzger DW. Inhibition of pulmonary antibacterial defense by interferon-γ during recovery from influenza infection. Nature Medicine. 2008;14(5):558-64.
230. Smith AM, Smith AP. A Critical, Nonlinear Threshold Dictates Bacterial Invasion and Initial Kinetics During Influenza. Scientific reports. 2016;6:38703-.
231. Califano D, Furuya Y, Metzger DW. Effects of Influenza on Alveolar Macrophage Viability Are Dependent on Mouse Genetic Strain. Journal of immunology (Baltimore, Md : 1950). 2018;201(1):134-44.
232. Doerschuk CM, Beyers N, Coxson HO, Wiggs B, Hogg JC. Comparison of neutrophil and capillary diameters and their relation to neutrophil sequestration in the lung. Journal of Applied Physiology. 1993;74(6):3040-5.
233. Holt PG, Strickland DH, Wikström ME, Jahnsen FL. Regulation of immunological homeostasis in the respiratory tract. Nature Reviews Immunology. 2008;8(2):142-52.
234. Tanino Y, Coombe DR, Gill SE, Kett WC, Kajikawa O, Proudfoot AEI, et al. Kinetics of Chemokine–Glycosaminoglycan Interactions Control Neutrophil Migration into the Airspaces of the Lungs. The Journal of Immunology. 2010;184(5):2677.
235. Guo L, Feng K, Wang YC, Mei JJ, Ning RT, Zheng HW, et al. Critical role of CXCL4 in the lung pathogenesis of influenza (H1N1) respiratory infection. (1935-3456 (Electronic)).
236. Wang H, Aloe C, Wilson N, Bozinovski S. G-CSFR antagonism reduces neutrophilic inflammation during pneumococcal and influenza respiratory infections without compromising clearance. Scientific Reports. 2019;9(1):17732.
237. Li H, Bradley KC, Long JS, Frise R, Ashcroft JW, Hartgroves LC, et al. Internal genes of a highly pathogenic H5N1 influenza virus determine high viral replication in myeloid cells and severe outcome of infection in mice. PLOS Pathogens. 2018;14(1):e1006821.
238. Rudd JM, Pulavendran S, Ashar HK, Ritchey JW, Snider TA, Malayer JR, et al. Neutrophils Induce a Novel Chemokine Receptors Repertoire During Influenza Pneumonia. Frontiers in cellular and infection microbiology. 2019;9:108-.
239. Lillard James W, Boyaka Prosper N, Chertov O, Oppenheim Joost J, McGhee Jerry R. Mechanisms for induction of acquired host immunity by neutrophil peptide defensins. Proceedings of the National Academy of Sciences. 1999;96(2):651-6.
240. Jenne Craig N, Wong Connie HY, Zemp Franz J, McDonald B, Rahman Masmudur M, Forsyth Peter A, et al. Neutrophils Recruited to Sites of Infection Protect from Virus Challenge by Releasing Neutrophil Extracellular Traps. Cell Host & Microbe. 2013;13(2):169-80.
241. Brandes M, Klauschen F, Kuchen S, Germain RN. A systems analysis identifies a feedforward inflammatory circuit leading to lethal influenza infection. Cell. 2013;154(1):197-212.
242. Stacey Hannah D, Golubeva D, Posca A, Ang Jann C, Novakowski Kyle E, Zahoor Muhammad A, et al. IgA potentiates NETosis in response to viral infection. Proceedings of the National Academy of Sciences. 2021;118(27):e2101497118.
243. Maus UA, Waelsch K, Kuziel WA, Delbeck T, Mack M, Blackwell TS, et al. Monocytes Are Potent Facilitators of Alveolar Neutrophil Emigration During Lung Inflammation: Role of the CCL2-CCR2 Axis. The Journal of Immunology. 2003;170(6):3273.
244. Seo SU KH, Ko HJ, Byun YH, Seong BL, Uematsu SU, Akira S, Kweon MN. Type I interferon signaling regulates Ly6C(hi) monocytes and neutrophils during acute viral pneumonia in mice. PLOS Pathogens. 2011;7(2)(1553-7374 (Electronic)).
245. Cabeza-Cabrerizo M, Minutti CM, da Costa MP, Cardoso A, Jenkins RP, Kulikauskaite J, et al. Recruitment of dendritic cell progenitors to foci of influenza A virus infection sustains immunity. Science immunology. 2021;6(65):eabi9331-eabi.

246. Allavena P, Giardina G Fau - Bianchi G, Bianchi G Fau - Mantovani A, Mantovani A. IL-15 is chemotactic for natural killer cells and stimulates their adhesion to vascular endothelium. (0741-5400 (Print)).
247. Cooper MA, Fehniger TA, Turner SC, Chen KS, Ghaheri BA, Ghayur T, et al. Human natural killer cells: a unique innate immunoregulatory role for the CD56bright subset. Blood. 2001;97(10):3146-51.
248. Arnon TI, Lev M Fau - Katz G, Katz G Fau - Chernobrov Y, Chernobrov Y Fau - Porgador A, Porgador A Fau - Mandelboim O, Mandelboim O. Recognition of viral hemagglutinins by NKp44 but not by NKp30. (0014-2980 (Print)).
249. Mandelboim O, Lieberman N, Lev M, Paul L, Arnon TI, Bushkin Y, et al. Recognition of haemagglutinins on virus-infected cells by NKp46 activates lysis by human NK cells. Nature. 2001;409(6823):1055-60.
250. Gazit R GR, Elboim M, Arnon TI, Katz G, Achdout H, Hanna J, Qimron U, Landau G, Greenbaum E, Zakay-Rones Z, Porgador A, Mandelboim O. Lethal influenza infection in the absence of the natural killer cell receptor gene Ncr1. Nat Immunol. 2006(1529-2908 (Print)).
251. Flynn KJ, Belz GT, Altman JD, Ahmed R, Woodland DL, Doherty PC. Virus-Specific CD8+ T Cells in Primary and Secondary Influenza Pneumonia. Immunity. 1998;8(6):683-91.
252. Low JS, Farsakoglu Y, Amezcua Vesely MC, Sefik E, Kelly JB, Harman CCD, et al. Tissue-resident memory T cell reactivation by diverse antigen-presenting cells imparts distinct functional responses. Journal of Experimental Medicine. 2020;217(8):e20192291.
253. Butler A, Hoffman P, Smibert P, Papalexi E, Satija RA-O. Integrating single-cell transcriptomic data across different conditions, technologies, and species. (1546-1696 (Electronic)).
254. Aran D, Looney AP, Liu L, Wu E, Fong V, Hsu A, et al. Reference-based analysis of lung single-cell sequencing reveals a transitional profibrotic macrophage. Nature Immunology. 2019;20(2):163-72.
255. Labiris NR, Dolovich MB. Pulmonary drug delivery. Part I: physiological factors affecting therapeutic effectiveness of aerosolized medications. British journal of clinical pharmacology. 2003;56(6):588-99.
256. Fröhlich E MA, Wu S, Salar-Behzadi S. Measurements of Deposition, Lung Surface Area and Lung Fluid for Simulation of Inhaled Compounds. Front Pharmacol. 2016(1663-9812 (Print)).
257. Bayat B, Werth S, Sachs UJH, Newman DK, Newman PJ, Santoso S. Neutrophil Transmigration Mediated by the Neutrophil-Specific Antigen CD177 Is Influenced by the Endothelial S536N Dimorphism of Platelet Endothelial Cell Adhesion Molecule-1. The Journal of Immunology. 2010;184(7):3889.
258. Walzer T, Bléry M, Chaix J, Fuseri N, Chasson L, Robbins Scott H, et al. Identification, activation, and selective in vivo ablation of mouse NK cells via NKp46. Proceedings of the National Academy of Sciences. 2007;104(9):3384-9.
259. Luster AD, Ravetch JV. Biochemical characterization of a gamma interferon-inducible cytokine (IP-10). Journal of Experimental Medicine. 1987;166(4):1084-97.
260. Cole KE, Strick CA, Paradis TJ, Ogborne KT, Loetscher M, Gladue RP, et al. Interferon–inducible T Cell Alpha Chemoattractant (I-TAC): A Novel Non-ELR CXC Chemokine with Potent Activity on Activated T Cells through Selective High Affinity Binding to CXCR3. Journal of Experimental Medicine. 1998;187(12):2009-21.
261. Liberzon A, Birger C, Thorvaldsdóttir H, Ghandi M, Mesirov JP, Tamayo P. The Molecular Signatures Database (MSigDB) hallmark gene set collection. (2405-4712 (Print)).
262. Lusty E, Poznanski SM, Kwofie K, Mandur TS, Lee DA, Richards CD, et al. IL-18/IL-15/IL-12 synergy induces elevated and prolonged IFN-γ production by ex vivo expanded NK cells which is not due to enhanced STAT4 activation. (1872-9142 (Electronic)).
263. Pirhonen J ST, Julkunen I, Matikainen S. Virus infection induces proteolytic processing of IL-18 in human macrophages via caspase-1 and caspase-3 activation. Eur J Immunol. 2001(0014-2980 (Print)).

264. Novick D KS, Fantuzzi G, Reznikov LL, Dinarello CA, Rubinstein M. Interleukin-18 binding protein: a novel modulator of the Th1 cytokine response. Immunity. 1999(1074-7613 (Print)).
265. Mizutani T, Neugebauer N, Putz EM, Moritz N, Simma O, Zebedin-Brandl E, et al. Conditional IFNAR1 ablation reveals distinct requirements of Type I IFN signaling for NK cell maturation and tumor surveillance. OncoImmunology. 2012;1(7):1027-37.
266. Madera S, Rapp M, Firth MA, Beilke JN, Lanier LL, Sun JC. Type I IFN promotes NK cell expansion during viral infection by protecting NK cells against fratricide. Journal of Experimental Medicine. 2016;213(2):225-33.
267. Nguyen KB, Salazar-Mather TP, Dalod MY, Van Deusen JB, Wei X-q, Liew FY, et al. Coordinated and Distinct Roles for IFN-αβ, IL-12, and IL-15 Regulation of NK Cell Responses to Viral Infection. The Journal of Immunology. 2002;169(8):4279.
268. Lee PY, Kumagai Y Fau - Xu Y, Xu Y Fau - Li Y, Li Y Fau - Barker T, Barker T Fau - Liu C, Liu C Fau - Sobel ES, et al. IL-1α modulates neutrophil recruitment in chronic inflammation induced by hydrocarbon oil. J Immunol. 2011(1550-6606 (Electronic)).
269. Eigenbrod T PJ, Harder J, Iwakura Y, Núñez G. Cutting edge: critical role for mesothelial cells in necrosis-induced inflammation through the recognition of IL-1 alpha released from dying cells. (1550-6606 (Electronic)).
270. Rider P, Carmi Y, Guttman O, Braiman A, Cohen I, Voronov E, et al. IL-1α and IL-1β Recruit Different Myeloid Cells and Promote Different Stages of Sterile Inflammation. The Journal of Immunology. 2011;187(9):4835.
271. Bradley LM, Douglass MF, Chatterjee D, Akira S, Baaten BJG. Matrix metalloprotease 9 mediates neutrophil migration into the airways in response to influenza virus-induced toll-like receptor signaling. PLoS pathogens. 2012;8(4):e1002641-e.
272. Lam WY YA, Chu IM, Chan PK. Profiles of cytokine and chemokine gene expression in human pulmonary epithelial cells induced by human and avian influenza viruses. Virol J. 2010(1743-422X (Electronic)).
273. Xing Z, Harper R, Anunciacion J, Yang Z, Gao W, Qu B, et al. Host immune and apoptotic responses to avian influenza virus H9N2 in human tracheobronchial epithelial cells. American journal of respiratory cell and molecular biology. 2011;44(1):24-33.
274. Ichinohe T LH, Ogura Y, Flavell R, Iwasaki A. Inflammasome recognition of influenza virus is essential for adaptive immune responses. J Exp Med. 2009(1540-9538 (Electronic)).
275. Roco JA, Mesin L, Binder SC, Nefzger C, Gonzalez-Figueroa P, Canete PF, et al. Class-Switch Recombination Occurs Infrequently in Germinal Centers. Immunity. 2019;51(2):337-50.e7.
276. Heng TS ea, Immunological Genome Project Consortium. The Immunological Genome Project: network of gene expression in immune cells. . Nat Immunol. 2008;10:1091.
277. Zan H, Casali P. Regulation of Aicda expression and AID activity. Autoimmunity. 2013(1607-842X (Electronic)).
278. Mai T ZH, Zhang J, Hawkins JS, Xu Z, Casali P. Estrogen receptors bind to and activate the HOXC4/HoxC4 promoter to potentiate HoxC4-mediated activation-induced cytosine deaminase induction, immunoglobulin class switch DNA recombination, and somatic hypermutation. J Biol Chem. 2010(1083-351X (Electronic)).
279. Gallo MA, Kaufman D. Antagonistic and agonistic effects of tamoxifen: significance in human cancer. (0093-7754 (Print)).
280. Haas KM, Poe JC, Steeber DA, Tedder TF. B-1a and B-1b Cells Exhibit Distinct Developmental Requirements and Have Unique Functional Roles in Innate and Adaptive Immunity to S. pneumoniae. Immunity. 2005;23(1):7-18.
281. Lu Z YL, Zhou X, Sotomayor E, Levitsky HI, Pardoll DM. CD40-independent pathways of T cell help for priming of CD8(+) cytotoxic T lymphocytes. J Exp Med. 2000(0022-1007 (Print)).
282. Lane P, Burdet C, McConnell F, Lanzavecchia A, Padovan E. CD40 ligand-independent B cell activation revealed by CD40 ligand-deficient T cell clones: evidence for distinct activation

requirements for antibody formation and B cell proliferation. European Journal of Immunology. 1995;25(6):1788-93.
283. Muehlinghaus G, Cigliano L, Huehn S, Peddinghaus A, Leyendeckers H, Hauser AE, et al. Regulation of CXCR3 and CXCR4 expression during terminal differentiation of memory B cells into plasma cells. Blood. 2005;105(10):3965-71.
284. Bouvier NM, Lowen AC. Animal Models for Influenza Virus Pathogenesis and Transmission. (1999-4915 (Electronic)).
285. Marois I CA, Garneau É, Richter MV. Initial infectious dose dictates the innate, adaptive, and memory responses to influenza in the respiratory tract. J Leukoc Biol. 2012(1938-3673 (Electronic)).
286. Wang CC, Prather KA, Sznitman J, Jimenez JL, Lakdawala SS, Tufekci Z, et al. Airborne transmission of respiratory viruses. Science. 2021;373(6558).
287. Longest PW, Golshahi L, Behara SRB, Tian G, Farkas DR, Hindle M. Efficient Nose-to-Lung (N2L) Aerosol Delivery with a Dry Powder Inhaler. Journal of aerosol medicine and pulmonary drug delivery. 2015;28(3):189-201.
288. Oh JE, Iijima N, Song E, Lu P, Klein J, Jiang R, et al. Migrant memory B cells secrete luminal antibody in the vagina. Nature. 2019;571(7763):122-6.
289. Oh JE SE, Moriyama M, Wong P, Zhang S, Jiang R, Strohmeier S, Kleinstein SH, Krammer F, Iwasaki A. Intranasal priming induces local lung-resident B cell populations that secrete protective mucosal antiviral IgA. Sci Immunol. 2021;10(2470-9468 (Electronic)).
290. Dogan I, Bertocci B, Vilmont V, Delbos F, Mégret J, Storck S, et al. Multiple layers of B cell memory with different effector functions. Nature Immunology. 2009;10(12):1292-9.
291. Kenderes KJ, Levack RC, Papillion AM, Cabrera-Martinez B, Dishaw LM, Winslow GM. T-Bet+ IgM Memory Cells Generate Multi-lineage Effector B Cells. Cell Reports. 2018;24(4):824-37.e3.
292. Knust J, Ochs M, Gundersen HJG, Nyengaard JR. Stereological Estimates of Alveolar Number and Size and Capillary Length and Surface Area in Mice Lungs. The Anatomical Record. 2009;292(1):113-22.
293. Atkinson J CY, Pessoa-Silva CL, et al. Natural Ventilation for Infection Control in Health-Care Settings. Geneva: World Health Organization. 2009.
294. Southam DS, Dolovich M, O'Byrne PM, Inman MD. Distribution of intranasal instillations in mice: effects of volume, time, body position, and anesthesia. American Journal of Physiology-Lung Cellular and Molecular Physiology. 2002;282(4):L833-L9.
295. Kiyono H, Fukuyama S. NALT- versus PEYER'S-patch-mediated mucosal immunity. Nature Reviews Immunology. 2004;4(9):699-710.
296. Liang B HL, Hou S. Nasal-associated lymphoid tissue is a site of long-term virus-specific antibody production following respiratory virus infection of mice. J Virol. 2001(0022-538X (Print)).
297. Pizzolla A, Wang Z, Groom Joanna R, Kedzierska K, Brooks Andrew G, Reading Patrick C, et al. Nasal-associated lymphoid tissues (NALTs) support the recall but not priming of influenza virus-specific cytotoxic T cells. Proceedings of the National Academy of Sciences. 2017;114(20):5225-30.
298. Johnston SL, Pattemore PK, Sanderson G, Smith S, Lampe F, Josephs L, et al. Community study of role of viral infections in exacerbations of asthma in 9-11 year old children. Bmj. 1995;310(6989):1225-9.
299. Yoo JK KT, Hufford MM, Braciale TJ. Viral infection of the lung: host response and sequelae. J Allergy Clin Immunol. 2013(1097-6825 (Electronic)).
300. Habener A, Grychtol R, Gaedcke S, DeLuca D, Dittrich AM, Happle C, et al. IgA+ memory B cells are significantly increased in patients with asthma and small airways dysfunction. European Respiratory Journal. 2022:2102130.

301. Habener A, Happle C, Grychtol R, Skuljec J, Busse M, Dalüge K, et al. Regulatory B cells control airway hyperreactivity and lung remodeling in a murine asthma model. (1097-6825 (Electronic)).
302. Coughlan L, Palese P. Overcoming Barriers in the Path to a Universal Influenza Virus Vaccine. Cell Host & Microbe. 2018;24(1):18-24.
303. Isakova-Sivak I, Rudenko L. The future of haemagglutinin stalk-based universal influenza vaccines. The Lancet Infectious Diseases. 2022;22(7):926-8.
304. Folschweiller N, Vanden Abeele C, Chu L, Van Damme P, García-Sastre A, Krammer F, et al. Reactogenicity, safety, and immunogenicity of chimeric haemagglutinin influenza split-virion vaccines, adjuvanted with AS01 or AS03 or non-adjuvanted: a phase 1–2 randomised controlled trial. The Lancet Infectious Diseases. 2022;22(7):1062-75.
305. Nachbagauer RA-O, Feser J, Naficy A, Bernstein DI, Guptill J, Walter EB, et al. A chimeric hemagglutinin-based universal influenza virus vaccine approach induces broad and long-lasting immunity in a randomized, placebo-controlled phase I trial. Nat Med. 2021;27(1546-170X (Electronic)).
306. Shlomchik MJ. Sites and Stages of Autoreactive B Cell Activation and Regulation. Immunity. 2008;28(1):18-28.
307. Cashman KS, Jenks SA, Woodruff MC, Tomar D, Tipton CM, Scharer CD, et al. Understanding and measuring human B-cell tolerance and its breakdown in autoimmune disease. Immunological reviews. 2019;292(1):76-89.
308. Ghosh S, Hoselton SA, Asbach SV, Steffan BN, Wanjara SB, Dorsam GP, et al. B lymphocytes regulate airway granulocytic inflammation and cytokine production in a murine model of fungal allergic asthma. Cellular & Molecular Immunology. 2015;12(2):202-12.
309. De Vooght V, Carlier V, Devos FC, Haenen S, Verbeken E, Nemery B, et al. B-lymphocytes as key players in chemical-induced asthma. PloS one. 2013;8(12):e83228-e.